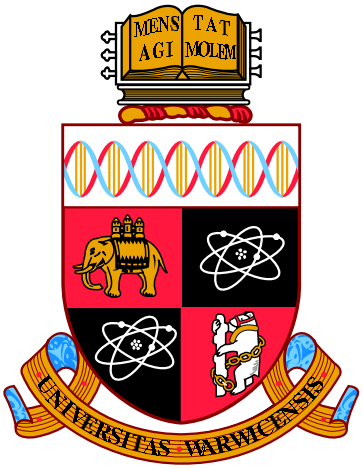

Dynamics of Condensation in Stochastic Particle Systems

by

Jiarui Cao

Thesis

Submitted to the University of Warwick

for the degree of

Doctor of Philosophy

Mathematics Institute

January 2016

THE UNIVERSITY OF WARWICK

Contents

List of Figures

Acknowledgments

I would like to express my sincere gratitude to my supervisor Stefan Grosskinsky for the continuous guidance of my Ph.D study and research, for his patience, motivation and support. He always found time for very useful discussions, during which I learnt extensive knowledge and more importantly the insight into scientific research. I could not have imagined having a better mentor and advisor for my Ph.D study.

I would like to thank my second supervisor Paul Chleboun for his guidance and help. His previous contribution to this area laid the cornerstone of this work and I learnt many advanced numerical methods from him. I am also very grateful for the many fruitful discussions and meetings with the colleagues in our Warwick Interacting Stochastic Particle Systems (WISPS) group. I would like to thank all members in the mathematics institute and centre for complexity science, in particular Xue-Mei Li for carefully reading my annual reports and gave very helpful feedbacks.

Additional thanks go to many people outside of the department who also helped with this work and provided inspiring discussions. I am very grateful to Frank Redig for inviting me to Delft, sharing his insights in many discussions and teaching me the theory of duality. I would also like to thank Martin Evans for his support and advice.

Finally, I would like to thank my family for the support throughout my entire Ph.D study. I am specially grateful to my wife, Yang, without whose love and encouragement, I would not have finished this thesis.

This work is funded by the University of Warwick through the Chancellor's International Scholarship and the Mathematics Institute.

Declarations

The large majority of the original content of this thesis was conducted in collaboration with my supervisors Stefan Grosskinsky and Paul Chleboun and has not been submitted for any other degree or professional qualification.

- Chapter 2 introduces standard notations and well known results from recent literatures.
- Chapter 3 contains original work, which was jointly conducted with Stefan Grosskinsky and Paul Chleboun, and has largely been published in [1].
- Chapter 4 and Chapter 5 contains original work, which was jointly conducted with Stefan Grosskinsky and Paul Chleboun. This work is in preparation for publication.
- Chapter 6 contains original work in collaborations with Stefan Grosskinsky and Frank Redig from Delft University of Technology. This work is in preparation for publication.

Abstract

Condensation is a special class of phase transition which has been observed throughout the natural and social sciences. The understanding of the critical behaviour of such systems is a very active area of current research, in particular a mathematical description of the formation and time evolution of the condensate. In this thesis we study these phenomena in several models. In particular we focus on the recently introduced inclusion process, and we compare it with related classical mass transport models such as zero range processes.

We first give a brief review of relevant definitions and properties of interacting particle systems, in particular recent literatures on the condensation and stationary behaviour of a large class of interacting particle systems with stationary product measures, which forms the theoretical basis of this thesis.

The second part of this thesis is on the dynamics of condensation in the inclusion process on a one-dimensional periodic lattice in the thermodynamic limit. This generalises recent results which were limited to finite lattices and symmetric dynamics. Our main focus is firstly on totally asymmetric dynamics which have not been studied before, which we compare to exact solutions for symmetric systems. We identify all the relevant dynamical regimes and corresponding time scales as a function of the system size, including a coarsening regime where clusters move on the lattice and exchange particles, leading to a growing average cluster size. After establishing the general approach to study dynamics of condensation in totally asymmetric processes, we extend the results to more general partially asymmetric cases as well as higher dimensional cases.

In the third part of this thesis we derive some preliminary exact results on symmetric systems through duality, which recovers heuristic results in previous chapter and allows us to treat coarsening in the infinite lattice directly.

Notation

$\bar{\nu}_\phi(\eta_x)$	Grand canonical marginal density w.r.t counting measure $d\boldsymbol{\eta}$. (p. 15)
$\boldsymbol{\eta} = (\eta_x : x \in \Lambda)$	Full configuration (p. 6)
$\mathcal{R}$	Fraction of occupied sites (random) after nucleation (p. 35)
η_x	Particle number (local configuration) on site x (p. 6)
$\hat{d}$	Dimension of the lattice (p. 23)
Λ , Λ_L	Lattice (of L sites) (p. 6)
$\langle\cdot\rangle$	Simulation averaged over a large number of realisations (p. 32)
$\mathbb{E}^{\boldsymbol{\eta}}[f]$	Expectation with respect to path measure $\mathbb{P}^{\boldsymbol{\eta}}$ (p. 7)
$\mathbb{P}^{\boldsymbol{\eta}}[\ ]$	Probability path measure starting from initial state $\boldsymbol{\eta}$ (p. 7)
$\mathcal{L}$, $\mathcal{L}_L$	The infinitesimal generator (p. 9)
$\mathbb{I}, \mathbb{I}_{\boldsymbol{\eta}}(\boldsymbol{\zeta})$	Indicator function, with shorthand $\mathbb{I}\{x \in A\} = \mathbb{I}_A(x)$ (p. 10)
$\nu(f)$	Expectation of f w.r.t. the measure ν, $\nu(f) = \int_X f\, d\nu$ (p. 11)
$\nu_\phi^\Lambda[d\boldsymbol{\eta}]$	Stationary product measure. (p. 15)
$\phi \geq 0$	Fugacity parameter (p. 16)
π, $\pi_{L,N}$	Stationary distribution (p. 12)
ρ	Particle density in the thermodynamic limit (p. 19)
ρ_c	Critical density $\rho_c = \lim_{\phi \nearrow \phi_c} R(\phi)$ (p. 19)
$\sigma^2(t)$	Second moment $\sigma^2(t) = \mathbb{E}[\eta_x^2(t)]$ (p. 8)
τ	Time scale of expectation of a hitting time (p. 44)
$\{S(t), t \geq 0\}$	Markov semigroup (p. 8)
A_x	Set of all nearest-neighbours of site x (p. 91)

$c(1,t)$	Nearest-neighbour product $c(1,t) = \mathbb{E}[\eta_x \eta_{x+1}]$ (p. 8)
$c(\boldsymbol{\eta}, \boldsymbol{\eta}') \geq 0$	Transition rate from state $\boldsymbol{\eta}$ to state $\boldsymbol{\eta}'$ (p. 7)
$C^b(X)$	Collection of continuous and bounded functions on X (p. 8)
d, d_L, d_N	Diffusion parameter in inclusion process (p. 26)
D_ϕ^Λ	Domain of the stationary product measure (p. 16)
$E \subseteq \mathbb{N}$	Local state space (p. 6)
$f(h) = o(h)$	$f(h)/h \to 0$ as $h \to 0$ (p. 7)
$f(n) = \Theta(n)$	$k_1 n < f(n) < k_2 n$, for some k_1, $k_2 > 0$ and n sufficiently large (p. 40)
$f_n \sim g_n$	Asymptotically proportional $f_n = C g_n + o(1)$ (p. 33)
$f_n \simeq g_n$	Asymptotically equivalent $f_n = g_n + o(1)$ (p. 28)
$j_{\Lambda,N}$	Canonical current (p. 21)
j_{gc}	Grand canonical current (p. 20)
m, $m(t)$	Size of a typical cluster (p. 40)
N	Total number of particles in the system (p. 14)
$p_t[\boldsymbol{\eta}]$, $\nu[\boldsymbol{\eta}]$	Probability distribution on state space X (p. 11)
$R(\phi)$	Average particle density (p. 16)
T	Hitting time (random) (p. 35)
X	State space (p. 6)
x, y	Lattice site (p. 6)
$z(\phi)$	Partition function (normalisation) of $\nu_\phi^\Lambda[d\boldsymbol{\eta}]$ (p. 15)
$Z_{\Lambda,N}$	Partition function (normalisation) of $\pi_{L,N}$ (p. 18)

Chapter 1

Introduction

Since the fundamental work initiated by Boltzmann in 1870s, the aim of statistical mechanics has been to understand a large class of phenomena in macroscopic systems in terms of microscopic components governed by local dynamics. Such systems exist everywhere in natural and social sciences, from granular materials to quantum gravity, from molecular and cellular biology systems to generic dynamics in evolution, from traffic dynamics to wealth distributions. In principle, microscopic dynamics in such systems usually follow well-known, relatively simple dynamics and interactions. Since a precise description of the system at the microscopic level is unrealistic due to the large number of particles involved, it is possible to approximate such systems in a probabilistic way. It is neither feasible nor required, to predict the accurate dynamics of a single component in the system, since they are usually sensitive to initial conditions and microscopic details. One is rather interested in understanding macroscopic measurable quantities of the system, such as granular clustering rates or critical car density on motorways causing traffic congestion. Therefore the microscopic components can be approximated as certain postulated distributions with effective noise. The exact origin of this noise is usually ignored, since macroscopically behaviour of the system is robust with respect to such details.

Mathematically, expected values of a number of chosen observables corresponding to measurable functions of the microscopic states are often used to describe the system. These observables are in general determined by macroscopic quantities, such as temperature, particle density and total energy, in the limit of large systems and possibly after appropriate equilibration of time. Macroscopic quantities are usually time invariant or slowly varying with respect to microscopic interacting dynamics, and a system is often observed in a stationary situation. However, continuously varying system parameters across certain critical values could lead to a qualitative differences in the stationary behaviour, which is often linked to

singularities in some thermodynamic functions. This phenomenon is known as a phase transition. Understanding how the phase transitions, and their associated macroscopic dynamics, depend on the system's microscopic dynamics is one of the fundamental tasks of statistical mechanics, and also the primary aim of this thesis.

Through the past century, there has been a very well developed understanding of systems in equilibrium with their surroundings. In such systems, an energy function governs the dynamics and the stationary behaviour. The dynamics, if considered at all, are assumed to be ergodic and reversible with respect to the stationary distribution. While there is a general theory of phase transitions in equilibrium systems [2] in the context of Gibbs measures [3], the phase transition of systems out of equilibrium lacks a general formalism and has drawn great research interests since the 1970s. To better understand the phenomenon of phase transitions, a branch of probability theory, namely the interacting particle systems, has been developed in the 1970s by Spitzer [4]. The original objective of interacting particle systems was to describe and analyse stochastic models for the temporal evolution of systems where equilibrium measures are the classical Gibbs states. Then, research in recent decades has shown that a wide variety of models with similar mathematical structures can be naturally formulated in the same way. Precisely, interacting particle systems are defined as continuous-time Markov processes on discrete state spaces (see details in Chapter 2). The microscopic behaviour is described through certain dynamics of jumping particles and their interactions. For its applications in natural and social sciences, the concept of 'particles' can be adapted in specific applications to represent various objectives far beyond physical particles, such as vehicles in a motorway, birds in a flock, proteins in a biological tissue or even certain information in a network.

For an interacting particle system, a conservation law is one of the main features determining its behaviour, both dynamical and stationary. In many systems, there are quantities locally conserved with respect to time evolution and can only be transported to or from other systems through boundaries, for example vehicles moving in a single direction motorway between two junctions. Systems without conservation laws are also common, examples include opinions in an election or people infected by certain diseases. These systems are often characterised by different dynamics and contain phase transitions into absorbing states, such as all patients are recovered or infected in an infection model. In this thesis, we focus on interacting particle systems defined on lattices with local conservation of the number of particles. A series of simplified models has been introduced in [4] to provide insights into the essential features in such systems, which can be divided into two

basic types depending on the restriction of number of particles per site. The first type is restricted to maximally one or a finite number of particles per site, and among them the asymmetric simple exclusion process (ASEP) is the elementary model, where particles on a one-dimensional lattice can only jump to nearest neighbour empty sites with biased rates. It was first introduced in [5] and then studied in a large volume of publications summarised in, e.g., [6, 7, 8]. The second type, without restrictions on particles residing per site, are relatively more complicated, and have drawn great research interests recently. The most basic such model is the zero range process (ZRP), where particles jump to other sites on the lattice with a rate that only depends on the number of particles residing on the departure site (zero-range interaction). Its simple product form of stationary measures (see details in Chapter 2) allows for a detailed analysis of its phase transitions on a rigorous level [9, 10, 11, 12]. Recent results and applications of the ZRP can be found in [9, 13, 14] and references therein.

The main model in this thesis, the inclusion process, is a recently introduced interacting particle system, in which particles perform independent random walks on a lattice and interact via an attractive mechanism. The interaction rates depend on occupation numbers of both departure and target sites. It was originally introduced in 2007 as a dual process of a heat conduction model [15], and then further developed as a bosonic counterpart of the exclusion process in [16]. Besides its application in energy transportation, this model can also be interpreted as a multi-allele version of the Moran model [17] which describes generic dynamics in finite populations. It can also be applied in the field of econophysics as a model of kinetic wealth distribution, which is a large class of processes modelling the transitions of preserved total wealth between agents in an economy.

As mentioned above, phase transition is a main research area in statistical mechanics, and one of the most ubiquitous forms of phase transitions in nature is condensation. In a narrow sense, condensation is defined as a certain type of matter transition from a gas form to a liquid form. Fog in a cold morning, water drops on a bottle of cold beer and rain or snow formation within clouds are all examples of condensation. It is also widely used in industries such as liquid oxygen production and oil refinery. In statistical mechanics, the concept of condensation has been generalised to describe systems where a finite fraction of a conserved quantity becomes localised in the phase space with respect to real or momentum space. Condensation in this generalised sense has been observed in a wide variety of fundamental models of dynamical processes. These include traffic flow [18, 19, 20, 21], the flow of wealth [22] and hub formation in complex networks [23, 24], where zero range processes have

been established as fundamental and minimal models to well describe such systems. In fact, the condensed phases can have variant forms from the ones described in those models. For example, the fraction of the total system mass in the condensate can be 1, leading to a complete condensate [25, 26]; the condensed phase can present a number of smaller mesocondensates [27] or finite-size quasi-condensates [28]. Notice, the existence of a condensed phase is not unique to models based on the ZRP or with factorised steady states [29]. A recent study in [30] show that a non-Markovian simple exclusion process exhibits an immobile condensate phase. The condensates discussed above are static, in the sense that they reside on certain parts of space for a long time then dissolve due to large fluctuations and reform somewhere else [10]. However, mobile condensates are often observed in a variety of physical models, and models with moving condensates are in general less well understood compared with the static ones, and so far there is no general theory about this phenomenon. The inclusion process studied in this thesis is thought to be one fundamental model to understand such systems. A similar model with interactions in a non-linear form has also been studied recently in [31, 32]. Other related models that have been studied in this area include the chipping model [33, 34] where all the mass from a site can move to a neighbouring site while a single unit of mass can chip off from the departure site and jump to an adjacent site, and a ZRP-like model with non-Markovian transition rates [35, 36].

In addition to characterising the stationary properties of condensation in interacting particle systems, understanding the dynamics of condensation poses a very natural and interesting problem. The coarsening behaviour in condensing systems has been studied heuristically in [11] and subsequent work for ZRP [9, 10, 12, 13, 37] and related models [38, 39, 40]. There is also a significant literature on the dynamics of condensation in spatially heterogeneous models (see [14] and references therein). For the symmetric inclusion process, the dynamics of the condensate formation and subsequent motion have been studied rigorously in [41] in the limit of infinitely many particles on a fixed, finite lattice. In this thesis we aim to investigate such dynamics in more general inclusion processes, both heuristically and rigorously, on one and two dimensional lattices.

The thesis is organised as follows: In Chapter 2 we give precise definitions of the models and mathematical tools used in this thesis and summarise results related to our work. In Chapter 3, we investigate the dynamics of condensation in the totally asymmetric inclusion process defined on a one-dimensional lattice, characterising four dynamical regimes. In Chapter 4, we extend our results to more general partially asymmetric inclusion process, which exhibit richer interaction mechanisms.

In Chapter 5 we investigate the dynamics of condensing inclusion process on two and higher dimensional lattices, with particular emphasis on symmetric systems. In Chapter 6, we derive some exact results on symmetric systems through duality.

Chapter 2

Interacting Particle Systems

In this chapter we give precise definitions of the stochastic particle systems that are studied in this thesis, and briefly review some relevant previous results. In Section 2.1 we introduce standard notations and results for general stochastic particle systems, including some key definitions used in this thesis, such as generator, stationary measure and transition rate. In Section 2.2 we briefly review results on a family of stochastic particle systems with stationary product measures following a recent review [42], with a particular emphasis on condensation. In Section 2.3 we summarise results of several particular models from a series of recent papers.

2.1 Definitions

In this section we give introductory definitions of stochastic particle systems largely following contents covered in [6, 43]. Definitions and theorems from a more mathematical point of view are put in Appendix A for completeness, and more results on general Markov chains can also be found in the literature, for example [44, 45].

2.1.1 Interacting particle system, Markov semigroup and generator

Interacting particle systems are continuous time Markov processes defined on discrete state spaces. The dynamics in these processes are specified by giving the infinitesimal rates at which particle transitions occur.

The **state space** of a process is the set containing all possible configurations and is denoted by $X = E^{\Lambda}$, where E is the countable local state space and Λ is the lattice. Throughout this thesis we restrict to $E = \mathbb{N}$ and Λ to be a finite subset of $\mathbb{Z}^{\hat{d}}$, and we denote a lattice that contains L sites as Λ_L. Configurations are denoted by $\boldsymbol{\eta} = (\eta_x : x \in \Lambda) \in X$, where $\eta_x \in E$ is the number of particles on site $x \in \Lambda$.

The generic probability space Ω of a continuous-time Markov chains is the space of right-continuous paths

$$\Omega = \left\{ \boldsymbol{\eta} : [0, +\infty) \to X \,\middle|\, \boldsymbol{\eta}(t) = \lim_{s \searrow t} \boldsymbol{\eta}(s) \right\} \quad .$$

For a given $\boldsymbol{\eta}(\cdot) \in \Omega$ the function $t \mapsto \boldsymbol{\eta}(t)$ is called a **sample path**.

Definition 2.1. A continuous-time stochastic process with state space X is a family $(\boldsymbol{\eta}(t) : t \geq 0)$ of random trajectories in the path space Ω. The process is called **Markov** if for all $A \subseteq \Omega$

$$\mathbb{P}^{\boldsymbol{\eta}} \left[\boldsymbol{\eta}(t + .) \in A | \left(\boldsymbol{\eta}(s) : s \leq t \right) \right] = \mathbb{P}^{\boldsymbol{\eta}(t)} \left[\boldsymbol{\eta}(.) \in A \right] \quad . \tag{2.1}$$

If X is discrete, the Markov process is called a continuous-time Markov chain.

The expectation with respect to $\mathbb{P}^{\boldsymbol{\eta}}$ is denoted by

$$\mathbb{E}^{\boldsymbol{\eta}}[f] = \int_{D[0,+\infty)} f \, d\mathbb{P}^{\boldsymbol{\eta}} \tag{2.2}$$

for any integrable function f on Ω. The local dynamics of interacting particle systems are described by a collection of **transition rates**, denoted by $c(\boldsymbol{\eta}, \boldsymbol{\eta}') \geq 0$, for every $\boldsymbol{\eta}, \boldsymbol{\eta}' \in X$. It represents the rate at which the system jumps from state $\boldsymbol{\eta}$ to state $\boldsymbol{\eta}'$. Intuitively we can write

$$\mathbb{P}^{\boldsymbol{\eta}} \left[\boldsymbol{\eta}(\delta t) = \boldsymbol{\eta}' \right] = c(\boldsymbol{\eta}, \boldsymbol{\eta}')\delta t + o(\delta t) \quad \text{as} \quad \delta t \searrow 0 \quad \text{for} \quad \boldsymbol{\eta} \neq \boldsymbol{\eta}'. \tag{2.3}$$

The probability of a transition from state $\boldsymbol{\eta}$ to state $\boldsymbol{\eta}'$ in a small time interval δt is then $c(\boldsymbol{\eta}, \boldsymbol{\eta}')\delta t$.

A variety of interacting particle systems have been introduced in [4]. Throughout this thesis we focus on processes with local conservation of particle numbers, called the **lattice gases**, where particles move on lattices without being created or annihilated. For compact local state spaces, there is a general theory on how to define interacting particle systems through continuous test functions and the Hille-Yosida theorem [43] even on infinite lattices. One may notice that strictly (2.3) can only hold on finite Λ, otherwise the probability on the left hand side is typically 0 for any $t > 0$. In fact, for infinite systems with non-compact state spaces, which include the models studied in this thesis, there is no general theory to guarantee a well defined process. The current method of definition on infinite lattices is case by case and requires more restrictive assumptions on test functions and transition

rates. An example of defining a ZRP on an infinite lattice can be found in [46] . The symmetric inclusion process on infinite lattices can be defined through duality (cf. [47]). However for general inclusion processes it is an interesting theoretical problem which has not been studied so far. In this thesis, we do not define the models on infinite lattices directly, but only study models defined on finite lattices in the limit of large system size. In this case, the state spaces are not compact, but countable. Therefore, we can define our models through standard methods for Markov chains [43, 45].

Let $C^b(X)$ denote the collection of continuous and bounded functions on X,

$$C^b(X) := \{f : X \to \mathbb{R} \quad | \quad f \text{ is continuous and bounded}\}.$$

Throughout this thesis, we regard functions in $C^b(X)$ as observables, and we study the dynamics through the time evolution of expected values of particular observables. For example, we study the dynamics of inclusion processes through second moment and nearest-neighbour product defined as the following:

Definition 2.2. For translation invariant interacting particle system $(\boldsymbol{\eta}(t), t \geq 0)$ defined on a lattice Λ, we define the **second moment** as

$$\sigma^2(t) := \mathbb{E}[\eta_x^2(t)] \quad \text{for some} \quad x \in \Lambda. \tag{2.4}$$

And the **nearest-neighbour product** as

$$c(1,t) := \mathbb{E}[\eta_x(t)\eta_{x+1}(t)] \quad \text{for some} \quad x \in \Lambda. \tag{2.5}$$

Both of these observables are x-independent if the initial distribution is translation invariant, and $\sigma^2(t)$ is the simplest observable capturing the temporal evolution of processes defined on lattices with periodic boundary conditions, like most models studied in this thesis. Generally, it is possible to consider functions outside $C^b(X)$, however $C^b(X)$ is sufficient to describe the distribution of Markov chains as a consequence of the Riesz representation theorem (see, e.g., [48, Theorem 2.14]).

For a given process $(\boldsymbol{\eta}(s), s \geq 0)$ on X and any $s \geq 0$, we now define an operator [1]

$$S(t) : C^b(X) \to C^b(X) \quad \text{as} \quad S(t)f(\boldsymbol{\eta}) = \mathbb{E}^{\boldsymbol{\eta}}\left[f(\boldsymbol{\eta}(t))\right], \tag{2.6}$$

to construct the Markov semigroup in the following sense.

[1] In general $f \in C^b(X)$ does not imply $S(t)f \in C^b(X)$, processes that have this property are called Feller processes (See Appendix A). All processes we consider throughout this thesis are Feller.

Definition 2.3. A collection of linear operators $\{S(t), t \geq 0\}$ on $C^b(X)$ is called a **Markov semigroup** if it satisfies the following properties:

(a) $S(0) = I$, the identity operator on $C^b(X)$.

(b) For every $f \in C^b(X)$, $t \mapsto S(t)f$ is right-continuous.

(c) $S(t+s)f = S(t)S(s)f$ for all $f \in C^b(X)$ and all $s, t \geq 0$ (Markov property).

(d) $S(t)1 = 1$ for all $t \geq 0$. [2]

(e) $S(t)f \geq 0$ for all non-negative $f \in C^b(X)$.

The importance of Markov semigroups lies in the fact there is an one-to-one correspondence between a Markov semigroup and a Markov process: for a Markov process $(\boldsymbol{\eta}(t), t \geq 0)$, a family of linear operators defined in Definition 2.3 is a Markov semigroup; on the other hand, for a Markov semigroup $\{S(t), t \geq 0\}$ defined on $C^b(X)$, there exists a unique Markov process $(\boldsymbol{\eta}(t), t \geq 0)$ such that $S(t)f(\boldsymbol{\eta}) = \mathbb{E}^{\boldsymbol{\eta}}[f(\boldsymbol{\eta}(t))]$ for all $t \geq 0$. Rigorous proofs of this property can be found in many text books, for example [43]. For a given Markov process, the corresponding semigroup could fully describe the time evolution of the expected values of observable $S(t)f \in C^b(X)$, and the expectation of observables at time $t > 0$ with respect to the initial distribution μ is given by

$$\mathbb{E}^{\mu}[f(\boldsymbol{\eta}(t))] = \int_X (S(t)f)(\boldsymbol{\zeta})\mu[d\boldsymbol{\zeta}] = \int_X S(t)f \, d\mu \quad \text{for all} \quad f \in C^b(X).$$

Intuitively, one can understand the semigroup defined in Definition 2.3 as being generated by the 'time derivative' of $S(t)$ at time zero, $S'(0)$, in an exponential form as $S(t) = \exp(tS'(0)) = \mathbb{1} + S'(0)t + o(t)$, as $t \to 0$. Formally, the generator of $\{S(t), t \geq 0\}$ is defined as the following.

Definition 2.4. The (infinitesimal) **generator** $\mathcal{L} : C^b(X) \to C^b(X)$ of a Markov semigroup $\{S(t), t \geq 0\}$ (see Definition 2.3) is given by

$$\mathcal{L}f = \lim_{\delta t \searrow 0} \frac{S(\delta t)f - f}{\delta t} \quad \text{for} \quad f \in C^b(X). \tag{2.7}$$

The Hille-Yosida theorem (see Theorem A.3 in Appendix A) says that, under certain conditions, there is a one-to-one correspondence between Markov generators and semigroups on $C^b(X)$. Formally, $S(t) = e^{t\mathcal{L}}$ in the sense that for every $f \in$

[2] Here 1 is the function constantly equal to 1

$C^b(X)$, $S(t)f$ is the solution of

$$\frac{d}{dt}S(t)f = S(t)\mathcal{L}f = \mathcal{L}S(t)f \tag{2.8}$$

which are called **forward** and **backward equation**, respectively. On finite state space X, $S(t) = e^{t\mathcal{L}}$ can be understood simply in terms of matrix exponentials.

With the transition rate $c(\boldsymbol{\eta}, \boldsymbol{\eta}')$ in (2.3), we can compute the generator directly as for small $\delta t \searrow 0$,

$$\begin{aligned} S(\delta t)f(\boldsymbol{\eta}) &= \mathbb{E}^{\boldsymbol{\eta}}\left[f(\boldsymbol{\eta}(\delta t))\right] = \sum_{\boldsymbol{\eta}' \in X} f(\boldsymbol{\eta}')\mathbb{P}^{\boldsymbol{\eta}}[\boldsymbol{\eta}(\delta t) = \boldsymbol{\eta}'] \\ &= \sum_{\boldsymbol{\eta}' \neq \boldsymbol{\eta}} c(\boldsymbol{\eta}, \boldsymbol{\eta}')f(\boldsymbol{\eta}')\delta t + f(\boldsymbol{\eta})\left(1 - \sum_{\boldsymbol{\eta}' \neq \boldsymbol{\eta}} c(\boldsymbol{\eta}, \boldsymbol{\eta}')\delta t\right) + o(\delta t), \end{aligned}$$

which implies

$$\mathcal{L}f(\boldsymbol{\eta}) = \sum_{\boldsymbol{\eta}' \in X} c(\boldsymbol{\eta}, \boldsymbol{\eta}')(f(\boldsymbol{\eta}') - f(\boldsymbol{\eta})),$$

where we used $c(\boldsymbol{\eta}, \boldsymbol{\eta}) = 0$ for all $\boldsymbol{\eta} \in X$. The definitions of semigroup and generator implies the following equation to describe the time evolution of expected values of an observable, which is used in the computations in following chapter,

$$\frac{d}{dt}\mathbb{E}^{\boldsymbol{\eta}}\left[f(\boldsymbol{\eta}(t))\right] = \mathbb{E}^{\boldsymbol{\eta}}\left[(\mathcal{L}f)(\boldsymbol{\eta}(t))\right] .$$

There is another common equivalent approach to describe above Markov chains in terms of the master equation, which we also briefly introduce here. Define the indicator function $\mathbb{I}_{\boldsymbol{\eta}} : X \to \{0, 1\}$ as

$$\mathbb{I}_{\boldsymbol{\eta}}(\boldsymbol{\zeta}) = \begin{cases} 1, & \text{if} \quad \boldsymbol{\zeta} = \boldsymbol{\eta} \\ 0, & \text{otherwise} \end{cases} ,$$

which is bounded and in fact forms a basis of $C^b(X)$ on finite lattices. Denote the probability distribution on X at time t starting from initial distribution μ as

$$p_t[\boldsymbol{\eta}] = \int_X S(t)\mathbb{I}_{\boldsymbol{\eta}} d\mu, \tag{2.9}$$

and substitute it into forward equation (2.8) to get

$$\begin{aligned}\frac{d}{dt}p_t[\boldsymbol{\eta}] &= \int_X S(t)\mathcal{L}\mathbb{I}_{\boldsymbol{\eta}}d\mu = \sum_{\boldsymbol{\zeta}\in X} p_t[\boldsymbol{\zeta}] \sum_{\boldsymbol{\zeta}'\in X} c(\boldsymbol{\zeta},\boldsymbol{\zeta}')(\mathbb{I}_{\boldsymbol{\eta}}(\boldsymbol{\zeta}') - \mathbb{I}_{\boldsymbol{\eta}}(\boldsymbol{\zeta})) \\ &= \sum_{\boldsymbol{\zeta}\in X} p_t[\boldsymbol{\zeta}]c(\boldsymbol{\zeta},\boldsymbol{\eta}) - p_t[\boldsymbol{\eta}] \sum_{\boldsymbol{\zeta}'\in X} c(\boldsymbol{\eta},\boldsymbol{\zeta}').\end{aligned}$$

The last line is indeed the **master equation**

$$\frac{d}{dt}p_t[\boldsymbol{\eta}] = \sum_{\boldsymbol{\zeta}\in X} \left(p_t[\boldsymbol{\zeta}]c(\boldsymbol{\zeta},\boldsymbol{\eta}) - p_t[\boldsymbol{\eta}]c(\boldsymbol{\eta},\boldsymbol{\zeta})\right), \tag{2.10}$$

where the two terms on the right-hand side are called **gain** and **loss terms**, respectively. It can be shown that it is equivalent to the forward equation (2.8) when the indicator functions form a basis of $C^b(X)$. This is valid on countable state space X only, which requires the lattice Λ to be finite.

2.1.2 Stationary measures

Definition 2.5. A probability measure ν defined on X is **stationary** or **invariant** if

$$\nu(S(t)f) = \nu(f), \quad \text{for all } f \in C^b(X).$$

Here and in the rest of this thesis, we use the notation $\nu(f) = \int_X f\, d\nu$ for the expectation of f with respect to a measure ν on the state space X. From the definition of the stationary measure, with notation (2.9) we have: if ν is stationary and $p_0 = \nu$, then $p_t = \nu$ for all $t \geq 0$. Recalling that indicator functions form a basis of $C^b(X)$ when Λ is finite and the master equation (2.10), it can be shown that a measure ν is stationary if and only if it solves the system of differential equations,

$$\frac{d}{dt}\nu[\boldsymbol{\eta}] = \sum_{\boldsymbol{\zeta}\in X} \left(\nu[\boldsymbol{\zeta}]c(\boldsymbol{\zeta},\boldsymbol{\eta}) - \nu[\boldsymbol{\eta}]c(\boldsymbol{\eta},\boldsymbol{\zeta})\right) = 0\,, \quad \text{for all } \boldsymbol{\eta} \in X.$$

In terms of the generator, this is equivalent to the following proposition.

Proposition 2.1. *A measure ν defined on X is stationary if and only if*

$$\nu(\mathcal{L}f) = 0 \quad \textit{for all} \quad f \in C(X)$$

Proof. See Proposition 2.13 in [43]. □

Recall the notation of the probability distribution at time t as p_t given in (2.9), we define ergodicity and irreducibility of a Markov process as the following:

Definition 2.6. A Markov process $(\boldsymbol{\eta}(t), t \geq 0)$ with semigroup $\{S(t), t \geq 0\}$ is **ergodic** if there exists a unique stationary distribution π and ,

$$\lim_{t\to\infty} p_t = \pi \quad \text{for any initial distribution } p_0 \ .$$

Definition 2.7. A Markov process $(\boldsymbol{\eta}(t), t \geq 0)$ is **irreducible** if for all $\boldsymbol{\eta}$, $\boldsymbol{\eta}' \in X$,

$$\mathbb{P}^{\boldsymbol{\eta}} \left[\boldsymbol{\eta}(t) = \boldsymbol{\eta}'\right] > 0 \quad \text{for some } \ t > 0$$

Generally, not every Markov process has a stationary distribution. But for all the models defined on finite state spaces and studied in this thesis, there exists at least one stationary distribution. Irreducibility of a Markov chain guarantees all states in the state space can be reached from any initial state. In fact, it also implies there is at most one stationary distribution (see detailed discussion in [45, Section 3.5]). An irreducible Markov process defined on a finite state space is always ergodic, this is the case for most processes we consider in the rest of this thesis.

Definition 2.8. A measure ν is **reversible** with respect to the semigroup $\{S(t), t \geq 0\}$ if

$$\nu(fS(t)g) = \nu(gS(t)f) \quad \text{for all } \ f, g \in C^b(X).$$

In terms of generator, this is equivalent to

$$\nu(f\mathcal{L}g) = \nu(g\mathcal{L}f) \quad \text{for all } f, g, \in C^b(X).$$

Every reversible measure is obviously stationary, which can by shown by taking $g = 1$ in the definition. If ν is stationary, the process $\boldsymbol{\eta}(t)$ with initial distribution ν has the same joint distributions as $\boldsymbol{\eta}(t+s)$ for $s \in [0, +\infty)$. It then can be extended to negative time $(-\infty, +\infty)$, and if ν is also reversible, $\boldsymbol{\eta}(t)$ and $\boldsymbol{\eta}(-t)$ have the same joint distributions. One can substitute indicator function into above definition to get the following proposition

Proposition 2.2. *A measure ν on a countable state space X is reversible for the process with transition rates $c(\cdot,\cdot)$ if and only if it fulfils the* ***detailed balance*** *conditions*

$$\nu(\boldsymbol{\eta})c(\boldsymbol{\eta}, \boldsymbol{\zeta}) = \nu(\boldsymbol{\zeta})c(\boldsymbol{\zeta}, \boldsymbol{\eta}) \quad \textit{for all } \ \boldsymbol{\eta}, \boldsymbol{\zeta} \in X \, .$$

For many problems related to interacting particle systems, proving limit theorems by developing and using estimates is usually very difficult and therefore one often takes advantages of any monotonicity that may be presented in the problem. We use the natural partial order on the state space X given by $\boldsymbol{\eta} \leq \boldsymbol{\zeta}$ if $\eta_x \leq \zeta_x$,

for all $x \in \Lambda$. A function $f \in C^b(X)$ is said to be increasing if $\boldsymbol{\eta} \leq \boldsymbol{\zeta}$ implies $f(\boldsymbol{\eta}) \leq f(\boldsymbol{\zeta})$. Two measures are stochastically ordered with $\mu_1 \leq \mu_2$ if for all increasing function $f \in C^b(X)$ we have $\mu_1(f) \leq \mu_2(f)$. A stochastic particle system on X with generator $\mathcal{L}$ and semigroup $S(t)$ is called **monotone (attractive)** if it preserves the stochastic order in time, i.e.

$$\nu_1 \leq \nu_2 \quad \Rightarrow \quad \nu_1 S(t) \leq \nu_2 S(t) \text{ for all } t \geq 0.$$

2.2 Condensation and equivalence of ensembles

As mentioned above, we focus on lattice gas models with a discrete, unbounded local state space $E = \mathbb{N} = \{0, 1, 2, ...\}$, i.e. without restriction on the number of particles per site. Examples of such models include zero-range process [4, 46, 49] and misanthrope processes [50], which is a large class of models containing the inclusion process and mass transport models [31, 32, 51]. These models with open boundaries have been studied in a series of papers [47, 52, 53], but in this thesis we only consider systems with periodic boundary conditions and the number of particles is a conserved quantity in finite systems. A **condensation transition** is said to occur when a non-zero fraction of all the particles typically accumulate on a vanishing volume fraction of the lattice, which has been the subject of recent research interest. Condensation phenomena have been observed in above lattice gases under certain geometries and particle interactions. When the particle density exceeds a critical value, the system phase separates into a condensed and a homogeneous or fluid phase. The fluid phase is distributed according to the maximal invariant measure with critical density and the excess mass concentrates on a subextensive part of the lattice, constituting the condensed phase. Condensation can be caused by spatial inhomogeneities or particle interactions in spatially homogeneous systems, and so far has mostly been studied for systems with stationary product measures.

Condensation in homogeneous systems was firstly studied in [9, 11], and then attracted research interests in the context of ZRP and related models. In homogeneous systems, the condensed phase is found to be delocalised, where the location of condensate is uniformly distributed on the lattice due to symmetry, and therefore not accessible in the thermodynamic limit under the usual local notions of convergence. Taking the maximum as a global observable, a series of papers [12, 26, 54, 55, 56] established rigorous results showing that the condensed phase in fact concentrates on a single lattice site, covering a relatively large class of systems with stationary product measures. Condensation in inhomogeneous systems in the

context of ZRP has been studied in [57, 58, 59, 60], and [61] covers more general models and provides a comprehensive review of related results on disordered systems. The condensed phase in such systems is localised on specific sites determined by geometric effects, such as exit/incoming rates of particles. The combination of inhomogeneous and interaction driven condensation has been studied in [62] for a system with a single defect site and more generally in [14, 63, 64]. Results on homogeneous mass transport models with continuous state space can be found in [65, 66, 67] and reference therein, and on related systems with pair-factorised stationary measures that give rise to a spatially extended condensates in [29, 68] and references therein.

In the rest of this section we focus on homogeneous systems and follow a recent review [42] to summarise previous results from a thermodynamic point of view, formulated in the context of the classical approach of the equivalence of ensembles [3].

2.2.1 Class of models with stationary product measures

We consider a family of lattice gases where the dynamics are given by the generator

$$\mathcal{L}f(\boldsymbol{\eta}) = \sum_{x,y\in\Lambda} p(x,y)u(\eta_x)v(\eta_y)\left[f\left(\boldsymbol{\eta}^{x,y}\right) - f(\boldsymbol{\eta})\right] \tag{2.11}$$

with the usual notation $\eta_z^{x,y} = \eta_z - \delta_{z,x} + \delta_{z,y}$ for a configuration where one particle has moved from site x to y. $p(x,y) \geq 0$ are transition rates of a single random walk on Λ with $p(x,x) = 0$, which we assume to be translation invariant $p(x,y) = q(y-x)$. We restrict the interaction part $u, v : \mathbb{N} \to [0,\infty)$ to satisfy

$$\begin{aligned} u(n) &= 0 \quad \text{if and only if} \quad n = 0 \\ v(n) &> 0, \ \forall n \geq 0. \end{aligned}$$

The number of particles is the only conserved quantity and on a finite lattice of size $|\Lambda| = L$ the process is irreducible on the subsets

$$X_{\Lambda,N} = \left\{ \boldsymbol{\eta} \in X \ : \ \sum_{x\in\Lambda} \eta_x = N \right\}, \ \text{for each} \ N \in \mathbb{N}.$$

The process is a finite state, irreducible Markov chain on $X_{\Lambda,N}$, and is therefore ergodic with a unique stationary measure $\pi_{\Lambda,N}$. Processes with such dynamics

include various models, such as[3]:

- zero-range processes (ZRP) [4]: $u(n)$ arbitrary, $v(n) \equiv 1$;
- Target processes (TP) [69]: $u(n) = 1 - \delta_{n,0}$, $v(n) > 0$ arbitrary;
- Inclusion processes (IP) [16, 65]: $u(n) = n$, $v(n) = d + n$, $d > 0$;
- Explosive condensation model (ECP) [32]:
  $u(n) = v(n) - v(0)$, $v(n) = (d + n)^\gamma$, $d, \gamma > 0$.

The family of processes (2.11) has some overlaps with the misanthrope process [50], which was originally defined on translation invariant lattices with a more general interaction function $g(\eta_x, \eta_y)$. All translation invariant examples of (2.11) are essentially special misanthrope processes, but (2.11) can be extended on more general lattices. It has been shown that (2.11) is attractive if and only if $u(n)$ is increasing and $v(n)$ is decreasing in n, which is analogous to results for misanthrope processes [50, 70]. However, condensation in homogeneous systems so far has only been observed if this condition is violated and the model is not attractive. In fact, whether the non-attractiveness is a necessary condition for condensation in homogeneous systems is an interesting question, recent results on this include [71, 72].

Under certain conditions (see Theorem 2.3 below) the process (2.11) admit stationary product measures which we denote

$$\nu_\phi^\Lambda[d\boldsymbol{\eta}] = \prod_{x\in\Lambda} \bar{\nu}_\phi(\eta_x) d\boldsymbol{\eta}\,, \tag{2.12}$$

and are defined by product densities with respect to the product counting measure $d\boldsymbol{\eta}$ on X_Λ. The marginals turn out to have the form

$$\nu_\phi[\eta_x = n] = \bar{\nu}_\phi(n) = \frac{1}{z(\phi)} w(n)\phi^n \tag{2.13}$$

with partition function (normalisation)

$$z(\phi) = \sum_{n=0}^{\infty} w(n)\phi^n.$$

The weights $w(n)$ are given by

$$w(n) = \prod_{k=1}^{n} \frac{v(k-1)}{u(k)}, \tag{2.14}$$

[3]Here we only list spatially homogeneous versions of these processes. Generally, the rates $u(n)$, $v(n)$ can both be site dependent.

encoding the interaction of the particles through the functional forms of u and v.

Since the number of particles is conserved, the measures can be indexed by a fugacity parameter $\phi \geq 0$ controlling the **average particle density**

$$R(\phi) = \nu_\phi(\eta_x) = \frac{1}{z(\phi)} \sum_{n=0}^{\infty} nw(n)\phi^n, \tag{2.15}$$

which is a strictly increasing function with $R(0) = 0$. This density can also be computed as $R(\phi) = \phi\partial_\phi \log z(\phi)$ since $z(\phi)$ is a generating function. Existence of (2.12) requires $z(\phi) < \infty$, so we define the domain of (2.12) as

$$D_\phi^\Lambda = \{\phi \geq 0 : \, z(\phi) < \infty, \} \, .$$

Notice $z(\phi)$ is a power-series in ϕ, the domain of each marginal ν_ϕ is $[0, \phi_c)$ or $[0, \phi_c]$ where

$$\phi_c = \left(\limsup_{n\to\infty} w(n)^{1/n} \right)^{-1}$$

is the radius of convergence of $z(\phi)$. The domain of (2.12) is then

$$D_\phi^\Lambda = [0, \phi_c) \quad \text{or} \quad [0, \phi_c], \tag{2.16}$$

and the right boundary of the domain depends on particular processes. For non-empty D_ϕ^Λ we require $\phi_c > 0$, and a sufficient condition is for example,

$$\frac{1}{n} \log w(n) = \frac{1}{n} \sum_{k=1}^{n} \log \frac{v(k-1)}{u(k)} \to \alpha \in [-\infty, \infty), \;\; \text{as} \;\; n \to \infty, \tag{2.17}$$

where α is some constant. This obviously holds whenever $v(n-1)/u(n)$ has a finite limit for all x as $n \to \infty$. A recent publication [42] summarises sufficient conditions for process (2.11) to have stationary product measures, from previous literature, for both spatially homogeneous and inhomogeneous systems. Here we only cover the homogeneous cases:

Theorem 2.3 (Stationary Product Measures)**.** *The processes with generator* (2.11) *have stationary product measures* ν_ϕ^Λ *of the form* (2.12)*, provided that one of the following conditions holds:*

1. $v(n) = 1$*, for all* $n \geq 0$ *(zero-range dynamics).*
2. $p(x, y) = p(y, x) \quad$ *for all* $\quad x, y \in \Lambda$*. In this case the measure is in fact reversible for the dynamics*(2.11)*.*

3. *Incoming and outgoing rates p are the same for each site,*

$$\sum_{y\in\Lambda} p(x,y) = \sum_{y\in\Lambda} p(y,x), \quad \textit{for all} \quad x \in \Lambda\,,$$

and $u(n)$ *and* $v(n)$ *fulfill*

$$u(n)v(m) - u(m)v(n) = v(0)(u(n) - u(m)) \quad \textit{for all } n, m \geq 0.$$

Proof. See, e.g., [42, Theorem 2.1]. □

Remarks

1. Cases 1 and 3 for ZRP have been covered in [4, 46, 73], and also been discussed in misanthrope processes [50] with some minor reformulation. Case 2 is analogous to a result for inclusion process in [74]. Cases 2 and 3 have also been studied in the context of target processes in [69]. Case 3 has been investigated in ECP in [32] as well.

2. In many instances, the above measures can be extended to infinite lattices in a generic way, even without guarantee of the existence of the dynamics of the process. If the dynamics exist, the measures are stationary for the limiting dynamics.

3. The result also holds for exclusion processes [43] or K-exclusion type models with $v(k) = 0$, $\forall k > K$, which results in restricted state space $E = \{0, 1, 2, ..., K\}$ (see [75, Section II.2.4] and reference therein).

4. The theorem can be generalised directly to systems with open boundaries of a particular type, where each boundary can be described consistently by a single auxiliary external site [42].

5. If above consistency relations do not hold, the stationary measures are in general not in product form. To study such systems, one approach is to describe the correlation structure using a matrix product formulation, which has been applied in the exclusion process in [76]. It is an interesting open question whether this technique can also be extended to the more general class of processes as described by (2.11).

2.2.2 Canonical measures and condensation

Results on stationary product measures discussed above can be applied in more general models, but in this thesis we are only interested in closed finite systems and their scaling limits. The total number of particles in such systems is conserved and there is no restriction on the number of particles per site. We further assume the weights $w(n) > 0$ are sub-exponential in the sense that

$$\frac{w(n+1)}{w(n)} = \frac{v(n)}{u(n-1)} \to 1, \quad \text{as} \quad n \to \infty. \tag{2.18}$$

If the limit is different from 1, it is equal to ϕ_c and by rescaling the rates we can always fix $\phi_c = 1$. The only exception is that w has super-exponential decay, then $\phi_c = \infty$ and there is no condensation, so we do not consider this case.

With product measures, the **canonical measures** $\pi_{\Lambda,N}$ on irreducible subsets $X_{\Lambda,N}$ have explicit formulae. Since the number of particles is conserved, the conditioned measures $\nu_\phi^\Lambda(d\eta|X_{\Lambda,N})$ are also stationary, and since the process is ergodic on $X_{\Lambda,N}$, these conditional measures are equal to $\pi_{\Lambda,N}$ and independent of the fugacity ϕ. Taking $\phi = 1$ for simplicity, we then have

$$\pi_{\Lambda,N}[d\boldsymbol{\eta}] = \nu_1^\Lambda[d\boldsymbol{\eta}|X_{\Lambda,N}] = \frac{1}{Z_{\Lambda,N}} \prod_{x\in\Lambda} w(\eta_x) d\boldsymbol{\eta}\,, \tag{2.19}$$

where $Z_{\Lambda,N} = \nu_1^\Lambda[X_{\Lambda,N}]$ is the normalisation.

The set of all stationary measures of processes with dynamics (2.11) is a convex subset of measures on X_Λ (see, e.g., [43, Proposition I.1.8]). On a finite lattice Λ, the canonical measures $\pi_{\Lambda,N}$ are the extreme points for this set, and the grand-canonical product measures ν_ϕ^Λ can be written as a convex combination

$$\nu_\phi^\Lambda = \sum_{N\in\mathbb{N}} \nu_\phi^\Lambda[X_{\Lambda,N}]\pi_{\Lambda,N},$$

which are not extremal. On finite lattices, it can be shown that there are no other extremal measures than the canonical ones, and therefore the full set of stationary distributions is given by their convex hull. However, on infinite lattice the problem is more complicated. In spatially homogeneous systems the grand-canonical measure are extremal, but there may be more non-homogeneous extremal measures, which are analogous to blocking measures for exclusion process (see, e.g., [43, Chapter.VIII]).

In the thermodynamic limit

$$L = |\Lambda|, N \to \infty, \quad \text{such that} \quad N/L \to \rho \geq 0,$$

the grand-canonical measures (with simple product structures) are usually expected to provide a good approximation to the sequence of canonical measures. In statistical mechanics this is called the **equivalence of ensembles** and one convenient way of quantifying the distance between two distributions is relative entropy. We do not use this technique directly in this thesis, and for its application in zero-range processes see [12] and more general discussion in [77]. Notice, for inclusion processes, we need to consider an adapted parameter-dependent thermodynamic limit to see the condensation where the equivalence of ensembles technique is not valid, which is discussed in details in Section 2.3.3.

Recall that the average particle density $R(\phi)$ (2.15) is strictly increasing in ϕ with $R(0) = 0$, we can define its critical limit as the following.

Definition 2.9. The **critical density** $\rho_c \in [0, \infty]$ is defined as

$$\rho_c := \lim_{\phi \nearrow \phi_c} R(\phi)\,, \quad \text{with } R(\phi) \text{ defined in (2.15)}, \tag{2.20}$$

and the system exhibits condensation if $\rho_c < \infty$.

It is clear that $\phi_c < \infty$ is a necessary condition for condensation, see, e.g., [73, Lemma II.3.3] for a proof in a special case. If the stationary weights had super-exponential decay, for example independent random walkers where η_x are i.i.d Poisson random variables, we have $\phi_c = \infty$ and $\rho_c = \infty$ and there is no condensation. This general connection between condensation and critical density works well in the thermodynamic limit for both homogeneous and inhomogeneous systems. It also works for systems with size-dependent parameters, e.g. inclusion processes. For other scaling limits such as $N \to \infty$ on a fixed lattice Λ, the above definition has to be adapted, see, e.g., [54]. Here we only review results on the connections between condensation, stationary currents as well as equivalence of ensembles for homogeneous systems. For results on inhomogeneous or more generalised systems, see [42, Section 4] and references therein.

Recall marginals (2.13)

$$\nu_\phi[\eta_x = n] = \frac{1}{z(\phi)} w(n)\phi^n, \quad \text{with} \quad z(\phi) = \sum_{n=0}^{\infty} w(n)\phi^n,$$

then the critical density (2.20) is

$$\rho_c = R(1) = \frac{1}{z(1)} \sum_{n=0}^{\infty} nw(n) \in (0, \infty].$$

It is easy to show $z(1) = \infty$ implies $\rho_c = \infty$ (see, e.g., [73, Lemma II.3.3]). Therefore, the system exhibits condensation with $\rho_c < \infty$ if and only if $nw(n)$ is summable, i.e. $w(n)$ must decay fast enough like a sub-exponential distribution, the measures are then defined for all $\phi \in [0, 1] = D_\phi$ and the range of densities is given by $R(D_\phi) = [0, \rho_c]$. Therefore, for $\rho_c < \infty$ the range of densities attainable by grand-canonical measures is a strict subset of $[0, \infty)$. For typical stationary configurations under canonical distributions $\pi_{\Lambda,N}$ with $N/L = \rho > \rho_c$, the system phase separates into a condensed and a fluid phase. It can be shown (see, e.g., a review in [42, Section 3]) that the bulk phase is distributed as the product measure ν_1 at the critical density ρ_c, and that the condensed phase containing a macroscopic amount of order $(\rho - \rho_c)L$ particles concentrates on a vanishing fraction of the lattice. This result is analogous to classical results on phase separation in the Ising model with spin-exchange (Kawasaki) dynamics (see, e.g., [43, Chapter 4]), where the main difference is that the models we discussed above have unbounded local state spaces and the condensed phase contributes only sub-extensively to the total entropy (or free energy) of the system. For the special cases where $w(n)$ have power law or stretched exponential tails, a series of papers [12, 26, 54, 55, 56] have shown that the condensed phase occupies a single site on the lattice.

The **stationary current** in a general lattice gas model is defined as the expected net number of particles crossing a bond in a (specified) positive direction per unit of time. The full current depends on the lattice geometry and vanishes for reversible systems, in which case one has to consider the diffusivity. The main interest for us will be the average jump rate of a particle per connecting bond. In the rest of this chapter we will simply call this the **current** for ease of presentation, even though in symmetric systems it is rather the activity. Since ν_ϕ^Λ is a homogeneous product measure, the **grand canonical current** can be defined for an arbitrary pair of sites $x \neq y \in \Lambda$ as

$$j_{\mathrm{gc}} := \nu_\phi^\Lambda(u(\eta_x)v(\eta_y)) = \nu_\phi^1(u)\nu_\phi^1(v) = \phi(\nu_\phi^1(v))^2, \tag{2.21}$$

where for the last representation we have used the following recursive property of

the stationary measures

$$\bar{\nu}_\phi(n+1)\bar{\nu}_\phi(k-1)u(n+1)v(k-1) = \bar{\nu}_\phi(n)\bar{\nu}_\phi(k)u(k)v(n), \quad \forall\, n \geq 0,\ k \geq 1,$$

which is implied by the form (2.13) and (2.14) of the marginals. Similarly, the **canonical current** can be defined as

$$j_{\Lambda,N} := \pi_{\Lambda,N}(u(\eta_x)v(\eta_y)), \tag{2.22}$$

which is still independent of $x \neq y \in \Lambda$ since the canonical measures are permutation invariant in homogeneous systems. The thermodynamic limit of the canonical current

$$j(\rho) = \lim_{L,N\to\infty} j_{\Lambda,N} \quad \text{for all } \rho \geq 0,$$

is usually named the **current-density relation** or the **fundamental diagram** of the process.

To compare both currents, it is often convenient to also view the grand-canonical one as a function of the density using the one-to-one relation $\rho = R(\phi)$ in (2.21), and in this case we write $j_{gc}(\rho)$ which exists only for densities in $[0, \rho_c]$.

The following theorem shows the weak convergence of the canonical measure to the grand-canonical measures on finite lattices. It was first published in [12] in terms of relative entropy and provided first rigorous results on the equivalence of ensembles.

Theorem 2.4. *1. We have weak convergence of the canonical measures to the grand-canonical measures in the sense that, for $f \in C^b(X)$,*

$$\pi_{\Lambda,N}(f) \to \begin{cases} \nu_\phi(f) \ \textit{with}\ R(\phi) = \rho & \textit{for} \quad \rho \leq \rho_c \\ \nu_{\phi_c}(f) & \textit{for} \quad \rho > \rho_c \end{cases}$$

as $L, N \to \infty$ and $N/L \to \rho > 0$.

2. For all $\rho > \rho_c$ we also have weak law of large numbers: denote $M_L := \max_{x\in\Lambda} \eta_x$, then

$$\frac{M_L}{(\rho - \rho_c)L} \to 1 \quad \textit{in distribution},$$

i.e. $\forall \epsilon > 0$, $\pi_{\Lambda,N}\left[\left|\frac{M_L}{(\rho-\rho_c)L} - 1\right| > \epsilon\right] \to 0$ as $L, N \to \infty$, $N/L \to \rho > \rho_c$.

Above theorem has been generalised in [42] for subcritical and supercritical cases. This result implies that the canonical measures converge locally to the grand-canonical measures for $\rho < \rho_c$, and for $\rho > \rho_c$ the canonical measure start to converge

locally to the critical grand-canonical measures, with density ρ_c, and the excess mass accumulates on a vanishing volume fraction. It is consistent with the study of ZRP in [78], while for IP it has been shown in [74] that $\rho_c = 0$ therefore the above theorem does not contribute to the study of condensation. We will discuss more details of both models in the next section.

2.3 Models

2.3.1 Zero range process

The zero-range process (ZRP) is a stochastic particle system with no restriction on the number of particles per site, and with jump rates depending only on the number of particles occupying on the departure site. It was originally introduced by Spitzer [4], and the stationary measure has a simple product structure [4, 46], as covered in Theorem 2.3. This model has recently drawn great research interests since a particular class of this model exhibits condensation transitions, which was established in a series of papers [9, 10, 11, 12]. And more variants of models in this class have been studied recently, including a non-Markovian version with slinky condensate motion [35, 79]. Recent reviews of the literature can be found in [14, 42]. If the particle density ρ in the system exceeds a critical value ρ_c, the system separates into a fluid phase at density ρ_c and a condensate, as explained in the previous section. The dynamics and time scaling of this condensation have been studied heuristically in [37]. For a large but finite system, the location of the condensate changes on a slow timescale and converges to a random walk on the lattice in the limit of diverging density [80, 81]. Recent extensions include a non-equilibrium version [82, 83] and models with size-dependent transition rates [84]. The zero range process so far has been the most studied model in the family of interacting particle systems without restrictions on local occupation numbers, and provides inspiring ideas to work on other models including the inclusion process. It is also well known that the zero range process can be mapped to simple exclusion process if sites are considered as particles and masses as hole clusters (see, e.g., [6, 85]). In this thesis we do not study the zero range process directly, but only extract ideas from the relevant work and extend them to the inclusion process, and in some cases compare these two models. In this section we give basic definitions and properties of the zero-range process. For further details see [4, 73].

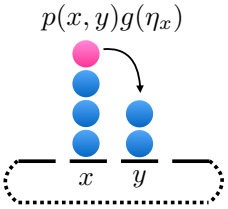

Figure 2.1: Illustration of the dynamics of zero-range process. Particles perform random walks with rate $p(x,y)g(\eta_x)$, which is independent of particles on target site y.

Definitions

The local state space of zero-range process is $E = \mathbb{N}$, and we focus on finite translation invariant lattices with periodic boundary conditions. Denote the one-dimensional torus by $\mathbb{T}_n = \mathbb{Z}/n\mathbb{Z} = \{1, 2, 3, ..., n\}$. We consider zero-range processes defined on $\hat{d}$-dimensional torus, $\Lambda_L = (\mathbb{T}_n)^{\hat{d}}$, of $L = n^{\hat{d}}$ sites. In one-dimensional case this is $\Lambda_L = \{1, 2, 3, ..., L\}$ with periodic boundary conditions. The state space is then

$$X_L = \{\boldsymbol{\eta} = (\eta_x)_{x\in\Lambda_L} \,:\, \eta_x \in \mathbb{N}\} = \mathbb{N}^{\Lambda_L},$$

where $\boldsymbol{\eta}$ is the full configuration and η_x is the local configuration on site x.

Particles on the lattice jump to other sites with rates depending only on the number of particles residing on departure sites (zero-range). This is a sharp contrast to the inclusion process and macroscopically makes a significant difference to the system's behaviour. The dynamics is described by the generator acting on bounded test functions $f \in C^b(X)$, choosing $u(n) = g(n)$ and $v(n) \equiv 1$ as given in (2.11)

$$\mathcal{L}_L f(\boldsymbol{\eta}) = \sum_{x,y\in\Lambda} p(x,y)g(\eta_x)\left(f(\boldsymbol{\eta}^{x,y}) - f(\boldsymbol{\eta})\right), \tag{2.23}$$

where $p(x,y) \geq 0$ are transition rates of an arbitrary, irreducible random walk on Λ_L. In this thesis we restrict jumps to be spatially homogeneous,

$$p(x,y) = q(y-x), \quad \text{for all } x, y \in \Lambda_L, \tag{2.24}$$

and $q(x)$ is further assumed to be normalised and of finite range,

$$\sum_{x\in\Lambda_L} q(x) = 1 \quad \text{and} \quad q(z) = 0 \text{ if } |z| > B, \text{ for some } B > 0, \tag{2.25}$$

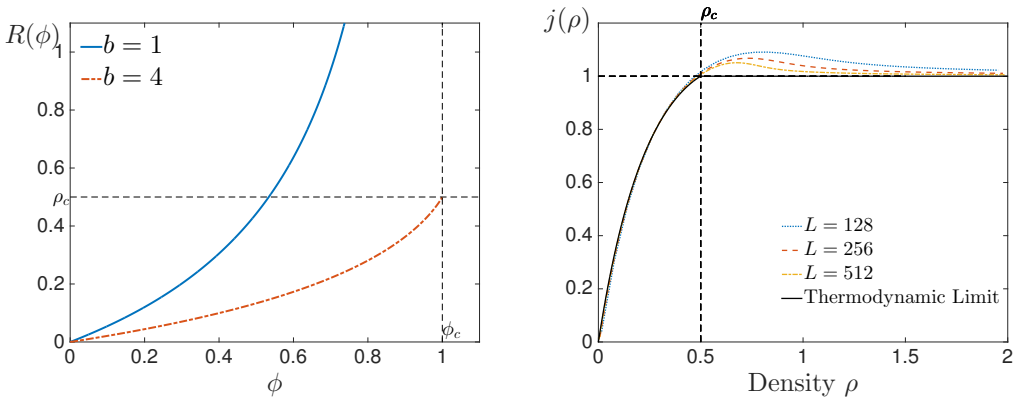

(a) (b)

Figure 2.2: Density and fundamental diagram of zero-range process (2.23) with $g(n)$ given in (2.26). (a): Density $R(\phi)$ (2.15) with $\gamma = 1$, $b = 1$ and $\gamma = 1$, $b = 4$. For $b = 4$, $\rho_c = 1/(b-2) = 1/2$ and $\phi_c = 1$. (b): Fundamental diagram. The canonical current with $\gamma = 1$ and $b = 4$ for various (finite) systems are plotted (see Algorithms in Appendix C). The black line is the thermodynamic current as a function of the system density ρ, given by the inverse of function $R(\phi)$ for $\rho \leq \rho_c$ and by $v_{\phi_c}(g) = 1$ for $\rho > \rho_c$ using Theorem 2.4.

where B is a bound independent of L. The jump rates $g(\eta_x)$ are assumed to be strictly positive on positive integers and have bounded variation,

$$\sup_{k\in\mathbb{N}} |g(k+1) - g(k)| < \infty \quad \text{and} \quad g(k) = 0 \Leftrightarrow k = 0.$$

The process can also be defined on infinite lattices under certain constraints, see [46, 86] for details.

Stationary measure

As discussed in previous section, the stationary product measures of zero-range processes are given by (2.12), where the weights can be specified as

$$w(n) = \prod_{k=1}^{n} g(k)^{-1}\,,\ n > 0.$$

Since $v \equiv 1$ in this model, the grand canonical current (2.21) can be written as $j_{gc} = \phi$. Recall the average particle density (2.15) can be computed as $R(\phi) = \phi\partial_\phi \log z(\phi)$. So $j_{gc}(\rho)$ in the zero-range process is then simply given by the inverse

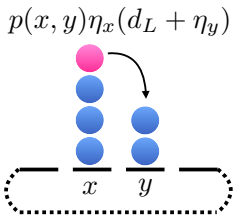

Figure 2.3: Illustration of the dynamics of one-dimensional inclusion process. Particles perform independent random walks with rate $p(x,y)d_L$ and attract each other with rate $p(x,y)\eta_x\eta_y$, which is called the inclusion part of the dynamics.

of $R(\phi)$. A standard example of zero-range process is given by

$$g(n) = 1 + \frac{b}{n^\gamma}, \quad \text{for all } n \geq 1, \quad \text{and } g(0) = 0, \tag{2.26}$$

which was first studied in [9]. Condensation as defined in Section 2.2 occurs for $\gamma \in (0,1)$, $b > 0$ or $\gamma = 1$ and $b > 2$, and the weights show a stretched exponential or power law decay, respectively (see [9, 12] for more details). Rigorous results on this transition have been published in a series of papers [12, 26, 54, 55, 56], and heuristic results on the dynamics have also been obtained in the areas like equilibration and coarsening [10, 12] and stationary dynamics of the condensate [37]. Figure 2.2 illustrates the density $R(\phi)$ (2.15) and the fundamental diagram of the zero-range process with (2.26) with numerics and the thermodynamic limit. In Figure 2.2(b) we observe that the canonical currents are converging to $j_{gc}(\rho)$, a consequence of weak convergence in Theorem 2.4.

2.3.2 Inclusion process

The inclusion process is a continuous-time stochastic particle system where particles perform independent random walks on a lattice and, in addition, interact via an attractive inclusion mechanism. The rates of the latter are proportional to the product of occupation numbers of departure and arrival sites. The process was first introduced in [15] as a dual of a model of heat conduction and has been further developed as a bosonic counterpart of the exclusion process in [16]. It has been shown that the system can exhibit a condensation transition in the limit of vanishing diffusion parameter d, which encodes the rates of independent motion of the

particles. The strong inclusion interaction leads to typical stationary configurations where a single lattice site contains almost all the particles in the system. This has been established rigorously on finite lattices in [74] and in the thermodynamic limit in [87]. Besides applications to energy transport [65], the inclusion process can also be interpreted as a multi-allele version of the Moran model [17], and condensation corresponds to fixation of a particular species in the limit of vanishing mutation rate, which is effectively given by the parameter d. There is also a different model [88, 89] that has been named inclusion process, where whole clusters of particles can jump simultaneously as opposed to the process studied in this thesis.

Definition

The inclusion process $(\boldsymbol{\eta}(t) : t \geq 0)$ is a lattice gas model defined on a $\hat{d}$-dimensional torus $\Lambda_L = (\mathbb{T}_n)^{\hat{d}}$, of $L = n^{\hat{d}}$ sites. The dynamics are defined by the generator acting on bounded test functions $f \in C^b(X_L)$, choosing $u(n) = n$, $v(n) = d_L + n$ as given in (2.11)

$$\mathcal{L}_L f(\boldsymbol{\eta}) = \sum_{x,y \in \Lambda_L} p(x,y)\eta_x(d_L + \eta_y)(f(\boldsymbol{\eta}^{x,y}) - f(\boldsymbol{\eta}))\,. \tag{2.27}$$

The parameter d_L scales with the system size, and determines the relative rate of the independent random walk of particles in comparison to the interacting inclusion part given by the product $\eta_x\eta_y$. The $p(x,y) \geq 0$ are transition rates of an arbitrary, irreducible random walk on Λ_L, with the same assumptions of spatial homogeneity (2.24), normalisation and finite range (2.25) as in the zero-range process. We focus on three types of nearest-neighbour dynamics (taking one-dimensional models as examples) :

(i) Symmetric (SIP): $p(x,y) = \frac{1}{2}(\delta_{y,x+1} + \delta_{y,x-1})$.

(ii) Partially Asymmetric (PASIP): $p(x,y) = p\delta_{y,x+1} + q\delta_{y,x-1}$, $p, q \in (0,1)$, $p+q = 1$.

(iii) Totally Asymmetric (TASIP): $p(x,y) = \delta_{y,x+1}$.

Details of inclusion processes on more general lattices including open boundaries can be found in [16, 65, 74, 90].

Stationary measure

Stationary product measures for the SIP were identified in [15, 65] and extended in [42, 74] to more general spatial rates $p(x,y)$, including the totally asymmetric case.

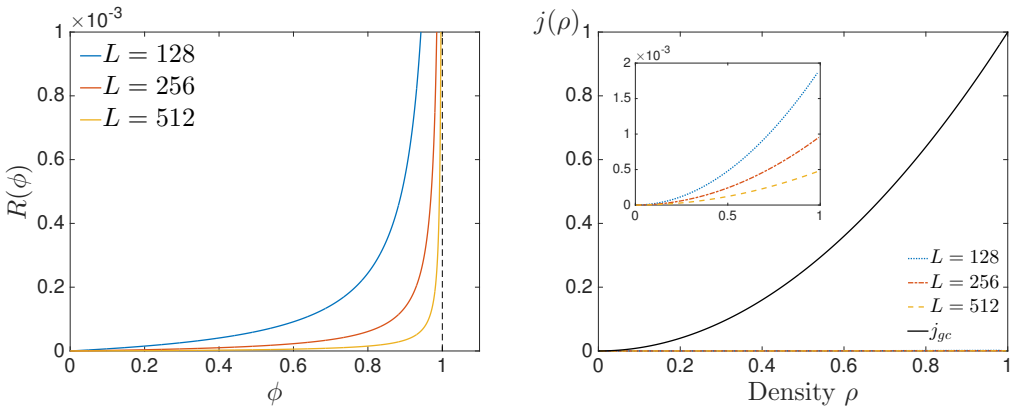

(a) (b)

Figure 2.4: Density and fundamental diagram of totally asymmetric inclusion process (2.27) with $d_L = 1/L^2$. (a): Density $R(\phi)$ (2.30) in systems of different sizes. (b): Fundamental diagram. The black curve is the grand canonical current (2.31), and other (dashed) curves are canonical current for finite systems from canonical recursion (see algorithms in Appendix C.1), coinciding with the prediction $j_{\Lambda,N} \simeq \rho^2 d_L L \to 0$ (2.34).

Since we focus on translation invariant systems, we have homogeneous product measures of the form (2.12) with stationary weights of the form

$$w(n) = \frac{\Gamma(d_L + n)}{n!\Gamma(d_L)}\,, \tag{2.28}$$

where Γ denotes the gamma function, and the single-site partition function is of the form

$$z(\phi) = \sum_{k=0}^{\infty} w(k)\phi^k = (1-\phi)^{-d_L}\,. \tag{2.29}$$

Since the partition function diverges as $\phi \nearrow 1$, the measures exist for all $\phi \in [0, 1)$ and constitute the grand canonical ensemble [42, 74]. The average particle density is given by

$$R(\phi) = \phi\partial_\phi \log z(\phi) = \frac{d_L\phi}{1-\phi}\,. \tag{2.30}$$

The grand canonical current is

$$j_{\mathrm{gc}}(\phi) = \mathbb{E}_\phi[\eta_x(d_L + \eta_{x+1})] = R(\phi)(R(\phi) + d_L)\,, \tag{2.31}$$

depending only on the particle density and d_L, and converges to ρ^2 for $d_L \to 0$.

2.3.3 Condensation in inclusion processes

In [87] it has been shown that to observe condensation in the inclusion process, the diffusion parameter d_L has to decay with the system size fast enough such that $d_L \ll 1/L$, and in the condensed regime all particles will concentrate on a single site. For L-independent d_L or not weak enough diffusion ($1/L \ll d_L \ll 1$), there is no condensation in the system. Therefore, in the rest of this thesis we always consider the following parameter-dependent thermodynamic limit for inclusion processes:

$$L, N \to \infty \ , \ d_L \to 0 \quad \text{such that} \quad \frac{N}{L} \to \rho > 0, \quad \text{and} \quad d_L L \to 0, \tag{2.32}$$

where we scale $d_L = L^{-\gamma}$ with $\gamma > 1$. Under the condition of $d_L \to 0$, the critical density (2.30) implies that the grand canonical ensemble degenerates as $L \to \infty$, $R(\phi) \to 0$, for all $\phi \in D_\phi$. And therefore the critical density $\rho_c = 0$ and the weak convergence of the grand canonical measures to the canonical measures stated in Theorem 2.4 is valid only for bounded local sets. Figure 2.4(b) shows that the canonical current does not converge to the grand canonical current for $\rho > 0$. The grand canonical current $j_{gc} = \rho^2$ is given by (2.31), and there is no closed form of the canonical current but we can use direct computations to calculate it (see detailed algorithms in Appendix C.1). In the condensed regime, the condensate contains all particles and can be localised on any site of the lattice. Therefore, the partition function $Z_{L,N}$ (cf.(2.19)) has a simple form as we have L equivalent states in total:

$$Z_{L,N} = L \prod_{i=1}^{L} w(\eta_i) = L w(N) = L d_L \prod_{i=2}^{N} \frac{d_L + i - 1}{i} \simeq \frac{L d_L}{N},$$

where we used the recursion property of weight $w(n) = \frac{d+n-1}{n} w(n-1)$ from (2.28) and $w(0) = 1$. With $d_L = L^{-\gamma}$, we can consider the following limit as

$$\frac{\log Z_{L,N}}{\log L} \simeq \frac{\log L + \log d_L - \log N}{\log L} \xrightarrow{L\to\infty} -\gamma, \quad \text{for } \rho > 0\,. \tag{2.33}$$

And for $\rho = 0$ the limit depends on the scaling of N with L, for example if $N = 0$ we have $Z_{L,N} = w(0)^L = 1$ and $\frac{\log Z_{L,N}}{\log L} \to 0$. The above divergence of grand canonical measures and canonical measures in the inclusion process has been studied rigorously in [87] through the non-equivalence of ensembles in this model. Indeed, (2.33) is the same as the result shown in [87, Proposition 6.3], where the above limit is called the canonical entropy density. Then one can compare it with the grand canonical

entropy density [4] , which is 0 for any $\rho > 0$ in the condensed regime, to prove the non-equivalence of ensembles. In [87], the authors also studied the case of fixed diffusion rate $d_L = d$ or weak diffusion but with$1/L \ll d_L \ll 1$ in IP. However, since in that case there will not be any condensation in the system and we focus more on the dynamics of the condensation throughout this thesis, we always study the thermodynamic limit (2.32) with $d_L \ll 1/L$ in the following chapters. In the next chapter, we will show that in the TASIP in the stationary regime, the jumps of an isolated condensate containing all the particles will dominate the stationary current (see Section 3.4.1 for details), and therefore we predict

$$j_{\Lambda,N} \simeq N d_L \frac{N}{L} \simeq \rho^2 d_L L \to 0 \quad \text{as } L \to \infty \text{ and } \frac{N}{L} \to \rho, \tag{2.34}$$

where Nd_L is the rate for a cluster to jump, this contributes N/L to the current. Above prediction is confirmed by numerical results shown in Figure 2.4(b).

[4] The grand canonical entropy density is defined as the Legendre-Fenchel transform of the grand canonical pressure (see, e.g., [91])

Chapter 3

Dynamics of Condensation in the Totally Asymmetric Inclusion Process

3.1 Introduction

In this chapter we investigate the dynamics of condensation in the totally asymmetric inclusion processes on a one-dimensional periodic lattice in the thermodynamic limit. Our main focus is on totally asymmetric dynamics which have not been studied before, and which we also compare to exact solutions for symmetric systems. We identify all relevant dynamical regimes and corresponding time scales as a function of the system size, including a coarsening regime where clusters move on the lattice and exchange particles, leading to a growing average cluster size. The second moment of occupation numbers is a suitable observable to characterise the transition, and exhibits a power law scaling in this regime, before saturation to stationarity following an exponential decay depending on the system size. Our results in this chapter are based on heuristic derivations for asymmetric systems and exact computations for symmetric systems, and are supported by detailed simulation data.

For the symmetric inclusion process, the dynamics of the condensate formation and subsequent motion have been studied rigorously in [41] in the limit of infinitely many particles on a fixed, finite lattice. In this chapter we extend these results in a non-rigorous way to spatially homogeneous, totally asymmetric systems in the thermodynamic limit, i.e. diverging lattice size with a finite particle density. For simplicity, we focus on the totally asymmetric system in one dimension with periodic boundary conditions, and also discuss some aspects of symmetric systems for comparison. We identify and describe in detail various regimes of the conden-

sation dynamics, including most importantly a coarsening regime where particle clusters move and exchange particles, following a power law scaling. We also describe the exponential approach to stationarity in the saturation regime, and the initial nucleation dynamics where isolated particle clusters form on a fast time scale.

The coarsening behaviour in condensing systems has already been studied heuristically in [11] and subsequent work for zero-range processes [9, 10, 12, 13, 37] and related models [38, 39, 40]. A rigorous description of the coarsening dynamics has also been studied recently in [92]. In contrast to zero-range models, in the inclusion process and related models condensates are mobile on the coarsening time scale and coarsening is in fact driven by condensate motion and interaction [31, 32, 41, 42]. Further developments in this direction include explosive condensation in a totally asymmetric model [31, 32] which exhibits a slinky motion of the condensate, also observed recently in [35] for non-Markovian zero-range dynamics. In this chapter we are able to give a detailed picture of this phenomenon in the totally asymmetric inclusion process by studying the interaction of two clusters. Further recent results on non-condensing inclusion processes include a hydrodynamic scaling limit for the symmetric system making use of self-duality of the model [93], which is not available for the totally asymmetric model we consider in this chapter and will be discussed later in Chapter 6.

3.2 Condensation and dynamical regimes

Recall the dynamics of the inclusion processes are defined by the generator acting on bounded test functions $f : X_L \to \mathbb{R}$,

$$\mathcal{L}_L f(\boldsymbol{\eta}) = \sum_{x,y\in\Lambda_L} p(x,y)\eta_x(d_L+\eta_y)(f(\boldsymbol{\eta}^{x,y}) - f(\boldsymbol{\eta}))\,. \qquad \text{(2.27 revisited)}$$

In this chapter we focus on TASIP and SIP on one-dimensional lattices as introduced in Section 2.3.2:

$$p(x,y) = \frac{1}{2}(\delta_{y,x+1} + \delta_{y,x-1}) \qquad \text{(SIP)}$$
$$p(x,y) = \delta_{y,x+1} \qquad \text{(TASIP)} \quad .$$

3.2.1 Condensation

For fixed L and d_L the range of densities is $R([0,1)) = [0,\infty)$ and the process does not exhibit condensation in the usual sense of zero-range processes [9, 12] or related

models [42], where this range is bounded. But it has been established in [74, 87] that in the thermodynamic limit (2.32) with vanishing diffusion rate

$$L, N \to \infty\,,\ d_L \to 0 \quad \text{such that} \quad \frac{N}{L} \to \rho > 0 \quad \text{and} \quad d_L L \to 0\ ,$$

the system exhibits complete condensation. In this case,

$$\max_{x\in\Lambda} \eta_x/N \to 1 \quad \text{in distribution } \pi_{L,N}\ , \tag{3.1}$$

so if the diffusion rate scales as $d_L \ll 1/L$ almost all particles in the system condense on a single site. Furthermore, in [87] stationary large deviations for the maximum occupation number are computed in the limit (2.32), and for condensing systems the most likely value for the maximum scales as the total number of particles N in the system. We will assume $d_L \ll 1/L$ for the rest of the chapter and for all simulation results presented we use $d_L = \frac{1}{L^2}$, but have checked the validity also for other scalings of d_L.

In contrast to zero-range processes, the condensate and large clusters move on the same time scale as the system approaches stationarity. The motion and interaction of clusters dominates the coarsening process, as will be explained in detail in the following. This has been established rigorously in [41] for the simpler setting of symmetric systems on fixed lattices. This mechanism is very similar to recent results in [31, 32] on explosive condensation, where the jump rates are essentially $\eta_x^\gamma(\epsilon + \eta_y)^\gamma$ with fixed $\epsilon > 0$ and $\gamma > 2$. In this case domination of attractive effects and condensation is caused by the non-linearity in the rates. For the inclusion process it is the scaling $d_L \to 0$ that causes domination of the attractive interaction.

To describe the dynamics of condensation we consider the second moment

$$\sigma^2(t) = \mathbb{E}\left[\eta_x^2(t)\right] \quad \text{for some } x \in \Lambda_L\ , \tag{2.4 revisited}$$

which does not depend on x since we will assume the initial distribution to be translation invariant. This is the simplest observable that captures the temporal evolution of the condensed phase, since the first moment is constant in time due to conservation of the number of particles. Due to spatial homogeneity, in simulations we measure $\sigma^2(t)$ by spatial average $\left\langle 1/L \sum_{x=1}^{L} \eta_x^2 \right\rangle$ to have better statistics, where $\langle\cdot\rangle$ denotes averaging over a large number (typically 200 in our simulations) of realisations.

We consider canonical initial conditions where N particles are placed uni-

formly and independently on the lattice, which leads to $\boldsymbol{\eta}(0)$ having a symmetric multinomial distribution with N trials and success probability $1/L$. For $L \to \infty$ and $N/L \to \rho$ the occupation numbers are asymptotically independent Poisson random variables $\eta_x(0) \sim \mathrm{Poi}(\rho)$, and have second moment $\sigma^2(0) = \rho(1+\rho)$. Furthermore, in stationarity as $t \to \infty$ we know that up to fluctuations all particles condense on a single site, and we expect $\sigma_L^2(t) \simeq \frac{1}{L}(\rho L)^2 = \rho^2 L$. So we consider the rescaled variable $\sigma_L^2(t)/\rho^2 L$, which increases from very small values of order $1/L$ to 1 during the formation of the condensate from homogeneous initial conditions. This process can be divided into four different regimes (see Figure 3.1):

(I). **Nucleation Regime**: Due to the inclusion rate $\eta_x\eta_y$, neighbouring pairs of sites exchange particles with order 1 rates until the process reaches a state where all occupied sites are separated by at least one empty site. This happens simultaneously everywhere on the lattice and takes at most of order $\log L$ time. After this regime, a fraction of at most $1/2$ of all sites is occupied and particles can only jump to another site by the diffusion part of the dynamics with slow rate d_L. Details can be found in Section 3.3.

(II). **Coarsening Regime**: Particle clusters formed in regime (I) can move to empty neighbouring sites or exchange particles at rate $\eta_x d_L$, but typically do not split on this timescale. This drives a coarsening process with a decreasing number of clusters of increasing size, which grow to large clusters of order N size. This coarsening process happens on a characteristic time scale $1/d_L$, as explained in detail in Section 3.5. As expected, $\sigma^2(t)$ follows an approximate power law in this regime.

(III). **Saturation Regime**: The coarsening scaling law no longer holds since the system reaches its finite size limit, and the remaining clusters merge to form a single condensate. As expected close to stationarity, the observable $\sigma^2(t)$ converges exponentially to its stationary value, as explained in detail in Section 3.5.2. The characteristic time scale for this regime is up to constant factors the relaxation time of the system, and turns out to be of order $\tau_L = L/d_L$ for the TASIP and L^2/d_L for the SIP (see Section 3.4.3).

(IV). **Stationary Regime**: Once there is only a single condensate left on the lattice, it continues to move according to the same rules and time scales as in regimes II and III. The observable σ^2 does not detect this motion, but it

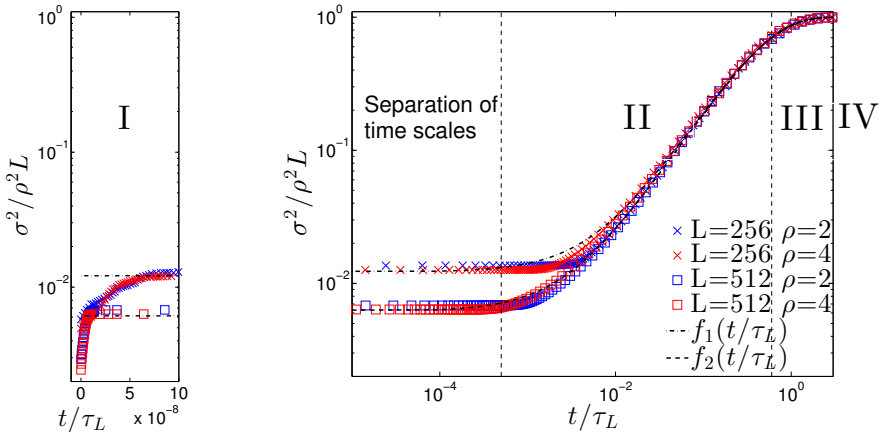

Figure 3.1: Illustration of different dynamical regimes in the TASIP. The rescaled observable $\sigma^2(t)/\rho^2 L$ (2.4) is shown against rescaled time t/τ_L with $\tau_L = L/d_L$ (cf. (3.28)) and $d_L = 1/L^2$. f_1 and f_2 are exponential functions (cf. (3.35)) describing the long-term asymptotic behaviour, with initial values $\sigma^2(0)$ fitted to data for $L = 256, \rho = 4$ and $L = 512, \rho = 4$, respectively. $\sigma^2(0)$ is calculated at the end of the fast nucleation process explained in Section 3.3. Data points are averaged over 200 realisations, errors are bounded by the size of the symbols.

can be studied by defining the location of the maximum occupation number as relevant observable as has been done on fixed lattices in [41], or in [80] for zero-range processes.

In Figure 3.1 we illustrate the condensation dynamics on the total relaxation time scale τ_L. Details of the time scale will be discussed in Section 3.4.3. As the nucleation regime occurs on a time scale of at most $\log L$, it finishes immediately on the time scale of the other regimes and just determines the initial condition for the coarsening regime. Note that the exponential approximation for the saturation regime also fits the data in the coarsening regime very well. This is a peculiarity due to the linear coarsening law for the TASIP as explained in Section 3.5, and does not hold for the SIP or in general.

3.3 Nucleation regime

The nucleation regime starts with the initial distribution of particles, which we take to be a uniform multinomial for simplicity. It ends when no particles reside on

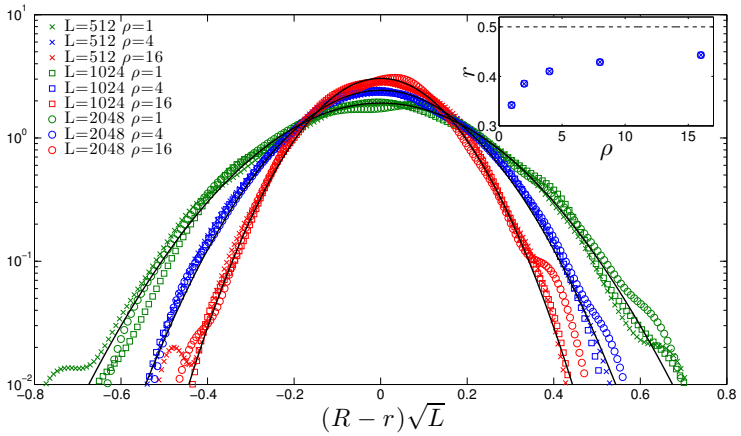

Figure 3.2: Distributions of the ratio of occupied sites $\mathcal{R}$ (3.3) (centred and scaled by $\sqrt{L}$) for TASIP. Black curves are probability density functions of Gaussians with mean 0 and standard deviations from data sets $L = 2048$ and corresponding ρ. The inset shows r for systems with size $L = 512, 1024, 2048$ and density $\rho = 1, 2, 4, 8, 16$. Data collapse confirms that r depends only on ρ, and has an upper bound 0.5 ($\rho \to \infty$). Distribution functions from data (2000 realisations) are a kernel density estimate computed by `ksdensity` with Matlab.

successive sites which can be defined by the hitting time

$$T := \inf \left\{ t \geq 0 : \sum_{x \in \Lambda_L} \eta_x(t)\eta_{x+1}(t) = 0 \right\} . \tag{3.2}$$

We denote the (random) fraction of occupied sites at the end of the nucleation regime at time T by

$$\mathcal{R} := \frac{1}{L} \sum_{x \in \Lambda_L} \mathbb{I}\{\eta_x(T) > 0\} , \quad \text{and its expectation by } r = \mathbb{E}[\mathcal{R}] . \tag{3.3}$$

Under our condition of weak diffusion $d_L \ll 1/L$, the inclusion effect completely dominates this regime and the time scale $\mathbb{E}[T]$ turns out to scale as $\log L$, which is much faster compared to all other regimes. The specific details of the scaling are therefore not relevant, a simple argument using a toy model can be found in the following section, we will then take two different approaches for the TASIP and the SIP, starting with the simpler symmetric case.

3.3.1 Toy model for the nucleation regime

We define a toy model for the number of occupied sites after the nucleation regime of the TASIP on the lattice $\Lambda_L = \{1, 2, 3, ..., L\}$ with periodic boundary conditions, where the modified state variable $\eta_x \in \{0, 1\}$ simply indicates whether site x is occupied. We consider the simplest uniform initial distribution $\eta_x(0) = 1$ for all $x \in \Lambda_L$. After waiting time T_x, the mass on site x tries to jump to site $x + 1$, where T_x are i.i.d. random variables. This jump is successful only if $\eta_{x+1}(T_x) = 1$, i.e. the mass on site $x + 1$ has not moved before, and after the jump we have $\eta_x = 0$ and $\eta_{x+1} = 1$. This is a simplified model of the inclusion interaction of the process in the nucleation regime, and keeps track only of occupied sites. The T_x can be interpreted as the random times when the full mass in the true TASIP has moved from site x to $x + 1$. The distribution of those times is not important for our argument, we only assume that they are independent, and their order therefore corresponds to a uniform permutation.

After some time all particles reside on non-successive sites and the toy model reaches an absorbing state. Such absorbing configurations are constructed of blocks of different lengths, where one block consists of empty sites and only one occupied site on the rightmost site of the block. In other words, the blocks are of the form $000 \ldots 001$. We denote the length of such a block (indexed by n) by $Y_n \in \mathbb{N}$, where $2 \leq Y_n \leq L$ and $\sum_n Y_n = L$. Assume that the occupied site of one such block is site z, then $\eta_{z-1} = \eta_{z-2} = ... = \eta_{z-k} = 0$ where $k + 1$ is the size of the block. The event $Y_n \geq k + 1$, i.e. the n-th block size is at least $k + 1$, is equivalent to the event

$$T_{z-k} < T_{z-k+1} < \ldots < T_{z-1} \ , \tag{3.4}$$

since each initial particle must have jumped before its right neighbour, so that all the mass on these sites moves up to site z. Since the times $\{T_x, \ x \in \Lambda\}$ are given by a uniform permutation, the probability for (3.4) determines

$$\mathbb{P}(Y_n - 1 \geq k) = \frac{1}{k!} \, .$$

We therefore get the following limiting behaviour for the expectation,

$$\mathbb{E}[Y_n] = \sum_{k=1}^{L-1} \frac{1}{k!} + 1 \to e \ , \ \text{ as } \ L \to \infty \ .$$

Note that the lengths of successive clusters are independent, so that the $(Y_n : n \geq 0)$

constitute a renewal process on Λ_L, and

$$n_L := \max\left\{ n \ : \ \sum_{i=1}^{n} Y_i \leq L \right\}$$

is the number of blocks in the absorbing state, which is equal to the number of remaining particles. From the standard renewal theorem (see, e.g., Chapter 10.2 in [94]) we get

$$\frac{n_L}{L} \to \frac{1}{\mu} \quad \text{as } L \to \infty \text{ almost surely } ,$$

where $\mu = \mathbb{E}[Y_1] = e$ is the expected block length. Therefore, we have an approximation of the ratio of occupied sites (3.3)

$$r \approx 1/e = 0.368 \ .$$

This is very close to the observed value in Section 3.3 for small densities $\rho \approx 1$, where we expect the toy model to give the best approximation. For very low densities r is dominated by the initial number of empty sites, whereas for high densities correlations build up over long distances leading to striped patterns, and r seems to grow slowly towards its maximal value 1/2 as $\rho \to \infty$.

With the above approach, the time scale for the nucleation regime can be approximated by the maximum of the order of L i.i.d random variables T_x. There is no evidence that the distribution of the T_x has heavy tails, which leads to a typical scaling of the maximum of order $\log(L)$. This is a good agreement with the nucleation time scaling which is also supported by unshown numerical results.

Striped patterns and ratio of occupied sites in the nucleation regime

The analysis of the toy model suggests that a striped pattern of the configuration is formed by the end of the nucleation regime. Indeed, we observe striped patterns emerging even before the first vacant site appears. The pattern is essentially caused by the inclusion interaction, and we can roughly understand it as follows. Assume $\eta_x = \rho$, $\forall x \in \Lambda_L$ at $t = 0$. Assume η_x loses some particles to η_{x+1}. This leads to $\eta_{x-2}\eta_{x-1} > \eta_x\eta_{x-1}$, which makes η_{x-1} more likely to gain particles from η_{x-2} than to lose particles to η_x, and thus a striped pattern is formed. The configurations of absorbing states are constructed by pieces of striped patterns in the shape '..$0\eta_x 0\eta_{x+2}0\eta_{x+4}$...' connected by a few empty sites. If we denote the length of such patterns by Z_k and the number of empty sites connecting them by M, then the

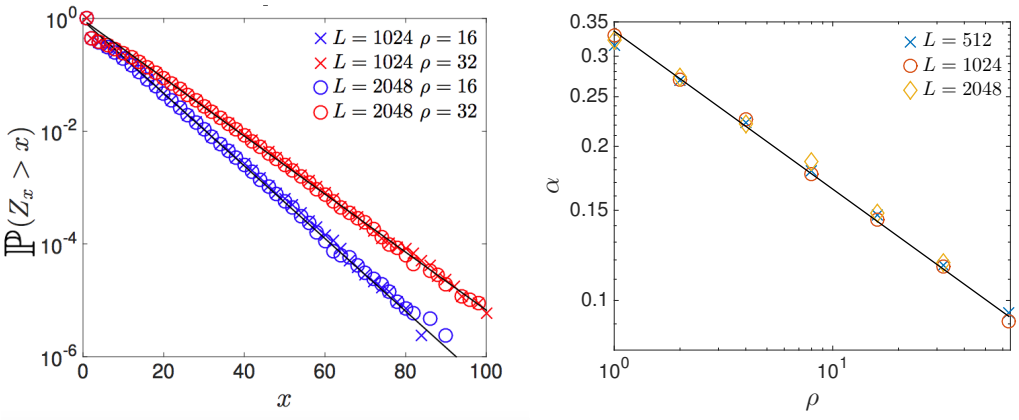

(a) (b)

Figure 3.3: Exponential behaviour of the length of striped patterns (3.5).(a): Empirical tail distribution (complementary cumulative distribution function) of Z_k with different system sizes and densities. The full lines are exponential function $f(x) = \exp(-\alpha x)$ with fitted rate parameters $\alpha = 0.1484$ for $\rho = 16$ and $\alpha = 0.1168$ for $\rho = 32$. (b): Power-law behaviour of the exponential rate parameter α against density ρ, where α fitted from unshown data with multiple system sizes and densities. The full line is fitted power-law function $\alpha = 0.3357\rho^{-0.3805}$, support out estimation $\alpha \sim \rho^{-1/3}$ in (3.6). Results are averaged over 2000 realisations and errors are bounded by the size of symbols.

fraction of the occupied sites at the end of the nucleation regime $\mathcal{R}$ (3.3) is given by

$$\mathcal{R} = \frac{1}{2}\frac{\sum_{k=1}^{n} Z_k}{L} \quad \text{and} \quad L = \sum_{k=1}^{n} Z_k + M. \tag{3.5}$$

Numerical results shown in Figure 3.3 strongly suggest that Z_k has an exponential distribution with the rate parameter depends only on density ρ, i.e.,

$$Z_k \sim \exp\left(f(\rho)\right) ,$$

where $f(\rho)$ is a function of density ρ and our numerical results suggest that it has a power-law form as $f(\rho) = C\rho^{\beta}$, where C is some positive constant and $\beta \approx -1/3$. Currently we do not have a very good argument of the rate parameter $f(\rho)$, which could be an interesting question for further investigation. But to understand the asymptotical behaviour of $\mathcal{R}$, it is enough to use the fact Z_k grows exponentially and approximately we have

$$\mathbb{E}[Z_k] \simeq \frac{1}{C}\rho^{\frac{1}{3}}. \tag{3.6}$$

Therefore, for high density Z_k converges to its upper bond L, which means the whole configuration is constructed by a single striped pattern with no extra empty sites. Then $M \to 0$ and $\mathcal{R} \to 1/2$, which agrees with previous numerical results of $\mathcal{R}$ in Figure 3.2.

3.3.2 Symmetric case

In the SIP we can derive closed equations for the dynamics of correlation functions due to the symmetry. We consider the nearest-neighbour product

$$c(1,t) := \mathbb{E}[\eta_x(t)\eta_{x+1}(t)] \quad \text{for some } x \in \Lambda_L\,, \tag{2.5 revisited}$$

since the observable $\eta_x\eta_{x+1}$ vanishes at the end of the nucleation regime. Similar to $\sigma^2(t)$, $c(1,t)$ is also x-independent due to translation invariance and in simulations we measure $c(1,t)$ by the spatial average $\left\langle 1/L \sum_{x=1}^{L} \eta_x\eta_{x+1} \right\rangle$ as described earlier. With our initial conditions we have $c(1,0) = \rho^2$ for large L, and $c(1,t) \to 0$ as $t \to \infty$. Applying the generator (2.27) to the test function $f(\boldsymbol{\eta}) = \eta_x\eta_{x+1}$ for some $x \in \Lambda_L$, we get

$$\begin{aligned}
\mathcal{L}(\eta_x\eta_{x+1}) &= \frac{1}{2}\eta_{x-1}(d_L+\eta_x)[(\eta_x+1)\eta_{x+1}-\eta_x\eta_{x+1}] \\
&+ \frac{1}{2}\eta_x(d_L+\eta_{x-1})[(\eta_x-1)\eta_{x+1}-\eta_x\eta_{x+1}] \\
&+ \frac{1}{2}\eta_x(d_L+\eta_{x+1})[(\eta_x-1)(\eta_{x+1}+1)-\eta_x\eta_{x+1}] \\
&+ \frac{1}{2}\eta_{x+1}(d_L+\eta_x)[(\eta_x+1)(\eta_{x+1}-1)-\eta_x\eta_{x+1}] \\
&+ \frac{1}{2}\eta_{x+1}(d_L+\eta_{x+2})[\eta_x(\eta_{x+1}-1)-\eta_x\eta_{x+1}] \\
&+ \frac{1}{2}\eta_{x+2}(d_L+\eta_{x+1})[\eta_x(\eta_{x+1}+1)-\eta_x\eta_{x+1}] \\
&= -\eta_x\eta_{x+1}+\frac{1}{2}d_L(-4\eta_x\eta_{x+1}+\eta_{x-1}\eta_{x+1}+\eta_x\eta_{x+2}+\eta_x^2+\eta_{x+1}^2-\eta_x-\eta_{x+1})\,.
\end{aligned}$$

In the nucleation regime all occupation numbers are of order 1, so the second term in the last line is of order d_L in expectation. Then by the standard evolution equation[1],

$$\frac{d}{dt}c(1,t) = \mathbb{E}[\mathcal{L}(\eta_x\eta_{x+1})] = -c(1,t) + \Theta(d_L)\,. \tag{3.7}$$

[1]Throughout this thesis we denote $f(n) = \Theta(n)$ as: $k_1 n < f(n) < k_2 n$, for some constants k_1, $k_2 > 0$ and n sufficiently large.

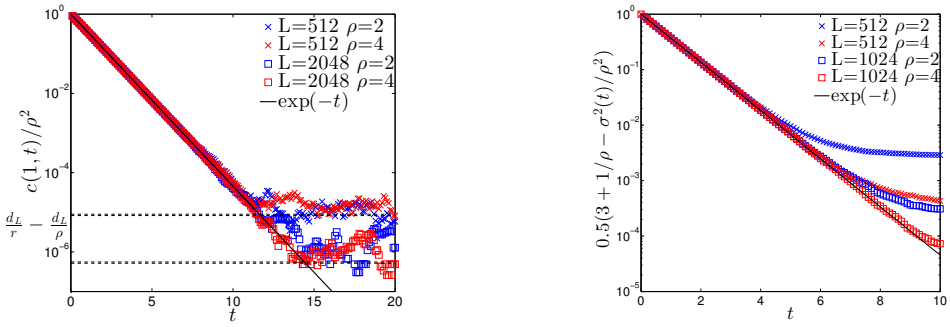

Figure 3.4: Exponential behaviour of $c(1,t)$ (2.5) and $\sigma^2(t)$ (2.4) for the SIP in the nucleation regime. (a) Exponential decay of $c(1,t)/\rho^2$ as given in (3.8). Dashed lines are fluctuation estimates $d_L/r - d_L/\rho$ for $L = 512, 1024$, where we used numerical values for the ratio r (3.3): $r|_{\rho=2} = 0.3747$ and $r|_{\rho=4} = 0.3865$. (b) Exponential convergence of $\sigma^2(t)/\rho^2$ as given in (3.14). The deviations for large time are determined by the finite size corrections in (3.12). Data points are averaged over 2000 realisations. Errors are of the order 10^{-4}.

For large systems, $d_L \ll 1/L$ is negligible, and we solve the above ODE with initial condition $c(1,0) = \rho^2$ to get

$$c(1,t) = \rho^2 e^{-t}\,. \tag{3.8}$$

Figure 3.4(a) shows a data collapse for $c(1,t)$ confirming this prediction. The large time plateau is dominated by attempted motion of clusters onto empty neighbouring sites with slow rate d_L. This motion leads to temporary nearest-neighbour occupation and produces finite size fluctuations of the asymptotic values of $c(1,t)$, which vanish with increasing system size. Their size can be estimated by considering the contribution to $c(1,t)$ during the step of a cluster as following. We consider a time $t_1 > \mathbb{E}[T]$ so that we expect to have reached the plateau in Figure 3.4(a). Then we can estimate $c(1,t_1)$ by the following ergodic average with duration T_{step}

$$c(1,t_1) \simeq \mathbb{E}\left[\int_{t_1}^{t_1+T_{step}} \eta_x(s)\eta_{x+1}(s)\,ds \middle| \eta_x(t_1) > 0\right] \frac{\mathbb{P}[\eta_x(t_1) > 0]}{\mathbb{E}[T_{\text{step}}]}\,, \tag{3.9}$$

where T_{step} is the random time duration for an attempted step of the cluster. It is not important if the cluster actually moves to site $y = x-1$ or $x+1$ or stays at x. As discussed in detail in Section 3.4.1, T_{step} is dominated by the slow rate to move the first particle, after which all remaining particles quickly follow due to the inclusion interaction, and we have $\mathbb{E}[T_{\text{step}}] \sim 1/(d_L m)$ where $m = \mathbb{E}[\eta_x(t_1)|\eta_x(t_1) > 0]$ is the size of a typical cluster. On the other hand, the integral in the numerator vanishes for most of the time, and the expected holding time in an intermediate state

$(\eta_x, \eta_{x+1}) = (k, m-k)$ for $k \in \{1, 2, ..., m-1\}$ is simply $\frac{1}{k(m-k)}$. The computation of $c(1, t_1)$ (3.9) reduces to a simple random walk problem as is described in Appendix B. We get

$$\mathbb{E}\left[\int_{t_1}^{t_1+T_{\text{step}}} \eta_x(s)\eta_{x+1}(s)\, ds \Big| \eta_x(t_1) > 0\right] = \mathbb{E}\left[\sum_{k=1}^{K_{\text{step}}} \frac{k(m-k)}{k(m-k)}\right] = m-1\ , \quad (3.10)$$

where we used that the expected number of steps K_{step} of an excursion starting with $(\eta_x, \eta_{x+1}) = (1, m-1)$ is $\mathbb{E}[K_{\text{step}}] = m-1$ (B.6). Recall the expected fraction of occupied sites at the end nucleation r (3.3). We have $\mathbb{P}[\eta_x(t_1) > 0] \simeq r$ and we get in (3.9)

$$c(1, t_1) \simeq r\frac{m-1}{1/(d_L m)} = rm(m-1)d_L = \rho^2 d_L\left(\frac{1}{r} - \frac{1}{\rho}\right) \quad (3.11)$$

using also $m = \rho/r$ for the average size of a cluster. This is confirmed by dashed lines in Figure 3.4(a). Note (3.11) only makes sense for $\rho > r$, but we are not interested in very small densities $\rho \leq r < 1$ where a large number of empty sites are already in the initial configuration and the nucleation dynamics we discussed above is heavily affected or destroyed .

To understand the evolution of the second moment $\sigma^2(t)$ (2.4) we take the test function $f(\boldsymbol{\eta}) = \eta_x^2$, for some $x \in \Lambda$. Similarly to the above computation we get

$$\mathcal{L}(\eta_x^2) = \eta_x\eta_{x+1} + \eta_{x-1}\eta_x + d_L\left(-2\eta_x^2 + \eta_x + \eta_x\eta_{x-1} + \eta_x\eta_{x+1} + \frac{1}{2}\eta_{x-1} + \frac{1}{2}\eta_{x+1}\right). \quad (3.12)$$

Again, the terms of order d_L are negligible for large L and in expectation

$$\frac{d}{dt}\sigma^2(t) = \mathbb{E}[\mathcal{L}(\eta_x^2(t))] = 2c(1, t) + \Theta(d_L)\,. \quad (3.13)$$

Integrating with initial condition $\sigma^2(0) = \rho(1+\rho)$ we get

$$\sigma^2(t) = 2\rho^2(1 - e^{-t}) + \rho^2 + \rho\ . \quad (3.14)$$

Note that this leading order behaviour is independent of L and converges to

$$\frac{\sigma^2(t)}{\rho^2} \to 3 + \frac{1}{\rho} = \sigma_0^2 \quad \text{as } t \to \infty\ . \quad (3.15)$$

This is the value of σ^2 after the nucleation regime on large systems and therefore gives the initial values σ_0^2 of coarsening regime up to finite size corrections as con-

firmed in Figure 3.6.

3.3.3 TASIP

The reason we could get closed equations for correlation functions in the previous section is related to self-duality of the SIP (see Chapter 6 for more details). Due to the asymmetry, the TASIP is not self-dual and therefore the above technique does not lead to closed equations for $c(1,t)$ or other observables. In this sub-section we will therefore focus mostly on simulations and approximations to understand the nucleation dynamics in the TASIP. Applying the TASIP generator to the test function $f(\boldsymbol{\eta}) = \eta_x\eta_{x+1}$ for some $x \in \Lambda_L$ we get analogously to the symmetric case

$$\begin{aligned}\mathcal{L}\left[\eta_x\eta_{x+1}\right] =&\eta_x\eta_{x+1}\left(-1+\eta_x-\eta_{x+1}+\eta_{x-1}-\eta_{x+2}\right)\\ &+d_L(\eta_{x-1}\eta_{x+1}-\eta_x\eta_{x+1}+\eta_x^2-\eta_x\eta_{x+1}-\eta_x)\\ =&\eta_x\eta_{x+1}(\eta_{x-1}-\eta_{x+2}+\eta_x-\eta_{x+1}-1)+\Theta(d_L)\,.\end{aligned}$$

Taking expectations and using translation invariance we get

$$\frac{d}{dt}c(1,t) = -c(1,t) + \mathbb{E}\left[\eta_x\eta_{x+1}(\eta_x-\eta_{x+1})\right]\,. \tag{3.16}$$

This equation involves higher order correlation functions, and simple mean-field type arguments trying to close it fail to give reasonable predictions. In the nucleation regime interactions between clusters are strong and complex, and correlations cannot be ignored. In fact, due to total asymmetry, given two neighbouring occupied sites the right one has higher occupation numbers on average and therefore the first order correction term in (3.16) is negative, which leads to a super-exponential decay. For small times, dominated by the initial conditions before correlations develop, the correction averages to zero, and we observe an exponential decay as illustrated in Figure 3.5. The bulk decay shows a significant density dependence, but is independent of the system size L for large enough systems. For large times, however, $c(1,t)/\rho^2$ converges to an L-dependent quasi-stationary value completely analogously to the symmetric case. Using the same arguments we get

$$c(1,t) \to \rho^2 d_L\left(\frac{1}{r}-\frac{1}{\rho}\right) \quad \text{for large } t\,, \tag{3.17}$$

as confirmed by dashed lines in Figure 3.5. Note that due to total asymmetry, the number of required particle moves for a cluster of m particles to hop one step on

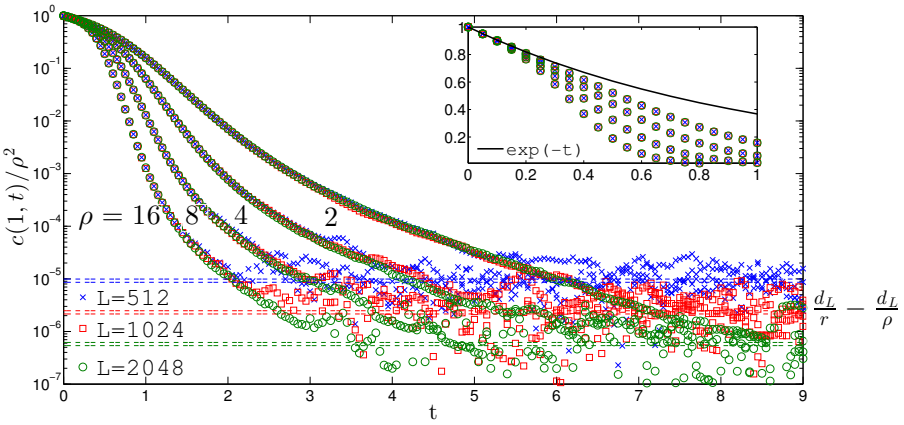

Figure 3.5: Super exponential decay of $c(1,t)$ for the TASIP in the nucleation regime. Dashed horizontal lines correspond to L-dependent corrections (cf (3.17)). For each system we give two lines by using the numerical maximal and minimal values of r and ρ, where $r_{max} = 0.4431$ for $\rho = 16$ and $r_{min} = 0.3850$ for $\rho = 2$. The inset shows the initial behaviour which is approximately exponential. Data points are averaged over 2000 realisations. Errors are bounded by the size of the symbols until we observe the L-dependent corrections.

the lattice is precisely $m - 1$, which simplifies the argument.

As is shown in Figure 3.2, the ratio $\mathcal{R}$ of occupied sites at the end of the nucleation regime follows a Gaussian distribution with density dependent fluctuations of order $1/\sqrt{L}$. The mean, r, monotonically increases with ρ from values around 0.35 for small densities $\rho \approx 1$. This can be consistently explained using the toy model of coalescing particles, as presented previously in Section 3.3.1. For large densities alternating occupied/empty patterns are observed with long correlation lengths, and in the limit $\rho \to \infty$ we expect the system to approach the maximal theoretical value $r = 0.5$. The inset in Figure 3.2 shows that this convergence is slow and is an interesting open question for further investigation. In this chapter we focus on other aspects of the dynamics, and will use the actual value of r as a fit parameter in the next sections.

3.4 Condensate motion and interaction

In this section we analyse the motion of an isolated macroscopic cluster which dominates the stationary dynamics of the model. We further study the interaction between condensates, which is the foundation of understanding the coarsening and

saturation dynamics as discussed in the next section.

3.4.1 Dynamics of isolated clusters

Totally asymmetric dynamics

Consider an isolated cluster of large size $m \gg 1$ on site x, and for simplicity on an otherwise empty lattice. The only possible transition is that a particle jumps to site $x+1$ with rate $d_L m$. Then the single particle could move to site $x+2$ at rate d_L, or the condensate could lose another particle which happens with much higher rate, $m-1$, due to the inclusion interaction. Thus, given that no particle exits to site $x+2$, the total time T^{step} for all particles to move to site $x+1$ is a sum of independent exponential variables with mean

$$\begin{aligned}\tau_m^{\text{step}} \simeq \mathbb{E}[T^{\text{step}}] &= \frac{1}{d_L m} + \sum_{k=1}^{m-1} \frac{1}{(m-k)k} \simeq \frac{1}{d_L m} + \frac{1}{m} \int_{1/m}^{(m-1)/m} \frac{1}{x(1-x)}\, dx \\ &\simeq \frac{1}{d_L m} + \frac{2}{m} \log(m)\,. \end{aligned} \tag{3.18}$$

Here we omitted terms involving d_L in the rates, which lead to sub-leading corrections. Due to the quadratic scaling of the inclusion interaction the process speeds up significantly after the first particle and the remaining time vanishes with respect to the time of the initial move. In particular T^{step} is dominated by the exponential time of the first particle, so to leading order $T^{\text{step}} \sim \exp(d_L m)$. The rate at which any particle escapes from site $x+1$ is bounded above by $d_L m \to 0$ with $L \to \infty$. Thus, in the limit a macroscopic cluster is stable and jumps to the right with vanishing rate $d_L m \to 0$ which is proportional to its size. In general, the time scale for motion of macroscopic clusters containing order L particles or the stationary single condensate is

$$\tau_L^{\text{move}} = \frac{1}{d_L L} \quad \text{(TASIP)}\,. \tag{3.19}$$

This is consistent with results in [87] on the vanishing stationary current, which is dominated by the motion of a single condensate as

$$j(\rho) \simeq d_L \rho^2 L^2 / L = \rho^2 d_L L\,. \tag{3.20}$$

Symmetric dynamics

For symmetric dynamics, a single cluster on an otherwise empty lattice is also stable, but performs a symmetric continuous-time random walk. Analogous to the above,

the first particle from site x moves with rate $d_L m$ to site $y = x - 1$ or $x + 1$. Then the inclusion interaction dominates the dynamics, and particles are exchanged symmetrically between sites x and y until one of them is again empty. We find

$$\mathbb{E}[T_{\text{step}}] \simeq \frac{1}{d_L m} + \Theta(1)\,, \tag{3.21}$$

since the expected number of steps is $m - 1$ (B.6) and the largest expected waiting time is $1/(m-1)$ (see Appendix B). So the step is again dominated by the motion of the first particle. The jump attempt of the cluster is only successful if all particles end up on the new site y rather than x, which happens with probability $1/m$ (B.3). So the cluster performs a symmetric random walk with effective rate d_L and the time scale for cluster motion is

$$\tau_L^{\text{move}} = \frac{1}{d_L} \quad (\text{SIP})\,. \tag{3.22}$$

3.4.2 Interaction of two clusters

Totally asymmetric dynamics

In the TASIP, we have seen above that the isolated clusters jump to the right with rates proportional to their sizes. Therefore, they move freely until a larger and faster cluster catches up with a smaller one. As soon as they are only one intermediate lattice site apart they start interchanging particles via a mechanism first observed in [32]. To describe this situation let $\eta_1 > \eta_3$ at time 0, both of order $m \gg 1$, and $\eta_2 = 0$ on the intermediate site. Then it is more likely that site 1 loses a particle to 2 rather than site 3 to 4 and the clusters start interacting. Notice, $d_L > 0$ is necessary for the first particle to move and the two clusters to get in contact and start interacting. From then on, the inclusion part of the rate $\eta_x \eta_y$ completely dominates the interaction and results in an effective symmetry. $d_L > 0$ only leads to higher order contributions and therefore does not affect the following argument. Ignoring jumps away from site 3, the only two events are jumps from site 1 to 2 or from site 2 to 3 with rates of order $\eta_1(t)\eta_2(t)$ and $\eta_2(t)\eta_3(t)$, respectively. Therefore, the probabilities for the next event to be a move from site 1 to 2 or site 2 to 3 are

$$\frac{\eta_1(t)}{\eta_1(t) + \eta_3(t)} \quad \text{and} \quad \frac{\eta_3(t)}{\eta_1(t) + \eta_3(t)}\,, \quad \text{respectively.} \tag{3.23}$$

The interaction process continues on the simplex $\Delta = \{\eta_1(t), \eta_3(t) \in \mathbb{N} \mid \eta_1(t) + \eta_3(t) \leq \eta_1(0) + \eta_3(0)\}$ following left-up paths due to total asymmetry, until the cluster on site 3 moves to site 4 which becomes more likely once $\eta_3(t) > \eta_1(t)$ and

$\eta_2(t) = 0$. Note that the result of the mass redistribution depends only on the discrete embedded chain with probabilities (3.23), which exhibit a symmetry under exchanging sites 1 and 3 with invariant diagonal $\eta_1 = \eta_3$. Since the whole process is invariant under time and space inversion, the statistics of all paths leading towards the diagonal for $\eta_1 > \eta_3$ is the same as that of all paths leading away. The cluster interaction is therefore symmetric, such that in distribution $\eta_1(T) \stackrel{dist}{=} \eta_3(0)$ and $\eta_3(T) \stackrel{dist}{=} \eta_1(0)$ where T is the time when the first particle moves from site 3 to 4 and the interaction terminates. So to leading order the clusters penetrate each other and just exchange places, and along the way exchange an unbiased amount of $\Theta(\sqrt{m})$ particles due to fluctuations.

Note that the above description is qualitative but exact, and can also be corroborated by the solution to a scaling limit of the standard evolution equations for the rescaled masses $\rho_x = \eta_x/N$. We consider the situation in which all N particles in the system reside on 3 sites $x = 1, 2, 3$, i.e. $\rho_1 + \rho_2 + \rho_3 = 1$ and $\rho_x = 0$ otherwise. Now consider the rescaled process $(\boldsymbol{\rho}(t) \,:\, t \geq 0)$ defined by

$$\boldsymbol{\rho}(t) := (\eta_x(t)/N \,:\, x \in \{1, 2, 3\}) \,.$$

This is a Markov process on the simplex $\Delta' = \left\{[0,1]^3, \sum_{x=1,2,3} \rho_x = 1\right\}$ with generator

$$\mathcal{L}_N f(\boldsymbol{\rho}) = \sum_{x=1,2} N\rho_x(d_L + N\rho_{x+1}) \left(f(\boldsymbol{\rho} - \frac{1}{N}\boldsymbol{e}_x + \frac{1}{N}\boldsymbol{e}_{x+1}) - f(\boldsymbol{\rho}) \right) , \qquad (3.24)$$

where $\boldsymbol{e}$ is the Cartesian basis vector and we can again ignore any particle leaving to site 4. In the beginning, a small initial mass is on site 2: $\rho_2 = \epsilon = 1 - \rho_1 - \rho_3 = \Theta(1/N) \ll 1$. Then assuming f is smooth, Taylor expansion of right hand side gives

$$\mathcal{L}_N f(\boldsymbol{\rho}) = \sum_{x=1,2} N\rho_x(d_L + N\rho_{x+1}) \left[\left(\frac{1}{N}\left(\partial_{\rho_{x+1}} - \partial_{\rho_x}\right) + \frac{1}{2N^2}\left(\partial_{\rho_{x+1}} - \partial_{\rho_x}\right)^2 \right) f(\boldsymbol{\rho}) + \Theta(\frac{1}{N^3}) \right] ,$$

where we use abbreviation

$$\left(\partial_{\rho_x} - \partial_{\rho_y}\right)^2 = \frac{\partial^2}{\partial {\rho_x}^2} - 2\frac{\partial^2}{\partial\rho_x\partial\rho_y} + \frac{\partial^2}{\partial\rho_y^2} \,.$$

For large systems d_L terms are negligible and for the test function $f(\boldsymbol{\rho}) = (\rho_1, \rho_3)$ we get,

$$\frac{1}{N}\mathcal{L}_N \begin{pmatrix} \rho_1 \\ \rho_3 \end{pmatrix} = -\rho_1\rho_2 \begin{pmatrix} 1 \\ 0 \end{pmatrix} + \rho_2\rho_3 \begin{pmatrix} 0 \\ 1 \end{pmatrix} + \Theta(\frac{1}{N}) \,. \qquad (3.25)$$

Note that to leading order the second order derivative terms cancel, so $\rho_i(t)$ is deterministic, and the order of the fluctuation terms are consistent with the unbiased exchange of order $\sqrt{N}$ particles as discussed above. Ignoring the correction term and slowing down time by taking $t \mapsto t/N$, with (3.25) the evolution equation gives

$$\frac{d}{dt}\begin{pmatrix}\rho_1(t)\\ \rho_3(t)\end{pmatrix} = \mathcal{L}_N \begin{pmatrix}\rho_1(t)\\ \rho_3(t)\end{pmatrix} = \begin{pmatrix}-\rho_1(t)\rho_2(t)\\ \rho_2(t)\rho_3(t)\end{pmatrix} = \begin{pmatrix}-\rho_1(t)^2 + \rho_1(t)\rho_3(t) - \rho_1(t)\\ -\rho_3(t)^2 - \rho_1(t)\rho_3(t) + \rho_3(t)\end{pmatrix}, \quad (3.26)$$

where we used $\mathbb{E}[\rho_x] = \rho_x$ in the first step and $\rho_2 = 1 - \rho_1 - \rho_3$ in the last step. For initial conditions $\rho_1(0)$ and $\rho_3(0)$ such that $(\rho_1(0) + \rho_3(0)) < 1$, $2\rho_1(0) > 1$, we have the solution:

$$\begin{aligned}
\rho_1(t) &= \frac{1}{2}\left(1 - B\tanh\left(\frac{Bt}{2} - A\right)\right) \to \frac{1-B}{2} \ \text{ as } \ t \to \infty\,,\\
\rho_3(t) &= \frac{2\rho_1(0)\rho_3(0)}{1 - B\tanh\left(\frac{Bt}{2} - A\right)} \to \frac{2\rho_1(0)\rho_3(0)}{1-B} \ \text{ as } \ t \to \infty\,, \qquad (3.27)\\
\text{where } \ B &= \sqrt{1 - 4\rho_1(0)\rho_3(0)} \ \text{ and } \ A = \tanh^{-1}\left(\frac{2\rho_1(0) - 1}{B}\right)\,.
\end{aligned}$$

We have $B = \sqrt{1 - 4\rho_1(0)(1 - \epsilon - \rho_1(0))} \to (2\rho_1(0) - 1) > 0$ as $\epsilon \to 0$, which implies $\rho_1(t) \to \rho_3(0)$ and $\rho_3(t) \to \rho_1(0)$ as $t \to \infty$, and the clusters exchange places.

Symmetric dynamics

For symmetric dynamics, the mechanism of cluster interaction is different and has been established in [41]. Two clusters on next-nearest neighbour sites, say 1 and 3, of rescaled sizes $\rho_1, \rho_3 \in [0, 1]$ with initially $\rho_1 = \rho_3 = 1$ can continuously exchange mass on the slow time scale d_L via the intermediate site according to the Wright-Fisher-type generator $\rho_1\rho_3(\partial_{\rho_3} - \partial_{\rho_1})^2$, which conserves the total mass. In addition, the two clusters can interact via site 2 in a jump event with rate $\rho_1 + \rho_3$, which includes the merging event. Since both clusters can separate only with site 1 moving to the left with rate ρ_1 and site 3 to the right with rate ρ_3, the jump event actually happens with probability 1/2. It can be shown that for each jump event, the two clusters merge with a probability of the order $1/((\rho_1 N + \rho_3 N)/2)$ (see more details later in Section 4.3.2). Due to the symmetry of the dynamics, for either cluster to move successfully away and finish one interaction event, it takes order ρ_1 or ρ_3 number of such jump events (see Appendix B). Therefore, the merge event during an interaction event actually happens with probability 1/2. But even without merging, the continuous exchange will lead to a finite fraction of particles being redistributed in an unbiased fashion, so that in a typical interaction event of order N particles

are exchanged, in contrast to $\sqrt{N}$ for totally asymmetric dynamics.

3.4.3 Derivation of time scale

The mechanism of cluster interaction together with the time scale for motion τ_L^{move} (3.19) and (3.22) determines the the time scale τ_L of coarsening and relaxation of the system, which we used in Figure 3.1. For the TASIP, condensates containing of order ρL particles have speed of order $d_L \rho L$. Then the relative speed between any two condensates is also of this order, which leads to the average time between two encounters to be of order $L \cdot \tau_L^{\text{move}} \sim 1/(\rho d_L)$. Since every interaction leads to an unbiased exchange of order $\sqrt{\rho L}$ particles, order ρL exchanges are necessary to achieve a macroscopic change, and it leads to the time scale

$$\tau_L^a = L/d_L \quad \text{(TASIP)} \ , \tag{3.28}$$

which is independent of the particle density ρ.

Following the similar argument for the SIP, the average time between successive encounters becomes $L^2 \cdot \tau_L^{\text{move}} \sim L^2/d_L$, since the condensates need to do order L^2 jumps to meet as they perform symmetric random walks with rate d_L. But as opposed to the TASIP, condensates can exchange a macroscopic number of particles so that we only need order 1 such encounters, leading to

$$\tau_L^s = L^2/d_L \quad \text{(SIP)} \ , \tag{3.29}$$

which is again independent of ρ.

3.5 Coarsening and saturation

3.5.1 Dynamics in the coarsening regime

We use heuristic arguments to derive the coarsening dynamics, based on the dynamics of a single 'typical' cluster and its interaction with others in a mean-field approximation.

Totally asymmetric dynamics

Let $m(t)$ denote the typical size of a cluster in the coarsening regime, and $n(t)$ the typical number of clusters per volume, so that we have $n(t)\, m(t) = \rho$. We denote the speed of a typical cluster by $v(t) = d_L m(t)$ and the typical distance of two clusters is given by $s(t) = m(t)/\rho$. Then the rate at which two clusters meet is

$v(t)/s(t) = \rho d_L$. As discussed in Section 3.4.2, when two clusters meet, they make an unbiased exchange of order $\sqrt{m}$ particles. So for one cluster to lose all its particles, it typically takes of order $m(t)$ exchanges. Therefore, each cluster independently disappears with rate $C_a \rho d_L / m(t)$, where C_a is a proportionality constant which is hard to predict and we will just fit it from simulation data. These death events, which happen typically after time $\Delta t = m(t)/(C_a \rho d_L n(t))$ per unit volume, drive the coarsening process. Each event effectively increases $m(t)$ by $\Delta m(t) = m(t)/n(t)$ per unit volume, which leads to

$$\frac{d}{dt} m(t) = \frac{\Delta m(t)}{\Delta t} = C_a \rho d_L \,. \tag{3.30}$$

The initial condition is

$$m(0) = \frac{\rho}{n(0)} = \frac{\rho}{r} \,,$$

where $n(0) = r$ (cf. (3.3)) is the expected ratio of occupied sites after nucleation which we also fit from the data. The solution to (3.30) is then simply

$$m(t) = C_a \rho d_L t + \frac{\rho}{r}. \tag{3.31}$$

Due to the clustered nature of configurations during the coarsening regime we have

$$\sigma^2(t) = \frac{m^2(t)}{s(t)} = \rho \, m(t) = C_a \rho^2 d_L t + \frac{\rho^2}{r} \,,$$

which implies

$$\frac{\sigma^2(t)}{\rho^2} = C_a d_L t + \frac{1}{r} \,. \tag{3.32}$$

Note that there is no explicit system size dependence in the above analysis and this scaling law also holds on infinite lattices (given a fixed small parameter d_L). On a finite lattice it only applies in a certain scaling window, after which the system saturates due to finite size effects (see Figure 3.6(a)), reminiscent of the classical Family-Viscek scaling for coarsening dynamics in surface growth (see, e.g., Chapter 3.3 in [95]). The time scale τ_L characterises this scaling window and the relaxation of the system, and is determined by the scaling solution reaching its maximal stationary value, i.e.

$$m(\tau_L^a) = C_a \rho d_L \tau_L^a + \frac{\rho}{r} = \Theta(N) \,.$$

This implies $\tau_L^a = \Theta(L/d_L)$ and corresponds to the time when all clusters have merged to a single condensate. This agrees with our previous prediction for the

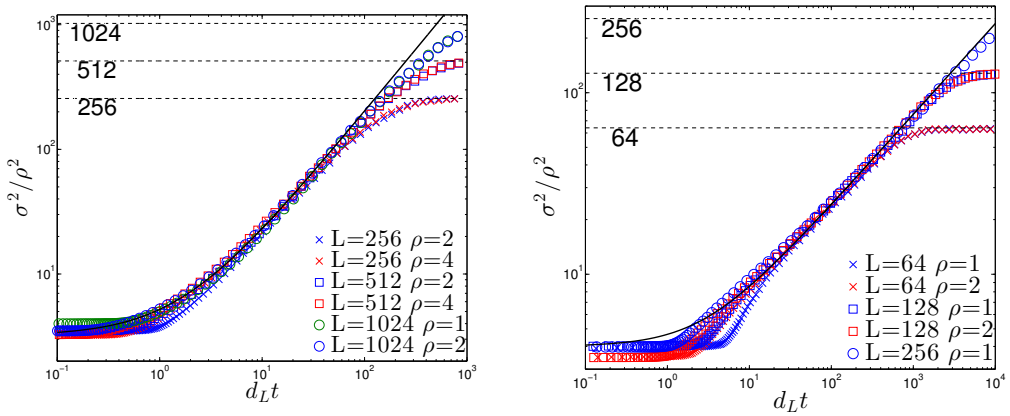

(a) (b)

Figure 3.6: Power-law scaling of $\sigma^2(t)/\rho^2$ in the coarsening regime. (a) Data for TASIP compared to the prediction (3.32) shown as a full line with fitted constant $C_a = 1.8961$ and initial condition $r = 0.3851$. (b) Data for SIP compared to the prediction (3.34) shown as a full line with fitted constant $C_s = 5.7614$. Data points are averaged over 200 realisations. Errors are bounded by the size of the symbols.

asymmetric time scale in (3.28).

Symmetric dynamics

We can apply the same argument to the SIP and get similar results. Since particles jump symmetrically, the velocity of clusters $v(t) = d_L$ is indeed the diffusivity(see (3.22)) but we keep $v(t)$ with a slight abuse of notation. With $s(t)$ being the typical distance between clusters, the interaction rate of clusters scales like $v(t)/s(t)^2$ in one dimension. Unlike the TASIP, a single interaction of two clusters in the SIP leads to a macroscopic exchange of order $m(t)$ particles as was derived in Section 3.4.2. Then we have

$$\frac{d}{dt}m(t) = C_s \frac{v(t)m(t)}{s(t)^2} = C_s \frac{d_L \rho^2}{m(t)} \ , \tag{3.33}$$

where C_s is again a proportionality constant for cluster interaction. With initial condition $m(0)$, we have the solution

$$m(t) = \sqrt{2C_s \rho^2 d_L t + m(0)^2} \, .$$

As before, the second moment can be written as

$$\sigma^2(t) = \rho m(t) = \rho^2 \sqrt{2C_s d_L t + (\sigma^2(0)/\rho^2)^2},$$

and for the initial condition we now have the exact result of the nucleation regime (3.15) where $\sigma^2(0)/\rho^2 = 3 + 1/\rho$. This leads to

$$\frac{\sigma^2(t)}{\rho^2} = \sqrt{2C_s d_L t + \left(3 + \frac{1}{\rho}\right)^2}, \tag{3.34}$$

where we only have to fit the parameter C_s. This scaling law is confirmed in Figure 3.6(b), and the scaling window and time scale can again be determined from

$$m(\tau_L^s) = \sqrt{2C_s \rho^2 d_L \tau_L^s + \frac{\rho^2}{r^2}} = \Theta(N) \ .$$

This implies $\tau_L^s = \Theta(L^2/d_L)$ which agrees with our previous prediction in (3.29).

3.5.2 Exponential saturation and stationarity

Having identified the time scales τ_L of the coarsening window for symmetric and asymmetric dynamics, we expect that the power-law behaviour turns into an exponential saturation of the system to the stationary value 1 of our observable $\sigma^2(t)/(\rho^2 L)$, i.e.

$$\frac{\sigma^2(t)}{\rho^2 L} \simeq 1 - e^{-C't/\tau_L} \quad \text{as } t \to \infty \ . \tag{3.35}$$

This is essentially equivalent to the assertion that C'/τ_L is indeed the spectral gap of the generator of the system, which usually describes the exponential approach to stationarity in finite systems as shown previously in Figure 3.1.

For symmetric dynamics, we can provide a simple derivation which includes a rough estimate of the constant C_s'. The late stage of the dynamics is dominated by 2 remaining clusters competing for particles. On average, both of them have roughly size $m \simeq N/2$, and from the derivation of (3.33) in the previous sub-section we see that under that assumption they meet at rate

$$C_s \frac{v(t)}{s(t)^2} = C_s \frac{4d_L}{L^2} = 4C_s/\tau_L^s \quad \text{since} \quad s = m/\rho = L/2 \ .$$

As mentioned in Section 3.4.3, at each encounter the clusters can merge with probability 1/2, which would lead to a single condensate and remaining in a typical stationary configuration. Since merge attempts are independent, this leads to an

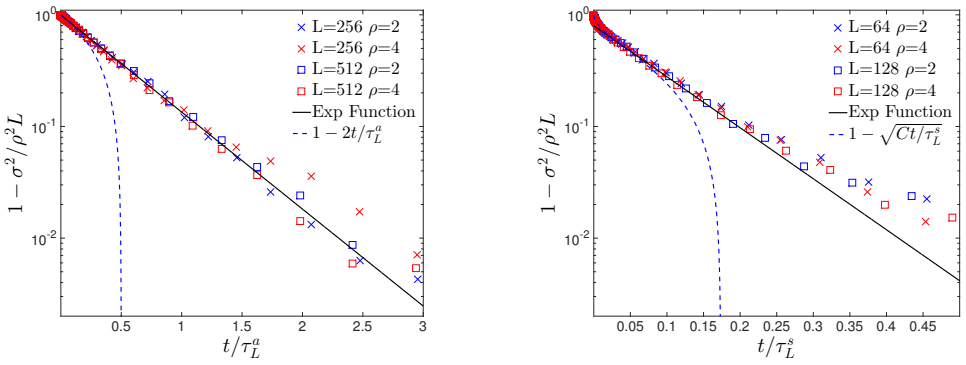

Figure 3.7: Exponential relaxation in the saturation regime for TASIP (a) and SIP (b). The predictions (3.35) are shown as a full lines with best fit constants $C'_a = 2.00$ and $C'_s = 10.51$. In both cases we plot the coarsening scaling law (dashed line) for comparison, which is only valid for short times on the scale τ_L^a or τ_L^s. Data points are averaged over 200 realisations. Errors are of the order 10^{-4}.

effective rate to reach stationarity roughly given by $2C_s/\tau_L^s$, and we expect

$$1 - \frac{\sigma^2(t)}{\rho^2 L} \simeq e^{-C'_s t/\tau_L^s} \quad \text{as } t \to \infty \,, \tag{3.36}$$

with $C'_s \simeq 2C_s$. This is confirmed in Figure 3.7(b), where we see a good data collapse with exponential decay with a best fit parameter $C'_s = 10.51$, which is similar to $2C_s$ as fitted in Figure 3.6. Given the crude approximation of two equal sized clusters in our derivation we cannot expect a perfect match of those constants.

For totally asymmetric dynamics two macroscopic clusters cannot merge in a single interaction event, but exchange only of order $\sqrt{L}$ particles in an unbiased fashion. Still, we expect the approach to stationarity to be governed by an exponential law of the form (3.35), and we can derive the constant by direct comparison with the coarsening dynamics. Expanding (3.35) for times $t \ll \tau_L$ we get

$$\frac{\sigma^2(t)}{\rho^2 L} \simeq 1 - e^{-C'_a t/\tau_L^a} \simeq C'_a \frac{t\, d_L}{L} \,,$$

where we used $\tau_L^a = L/d_L$. This matches the scaling law solution (3.32) and we see that in fact $C'_a = C_a$. Again this is confirmed in Figure 3.7(a), where the best fit parameter for C'_a is very close to 2 as is C_a. We currently do not have a good theoretical explanation to predict this value, but our numerics strongly suggest that the constant in the asymmetric case seems to be simply 2.

Note that the expansion of the exponential law matches with the coarsening

law only for the totally asymmetric case, since the coarsening law (3.32) is in fact linear. This leads to the fact that the whole coarsening and saturation dynamics are well described by the exponential law, as can be seen in Figure 3.1. For symmetric dynamics this matching argument would not work, since the coarsening law has exponent 1/2 and the exponential approximation is simply not valid in the coarsening window.

For large values of t the deviation from the exponential decay in Figure 3.7 is again a finite size effect. The stationary value of $\sigma^2/(\rho^2 L)$ is slightly smaller than 1, due to the fact that the single condensate continues to move on the time scale τ_L. During a step the mass is temporarily distributed on two lattice sites, which decreases the stationary average of σ^2. We have estimated a similar contribution to nearest-neighbour correlation functions in Section 3.3 using an ergodic average, and an analogous computation leads to stationary corrections of the order $1-\sigma^2/(\rho^2 L) \sim d_L/\rho$ for symmetric and totally asymmetric dynamics.

3.6 Summary

We have derived a heuristic description of the dynamics of condensation of the totally asymmetric inclusion process in the thermodynamic limit. We identified four dynamical regimes, and the main focus was the derivation of a coarsening scaling law. Our predictions have been confirmed by extensive simulations and describe the actual dynamics very well, in particular in the totally asymmetric case. Our arguments are based on the analysis of the dynamics of a typical cluster and interaction with others in a mean-field approximation, which is justified by observations of typical time evolutions of the system. This approach does not work for the explosive condensation model studied in [31, 32], where the full dynamics is dominated by a single large cluster and leads to a relaxation time scale that is decreasing with the system size.

The symmetric dynamics have been included mostly for comparison and to better understand the complicated dynamics for the totally asymmetric case in the nucleation regime. Since the symmetric inclusion process is self-dual, time dependent correlation functions can be computed exactly, which we have used indirectly for the nucleation regime. This holds, however, for the whole dynamics of the process, and a more detailed analysis of the duality structure of the process is expected to lead to a rigorous description of the full time evolution in the thermodynamic limit, which is discussed later in Chapter 6. A further interesting question arising for future work is a better understanding of the dynamics of the nucleation regime

in the totally asymmetric case.

Chapter 4

Results on General Asymmetric Inclusion Processes

4.1 Introduction

In this chapter, we extend the results of Chapter 3 to more general partially asymmetric inclusion processes, with focus on the dynamics of condensation in the thermodynamic limit. Comparing with the TASIP, in the partial asymmetric case there is no constraints on the jump direction of particles, which changes the behaviour of single clusters and their interactions on the microscopic level. We focus on the nearest-neighbour partially asymmetric inclusion process (PASIP) defined on a one-dimensional torus $\Lambda_L = \mathbb{T}_L$ of $|\Lambda_L| = L$ sites. The transition rates of the underlying random walk are given by

$$p(x,y) = p\delta_{y,x+1} + q\delta_{y,x-1}, \quad p,q \in (0,1), \quad p+q=1, \tag{4.1}$$

and the generator can be written explicitly as

$$\begin{aligned}\mathcal{L}_L f(\boldsymbol{\eta}) = \sum_x \Big\{ & p\eta_x(d_L + \eta_{x+1}) \left[f\left(\boldsymbol{\eta}^{x,x+1}\right) - f\left(\boldsymbol{\eta}\right) \right] \\ & + q\eta_x(d_L + \eta_{x-1}) \left[f\left(\boldsymbol{\eta}^{x,x-1}\right) - f\left(\boldsymbol{\eta}\right) \right] \Big\}. \end{aligned} \tag{4.2}$$

Partially asymmetric interacting particle systems have drawn large research interests in the last decade, often as a way to understand the crossover between symmetric and totally asymmetric models. As mentioned in Chapter 1, there is no general theory that can fully describe non-equilibrium systems, therefore the work on partially asymmetric models is also model specific, and the most studied one is

the partially asymmetric simple exclusion process (PASEP) due to its simple interaction mechanism. The asymptotic behaviour of the particle current of the totally asymmetric exclusion process has firstly been studied in [96] then similar results for the symmetric exclusion process (SEP) have also been established (see, e.g.,[97] and references therein). In [98, 99, 100], it has been shown that the same asymptotic description of the current in TASEP is still valid for PASEP with the only modification of a pre-factor in time variables, but the SEP shows qualitatively different behaviour. Then the crossover between the symmetric and asymmetric models, which corresponds to a weakly asymmetric simple exclusion Process (WASEP), has been extensively studied, including exact results related to random matrices (see, e.g.,[101, 102, 103, 104, 105, 106, 107]), as well as the exact crossover scale [108]. The partially asymmetric version of a special class of ZRP has also been studied in [109], where the hopping rates are set to be site dependent but not occupation number dependent. Since the ZRP can be mapped to ASEP, the spatial inhomogeneity of ZRP can be transformed to particle dependent hopping rates in ASEP (see [109, 110] and references therein for details).

Although the general dimensionless results on the inclusion process, reviewed in Chapter 2, are valid for the PASIP, as far as we know there have not been any results on the dynamics of the condensation. Inspired by the PASEP results, we expect the dynamical behaviour of condensation in the PASIP to share very similar features with the TASIP, with fundamental differences to SIP, and a weakly asymmetric version could provide a crossover. Compared with exclusion process, the interaction mechanism of inclusion process is more complicated and the local state space is unbounded. Therefore, one needs to carefully check the influences of the partial asymmetry on a microscopic level before considering the macroscopic behaviour of the clusters. We will show that the partial asymmetry slows down the movement of isolated clusters and also causes additional fluctuations to clusters' interactions.

The chapter is organised as follows. In Section 4.2 we look at the condensation and dynamical regimes in the PASIP. Mechanical laws of cluster motion and interaction are investigated in Section 4.3 based on results from previous chapters and detailed numerical studies. In Section 4.4, we discuss coarsening and saturation regimes and adapt scaling results in Chapter 3 to partially asymmetric systems. In Section 4.5 we introduce some interesting aspects for further study, in particular a weakly asymmetric inclusion process (WASIP) as the crossover between asymmetric and symmetric systems.

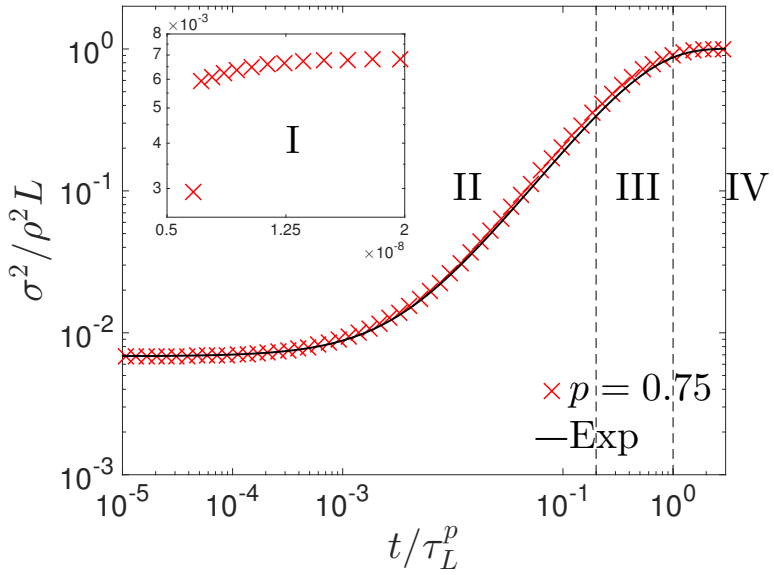

Figure 4.1: Different dynamical regimes in a PASIP system with $p = 0.75$, $L = 512$. I. Nucleation Regime. II. Coarsening Regime. III. Saturation Regime. IV. Stationary Regime. The normalised second moment $\sigma^2(t)/\rho^2 L$ is shown against scaled time t/τ_L^p, where τ_L^p is p-dependent and the exact form is given in (4.24). The black line is the same exponential prediction (3.35) as in the TASIP with predicted constant $C' \approx 2$. Data points are averaged over 200 simulations and errors are bounded by the size of symbols.

4.2 Condensation and dynamical regimes

Recall from Section 2.2 (see [74, Theorem 2.1] for further details) that the inclusion process exhibits a family of product stationary measures if $p(x, y)$ is doubly stochastic modulo a constant, i.e.

$$\sum_{j \in \Lambda_L} (p(i,j) - p(j,k)) = 0 \quad \text{for all } i, k \in \Lambda_L \,.$$

In particular this is the case for $p(x, y)$ in the PASIP (4.1). Therefore, there are stationary product measures denoted

$$\nu_\phi^L[d\boldsymbol{\eta}] = \prod_{x \in \Lambda_L} \bar{\nu}_\phi(\eta_x) d\boldsymbol{\eta} \qquad \text{with } \bar{\nu}_\phi(n) = \frac{1}{z(\phi)} w(n) \phi^n \,.$$

where

$$w(n) = \frac{\Gamma(d_L + n)}{n!\Gamma(d_L)}\,, \text{ and } z(\phi) = \sum_{k=0}^{\infty} w(k)\phi^k = (1-\phi)^{-d_L}\,.$$

The stationary distribution of PASIP is independent of the asymmetry p and is the same as the TASIP and the SIP. Therefore, the same condensation as discussed with general inclusion processes in Section 2.3.3,

$$\max_{x\in\Lambda_L} \eta_x/N \to 1 \quad \text{in distribution } \pi_{L,N}$$

still occurs under the thermodynamic limit (2.32):

$$L, N \to \infty\,,\ d_L \to 0 \quad \text{such that} \quad \frac{N}{L} \to \rho > 0 \quad \text{and} \quad d_L L \to 0\,,$$

where $d_L = L^{-\gamma}$ and $\gamma > 1$. Again, for numerical data in the rest of this chapter we use $d_L = \frac{1}{L^2}$ but have checked the validity of our results also for other scaling of d_L. Again, we will use $\sigma^2(t)$ as defined in (2.4) to quantify the time evolution towards condensation.

Although the stationary distribution of the PASIP is the same as for the TASIP and the SIP, the dynamics of PASIP are fundamentally different, especially from the SIP. In the rest of this chapter, we focus on the dynamics of PASIP from a spatially homogeneous initial distribution to the formation of the complete condensate. Without loss of generality, we always assume the particles have a drift to the right, i.e. $p > q$ in (4.1). Following the analysis in the previous chapter, the process of the formation of the complete condensate can be qualitatively divided into four different regimes: the nucleation regime, the coarsening regime, the saturation regime and the stationary regime, as illustrated with numerical results in Figure 4.1. In the following sections in this chapter, we can see these regimes exhibit similar characteristic behaviour as the TASIP, while the partial asymmetry brings more complicated details into the exact dynamics. Similar to the TASIP as discussed in Section 3.3, the PASIP does not have a self-duality property due to the asymmetry, and the correlation functions for clusters in the nucleation regime do not have closed forms. The same numerical approach as discussed in Section 3.3 for the TASIP can be applied to the nucleation regime, but does not lead to any significant differences. Although the nucleation itself has dynamics which may be of independent interest, we focus on the dynamics at larger time scales. Understanding the coarsening and saturation regimes is our main interest here and we will look at more details in Section 4.3. The stationary regime is a natural outcome of the isolated clusters movement and will also be discussed in detail in Section 4.3.

4.3 Condensate motion and interaction

In this section we first investigate the motion of a macroscopic isolated cluster which dominates the stationary regime. Then we look at the interaction of two clusters through a more detailed numerical approach, which extends results we have derived in Section 3.4.

4.3.1 Dynamics of isolated clusters

Consider an isolated cluster of size $m = \Theta(L)$[1] residing on site x of an otherwise empty lattice Λ_L. A single particle could move to site $x+1$ with rate pd_Lm, or to site $x-1$ with rate qd_Lm. First, we consider the case that it moves to $x+1$, where it could move one step further to site $x+2$ with rate pd_L, or return to site x with a much higher rate $q(m-1+d_L)$. In the meantime a particle on site x could move independently to site $x-1$ with rate $qd_L(m-1)$, or follow the previous particle to site $x+1$ with a higher rate $p(m-1)(1+d_L)$. Under the condition of small d_L, this interaction mechanism is dominated by inclusion rates between site x and $x+1$ and lasts until all particles are absorbed on either site. During this interaction, the rate of any particle escaping from these two sites is $pd_L\eta_{x+1} + qd_L\eta_x$, which is bounded above by d_Lm and vanishes as $L \to \infty$. For large clusters, we can omit the escaping events and the small d_L in inclusion rates, then the mass distribution between sites x and $x+1$ can be described by a simple asymmetric random walk on the state space $X_m = \{0, 1, 2, ..., m\}$ with jump rates p, q and absorbing sites at both boundaries. A macroscopic cluster successfully moving one step to the right is then equivalent to the event that the walker starting from $1 \in X_m$ and reaches m before being absorbed by 0. As derived in Appendix (B.2) the probability for such a successful step is

$$\frac{1-q/p}{1-(q/p)^m} \to 1 - \frac{q}{p} \quad \text{as} \quad m \to \infty, \tag{4.3}$$

which is now < 1 as opposed to the TASIP.

Analogously, if the first particle jumps left to the site $x-1$ with rate qd_Lm, it will trigger an interaction between particles on sites $x-1$ and x, where the rate of any particle to escape during the interaction is $qd_L\eta_{x-1} + pd_L\eta_x$. Again, the escaping rate is bounded by d_Lm and vanishes as $L \to \infty$. Using the same asymmetric random walk approximation, we have the probability for an isolated

[1]Recall the notation $f(n) = \Theta(n)$: $k_1 n < f(n) < k_2 n$, for some constants k_1, $k_2 > 0$ and n sufficiently large.

cluster to move one step to the left as

$$\frac{1-p/q}{1-(p/q)^m} \to 0 \quad \text{as} \quad m \to \infty. \tag{4.4}$$

This shows that the probability of a large cluster moving to the left vanishes since all particles would have to follow the first one against the bias.

Next, we compute the expected time of one such successful step of the cluster in the direction of the drift, and compare it with that in the TASIP and the SIP. This process is equivalent to a birth-death process on a finite state space $X_m = \{0, 1, 2, ..., m\}$ with site-dependent birth rates α_i and death rates β_i, $i = 0, 1, 2, ..., m$, which are given by the transition rates as

$$\alpha_i = p(m-i)(d_L+i), \beta_i = qi(d_L+m-i), \quad \text{for } i = 1, 2, 3, ..., m-1, \tag{4.5}$$

and at the boundaries

$$\alpha_0 = pd_Lm, \quad \beta_0 = 0, \quad \alpha_m = 0, \quad \beta_m = qd_Lm. \tag{4.6}$$

Denote the stationary distribution of this chain as $\boldsymbol{\mu}$, then by detailed balance (Proposition 2.2) we have $\mu_k\alpha_k = \mu_{k+1}\beta_{k+1}$ and then

$$\mu_k = \left(\prod_{i=1}^{k} \frac{\alpha_{i-1}}{\beta_i}\right)\mu_0, \quad \text{for } k = 1, 2, ..., n.$$

The expected hitting time of the boundary m starting from site k is derived in Appendix B and given by (B.1) as

$$\tau_k^m = \sum_{i=k}^{m-1} \frac{1}{\alpha_i\mu_i} \sum_{j=0}^{i} \mu_j.$$

Then τ_1^m with rates (4.5) (4.6) is the expected waiting time after the first particle jumps by diffusion until the whole cluster moves successfully one step to the drifted direction in the PASIP. Here we first compute a slightly more general formula of τ_k^m, then give an approximation of τ_1^m. To compute τ_k^m for a given $k \in \{1, 2, ..., m-1\}$,

using rates (4.5) (4.6) and ignoring d_L we have

$$\begin{aligned}\frac{\mu_j}{\mu_i} &= \frac{\left(\frac{p}{q}\right)^j \left(\prod_{l=1}^{j} \frac{(m-l+1)(d_L+l-1)}{l(d_L+m-l)}\right)\mu_0}{\left(\frac{p}{q}\right)^i \left(\prod_{l'=1}^{i} \frac{(m-l'+1)(d_L+l'-1)}{l'(d_L+m-l')}\right)\mu_0} \\ &\simeq \left(\frac{q}{p}\right)^{i-j} \frac{i(m-i)}{j(m-j)}\end{aligned} \tag{4.7}$$

for $j = 1, 2, 3, ..., i$ and $i = k, k+1, ..., m-1$. For $j = 0$ we keep one d_L in the denominator and use the approximation

$$\frac{\mu_0}{\mu_i} \simeq \left(\frac{q}{p}\right)^i \frac{i(m-i)}{md_L}, \quad \text{for } i = k, k+1, ..., m-1. \tag{4.8}$$

Notice that τ_k^m can be rearranged by μ_j in the numerators as

$$\begin{aligned}\tau_k^m &= \frac{\mu_0}{\alpha_k\mu_k} + \frac{\mu_1}{\alpha_k\mu_k} + \frac{\mu_2}{\alpha_k\mu_k} + ... + \frac{\mu_{k-1}}{\alpha_k\mu_k} + \frac{1}{\alpha_k} \\ &\quad + \frac{\mu_0}{\alpha_{k+1}\mu_{k+1}} + \frac{\mu_1}{\alpha_{k+1}\mu_{k+1}} + ... + \frac{\mu_{k-1}}{\alpha_{k+1}\mu_{k+1}} + \frac{\mu_k}{\alpha_{k+1}\mu_{k+1}} + \frac{1}{\alpha_{k+1}} \\ &\quad + ... \\ &\quad + \frac{\mu_0}{\alpha_{m-1}\mu_{m-1}} + ... + \frac{\mu_{k-1}}{\alpha_{m-1}\mu_{m-1}} + \frac{\mu_k}{\alpha_{m-1}\mu_{m-1}} + ... + \frac{1}{\alpha_{m-1}} \\ &= \sum_{i=k}^{m-1} \frac{\mu_0}{\alpha_i\mu_i} + \sum_{j=1}^{k-1}\sum_{i=k}^{m-1} \frac{\mu_j}{\alpha_i\mu_i} + \sum_{j=k}^{m-2}\sum_{i=j+1}^{m-1} \frac{\mu_j}{\alpha_i\mu_i} + \sum_{i=k}^{m-1} \frac{1}{\alpha_i},\end{aligned}$$

then we substitute (4.7) (4.8) and $\alpha_i \simeq pi(m-i)$ into the last line to get

$$\begin{aligned}\tau_k^m &\simeq \frac{\left(\frac{q}{p}\right)^k \left(1 - \left(\frac{q}{p}\right)^{m-k}\right)}{(p-q)md_L} + \frac{\left(\frac{q}{p}\right)^k \left(1 - \left(\frac{q}{p}\right)^{m-k}\right)}{(p-q)} \sum_{j=1}^{k-1} \left(\frac{q}{p}\right)^{-j} \frac{1}{j(m-j)} \\ &\quad + \sum_{j=k}^{m-2} \frac{\frac{q}{p}\left(1 - \left(\frac{q}{p}\right)^{m-j-1}\right)}{(p-q)j(m-j)} + \sum_{i=k}^{m-1} \frac{1}{pi(m-i)}.\end{aligned}$$

Notice this is a general expression of the expected hitting time starting from k particles on the target site. To see the motion of the cluster, we take $k = 1$ and then the second term of above equation vanishes, then we have the following results

for large clusters,

$$\tau_1^m \simeq \frac{q}{p(p-q)md_L} + \sum_{j=1}^{m-2} \frac{\frac{q}{p}\left(1-\left(\frac{q}{p}\right)^{m-j-1}\right)}{(p-q)j(m-j)} + \sum_{i=1}^{m-1} \frac{1}{pi(m-i)}\,.$$

We can find an upper and a lower bound for the second term as

$$\frac{q}{p^2}\sum_{j=1}^{m-2}\frac{1}{j(m-j)} \le \sum_{j=1}^{m-2} \frac{\frac{q}{p}\left(1-\left(\frac{q}{p}\right)^{m-j-1}\right)}{(p-q)j(m-j)} \le \frac{q}{p(p-q)}\sum_{j=1}^{m-2}\frac{1}{j(m-j)}.$$

Applying the same approximation as in (3.18) for the TASIP, we have

$$\sum_{j=1}^{m-2}\frac{1}{j(m-j)} \simeq \frac{1}{m}\int_{\frac{1}{m}}^{\frac{m-2}{m}}\frac{1}{x(1-x)}dx \simeq \frac{1}{m}\log\left(\frac{(m-2)(m-1)}{2}\right) \simeq \frac{2}{m}\log(m),$$

and

$$\sum_{j=1}^{m-1}\frac{1}{j(m-j)} \simeq \frac{1}{m}\int_{\frac{1}{m}}^{\frac{m-1}{m}}\frac{1}{x(1-x)}dx \simeq \frac{1}{m}\log\left((m-1)^2\right) \simeq \frac{2}{m}\log(m),$$

therefore

$$\tau_1^m \simeq \frac{q}{p(p-q)md_L} + \frac{2}{m}\log(m)\,.$$

Recall the first particle jumps by diffusion rate pd_Lm, the expected total time for all particles to move one step is therefore given by $\tau^{\text{step}} = \frac{1}{pd_Lm} + \tau_1^m$, with approximation

$$\tau^{\text{step}} \simeq \frac{1}{pd_Lm} + \frac{q}{p(p-q)md_L} + \Theta\left(\frac{\log m}{m}\right) = \frac{1}{(p-q)md_L} + \Theta\left(\frac{\log m}{m}\right) \quad (4.9)$$

Comparing with (3.18) in the TASIP, which we repeat here

$$\begin{aligned}\tau_{\text{TASIP}}^{\text{step}} &= \frac{1}{d_Lm} + \sum_{k=1}^{m-1}\frac{1}{(m-k)k} \simeq \frac{1}{d_Lm} + \frac{1}{m}\int_{1/m}^{(m-1)/m}\frac{1}{x(1-x)}\,dx \\ &\simeq \frac{1}{d_Lm} + \frac{2}{m}\log(m)\,, \qquad \text{(3.18 revisited)}\end{aligned}$$

we can see that (4.9) has an extra term $\frac{q}{p(p-q)md_L}$ which decreases with increasing $p \in (1/2, 1]$. This term corresponds to the event that the first particle, after it leaves the cluster by diffusion, jumps back rather than attracts more particles. Then the

cluster has to wait for the next particle leaving by diffusion with a lower rate. Obviously, this event occurs against the drift, and has more impact in a system with weaker drift strength, i.e. smaller p. In the extreme case when $p \to 1$, (4.9) converges to (3.18), and $\tau^{\text{step}} \to \tau^{\text{step}}_{\text{TASIP}}$, as the system itself converges to the TASIP.

4.3.2 Interaction of two clusters

Clusters move freely as described above until there is only one intermediate lattice site separating two of them, they then interact via a mechanism which is similar to but more complicated than the one discussed in Section 3.4.2 for the TASIP. The asymptotic behaviour of such interactions for large clusters in the PASIP can be studied following the same approach used for the TASIP, where we restrict all N particles on three lattice sites $x = 1, 2, 3$, and consider the rescaled process $\boldsymbol{\rho}(t) := (\eta_x(t)/N : x \in \{1,2,3\})$ on the simplex $\Delta' = \left\{[0,1]^3, \sum_{x=1,2,3} \rho_x = 1\right\}$. For the PASIP the generator of this process is then

$$\begin{aligned}\mathcal{L}_N f(\boldsymbol{\rho}) = &\sum_{x=1,2} pN\rho_x(d_L + N\rho_{x+1}) \left(f\left(\boldsymbol{\rho} - \frac{1}{N}\boldsymbol{e}_x + \frac{1}{N}\boldsymbol{e}_{x+1}\right) - f(\boldsymbol{\rho})\right) \\ &+ \sum_{x=2,3} qN\rho_x(d_L + N\rho_{x-1}) \left(f\left(\boldsymbol{\rho} - \frac{1}{N}\boldsymbol{e}_x + \frac{1}{N}\boldsymbol{e}_{x-1}\right) - f(\boldsymbol{\rho})\right) . \quad (4.10)\end{aligned}$$

For large systems d_L terms are negligible and for the test function $f(\boldsymbol{\rho}) = (\rho_1, \rho_3)$ we get,

$$\frac{d}{dt}\begin{pmatrix}\rho_1(t)\\ \rho_3(t)\end{pmatrix} = \begin{pmatrix}-(p-q)\rho_1(t)\rho_2(t)\\ (p-q)\rho_2(t)\rho_3(t)\end{pmatrix},$$

with solution under rescaled time $t \mapsto t/N$

$$\begin{aligned}\rho_1(t) &= \frac{1}{2}\left(1 - B\tanh\left(\frac{B(p-q)t}{2} - A\right)\right) \to \frac{1-B}{2} \text{ as } t \to \infty, \\ \rho_3(t) &= \frac{2\rho_1(0)\rho_3(0)}{1 - B\tanh\left(\frac{B(p-q)t}{2} - A\right)} \to \frac{2\rho_1(0)\rho_3(0)}{1-B} \text{ as } t \to \infty,\end{aligned}$$

where $B = \sqrt{1 - 4\rho_1(0)\rho_3(0)}$ and $A = \tanh^{-1}\left(\frac{2\rho_1(0)-1}{B}\right)$. This is the same result as (3.27), except for the factor $(p-q)$ in front of time t, which implies that asymptotically the interaction between large clusters are the same as TASIP, i.e. when a bigger cluster catches up with a smaller cluster (both of order L size), they exchange positions without exchanging a significant number of particles.

However, if we take a closer look at the dynamics in the PASIP, especially

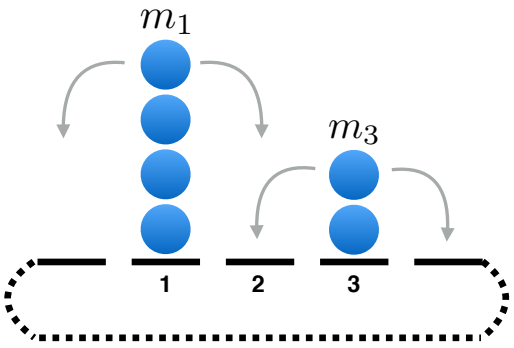

Figure 4.2: Sketch of the cluster interaction in the PASIP.

for interactions between small clusters (say of the order ρ) to leading order, the relevant quantity for the coarsening are the fluctuations which determine the amount of exchanged particles during a swap. This should increase as compared to the TASIP, since the interaction takes a longer time which is quantified by the pre-factor $(p-q)$ in the above equation. Therefore, the mean field approach yields the same mechanism of swapping positions as for the TASIP, but cannot account for the increased exchange of particles during that swap. In the rest of this section we describe this interaction mechanism through a different approach. The precise dynamics of this interaction is complicated and relatively difficult to derive in an explicit way, thus we first present a description from a more numerical perspective.

Observations

We now define one **sub-interaction process** starting when the first particle jumps to the intermediate site and finishing when this site becomes empty again or has absorbed all particles involved in the interaction (which happens with a very small probability). In the rest of this section we will refer to this sub-interaction process as interaction for ease of presentation. Notice, a typical 'catch up and swap' scenario of two clusters discussed above may consist of a number of such interactions. In the rest of this section, we use t to denote the interaction time and write the size of a cluster within an interaction as $m(t)$, and use $\bar{t}$ to denote the system time of the process. Regardless of the actual positions on the lattice, we always name the cluster on the left site m_1 containing $m_{1,\bar{t}}$ particles at time $\bar{t}$, the one on the right site m_3 containing $m_{3,\bar{t}}$ particles, and the cluster on the intermediate site m_2 containing $m_{2,\bar{t}}$ particles during one interaction (see Figure 4.2). Within an interaction, M denotes the total number of particles involved in one interaction i.e. $m_1(0) + m_3(0) = M$.

The duration of one interaction is then a stopping time:

$$T := \inf\{t > 0, m_1(t) + m_3(t) = 0 \quad \text{or} \quad m_1(t) + m_3(t) = M\}. \tag{4.11}$$

Figure 4.3 shows the observations of cluster interactions recorded in a single realisation of a full PASIP trajectory starting from a flat initial condition until only one cluster remains, for different values of p including $p = 0.5$ for the SIP and $p = 1.0$ for the TASIP. We record the ratio of m_1 to M before and after each interaction by the positions of markers, the size of M by the size of markers and the recorded time $\bar{t}$ by the colour of markers. Rich information about the interacting mechanism can be found in this figure, and we list several important aspects with analysis.

1. Most interactions occur between small clusters and in early stages of the coarsening regime (represented by small circles with blue colour in Figure 4.3).

2. Data points located on the main diagonal correspond to those clusters keeping their sizes after the interaction, where typically a particle jumps to the intermediate site then immediately jumps back to m_1. In the following we will refer the lower-left to upper-right diagonal as the **main diagonal** and the upper-left to lower-right diagonal as the **anti-diagonal**. Data around the main diagonal shows the fluctuations where m_1 loses or gains a small number of particles. The same fluctuations in the SIP (Figure 4.3(a)) are more obvious since interaction between two SIP clusters leads to an exchange of a large number of particles (see discussion in Section 3.4.2), and the data points distribute symmetrically along the diagonal due to the symmetry of transition rates. In contrast, there is only a few data points in the region above the main diagonal for the PASIP, which illustrates the difficulty for a cluster to gain particles against the drift. Naturally it is impossible for the TASIP by definition, as one can observe in Figure 4.3(c).

3. In Figure 4.3(b), 4.3(c), many data points are located on or around the anti-diagonal. This represents the 'swap' scenario, where $m_1(T) \simeq m_3(0)$. The reason we can only observe such data located on the right half of the diagonal is that bigger clusters have a higher speed and will catch up with smaller ones. Once they exchange positions, the bigger cluster tends to move away. Therefore we always observe $m_1(0) > m_3(0) \simeq m_1(T)$ in such interactions. Also, we find the large clusters prefer to follow the 'meet and swap' rule while small ones are more unpredictable, as indicated by the dispersed small circles. The pink arrows in 4.3(b) illustrate the following typical event: a large

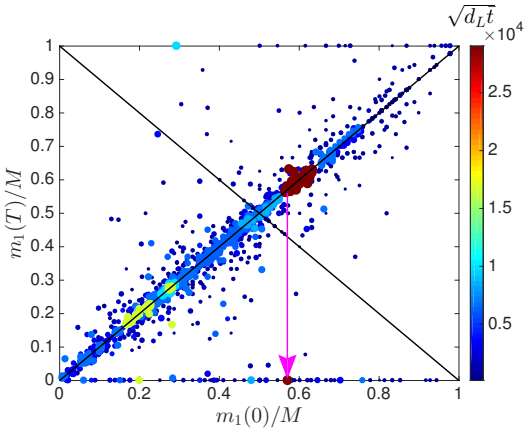

(a) $p = 0.5$

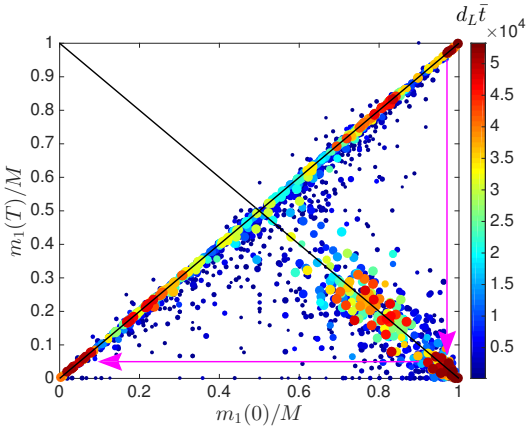

(b) $p = 0.75$

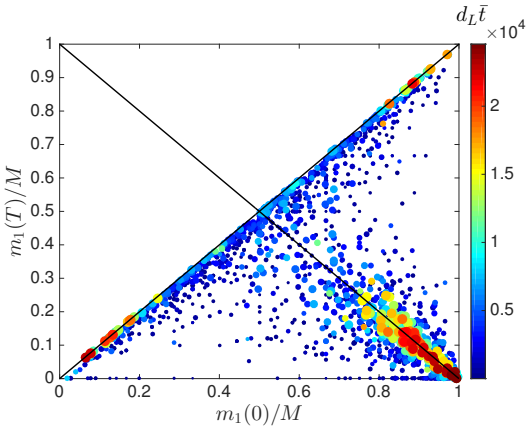

(c) $p = 1.0$

Figure 4.3: Scatter plot of normalised $m_1(0)/M$ and $m_1(T)/M$ (cf. (4.11)) in a single realisation of a full trajectory for SIP, PASIP and TASIP with $L = 256$, $N = 512$. Each point represents one interaction event. The number of particles M in these events varies, and is indicated by the size of the points, where colour indicates the time of the interaction. Two diagonals are shown as full lines. Purple arrows indicate a typical succession of interaction events, showing a merge for symmetric (a) and a flip for asymmetric dynamics (b) at a late stage in the dynamics.

cluster catches up with a smaller one and starts the interaction. Initially, a few particles jumps to the intermediate site but are immediately absorbed by either cluster, and the interaction finishes without significant impact on the mass distribution (data points on the diagonal close to upper-right corner). Then, after several such short interactions, one particle triggers a long interaction which ends up with the two clusters exchanging their positions (data points close to lower-right corner). Now, m_1 is the smaller cluster by definition and the bigger m_3 tends to move away with a higher speed. But before that further short interactions may occur (data points near lower-left corner). Thus, a typical event is finished, and when the bigger cluster travels around the whole lattice it will meet the smaller cluster again and start another such event until only a single cluster remains.

4. Data points located on the lower and upper boundaries indicate merge events. For the PASIP and the TASIP, a merge is typically observed for small clusters, and only on the lower boundary, i.e. the clusters did not merge on the left site 1. While for the SIP, we observe more merge events on both boundaries, including some big clusters. Note, we only record the change of m_1, thus the data on lower boundary ($m_1(T) = 0$) include the merge on both site 3 and the intermediate site 2. The merge events agree with our previous argument in Section 3.4.2 that order M particles can be exchanged in an interacting event in the SIP. Macroscopically, clusters in the PASIP and the TASIP move with the drift and only exchange a smaller number of particles when they meet. In contrast, after two clusters in the SIP meet, they typically keep their positions and interact for a longer time, until they either merge or one cluster moves away, which occurs with the same probability. In other words, the SIP clusters spend most of the time searching for other clusters then interact for a while, and the PASIP and the TASIP clusters meet more often but spend less time on each interaction. So the SIP interactions are more isolated than the PASIP and the TASIP in the space of time which is represented by colours in 4.3(a), and we observe the clustering of data with similar colour in the SIP while the colours of data in the TASIP and the PASIP are distributed more uniformly. The pink arrow in the Figure 4.3(a) illustrates a typical merge event in the SIP, where two big clusters meet and interact. For a long time they only exchange a few particles (the cluster of data points around the diagonal) until the merge event occurs (point moves to the lower boundary).

The above observations help us understand the interaction of two clusters

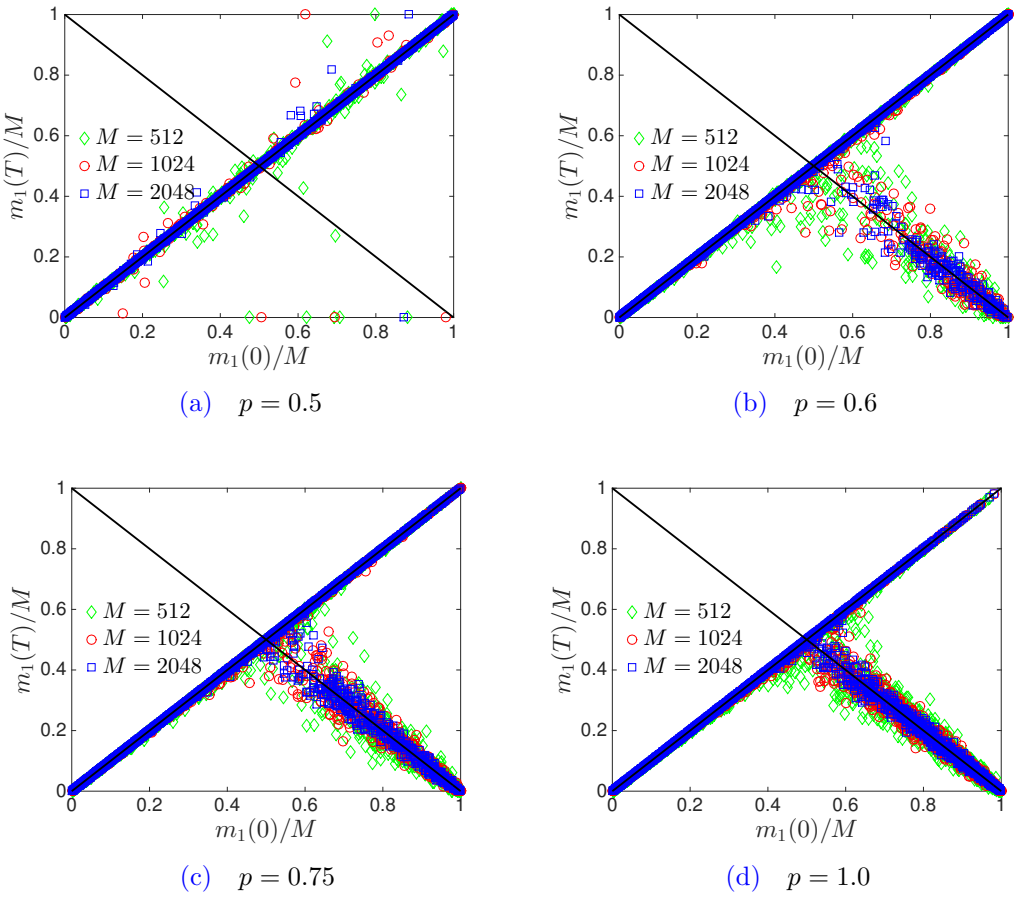

(a) $p = 0.5$ (b) $p = 0.6$

(c) $p = 0.75$ (d) $p = 1.0$

Figure 4.4: Scatter plot of normalised $m_1(0)$ and $m_1(T)$ for PASIP toy model (4.12) with uniform initial conditions. Note these data are not from full simulations. 2000 realisations are tested for each system size. Two diagonals are shown as full lines.

in different regimes qualitatively. But during a realisation, both the number of interactions and the size of clusters are random. Next, to investigate the interaction mechanism more precisely, we construct some artificial interacting models with a fixed number of particles and uniform initial distributions.

Analysis

We construct toy models of an interaction event as follows: First, fix the total number of particles $M = m_1(0) + m_3(0)$ to be relatively large. Then, distribute these particles on sites 1 and 3 with a uniform distribution

$$\mathbb{P}\left(m_1(0) = k, m_2(0) = 0, m_3(0) = M - k\right) = 1/(M-1), \quad k \in \{1, 2, ..., M-1\}.$$

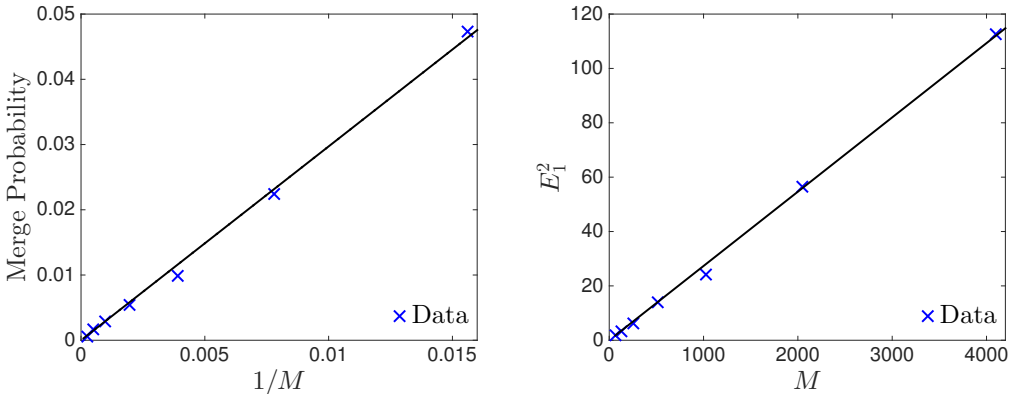

Figure 4.5: Interaction in the SIP. (a): Probability of condensates merging in the SIP. (b): Fluctuations (4.13) along the $m_1(0) = m_1(T)$ diagonal with tolerance $\epsilon = 0.1$. Fitted linear predictions $\mathbb{P}[\text{Merge}] = 2.9713(1/M)$ and $E_1^2 = 0.02733M$ are shown as full lines. 20000 realisations are tested for each M.

Pick the first particle from cluster m_1 or m_3 according to the jump rates $pd_M m_1(0)$ and $qd_M m_3(0)$, respectively, then start the interaction according to the generator

$$\begin{aligned}\mathcal{L}f(\boldsymbol{m}) = &\sum_{x=1,2} pm_x(d_M + m_{x+1})\left[f(\boldsymbol{m}^{x,x+1}) - f(\boldsymbol{m})\right] \\ &+ \sum_{x=2,3} qm_x(d_M + m_{x-1})\left[f(\boldsymbol{m}^{x,x-1}) - f(\boldsymbol{m})\right] ,\end{aligned} \tag{4.12}$$

where $f : X_M = \mathbb{N}^3 \to \mathbb{R}$ is the test function and $d_M \ll 1/M$. This is just the generator (4.2) restricted to three sites toy model. Then we record $m_1(T)$ when the interaction finishes. Figure 4.4 shows the results for this toy models with a large number of realisations with different p. Denote the probability of two cluster merge within an interaction as $\mathbb{P}[\text{Merge}] = \mathbb{P}[m_1(T) = 0 \text{ or } M]$, then in the SIP, two clusters either merge with a small probability $\mathbb{P}[\text{Merge}] \sim 1/M$ (see Figure 4.5 left) or keep their initial sizes with order $\sqrt{M}$ fluctuations (see Figure 4.5 right). The fluctuations are measured as

$$E_1^2 := \left\langle |m_1(T) - m_1(0)|^2 \mathbb{I}\{|m_1(T) - m_1(0)| < \epsilon M\} \right\rangle , \tag{4.13}$$

where $0 < \epsilon \ll 1$ is a constant (tolerance) ensuring that we only include data close to the main diagonal, and $\langle\cdot\rangle$ denotes the average on a large number of realisations. Notice, this merge probability is conditioned on the sub-interaction process here while an previously discussed interaction event, or an 'catch up and swap' scenario,

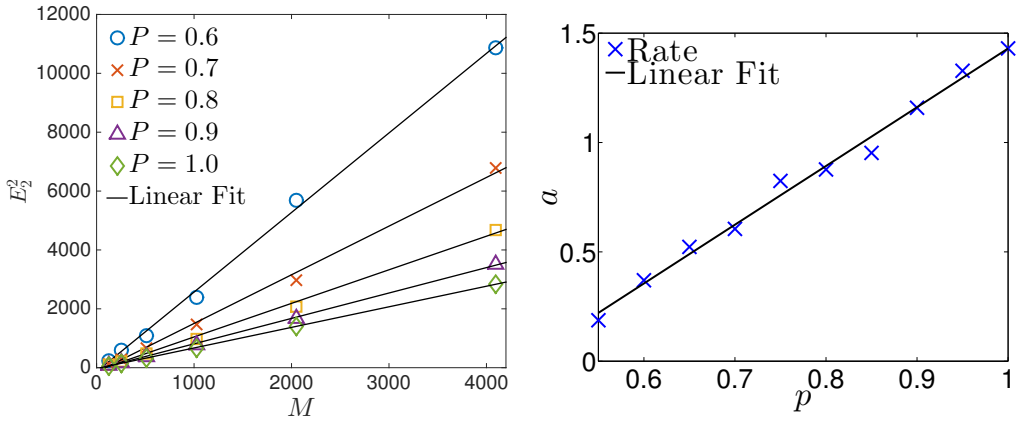

Figure 4.6: Left: Fluctuations (4.14) after two condensates exchange positions against system size. Fitted linear predictions $E_2^2 = (1/a)M$ with constants a are shown as full lines. Right: Linear fit rates against parameter p. Fitted linear predictions $a = 2.687p - 1.257$ are shown as full lines. 20000 realisations are tested for each system size.

consists order M such sub-interaction processes, which implies the merge probability within an interaction event to be of the order 1.

For $p > 0.5$, there are typically no merge events and we observe exchange events on the anti-diagonal. In Chapter 3 we predicted that the fluctuations of such an interaction are of order M in the TASIP (see Section 3.4.2). For the PASIP one can also measure such fluctuations as

$$E_2^2 := \left\langle |m_3(T) - m_1(0)|^2 \mathbb{I}\{m_1(0) > m_3(0) \text{ and } m_1(T) < m_3(T)\} \right\rangle . \tag{4.14}$$

Figure 4.6(a) shows that the fluctuations are all of order $\sqrt{M}$ for different p. Intuitively, we observe that the fluctuation after an interaction in the PASIP are the results of two parts: the same part as in the TASIP and an additional part caused by the partial asymmetry. The latter is crucial for investigating the coarsening dynamics. To further study these additional fluctuations, we map the interaction mechanism to a 2-dimensional random walk.

Each interaction is equivalent to a 2-dimensional random walk $S_1(t)$ with adapted jump rates in the (m_1, m_3) space. $S_1(t)$ is defined in the triangular lattice region $D_S = \{m_1 \geq 0, m_3 \geq 0, m_1 + m_3 \leq M\}$. The initial position of $S_1(0)$ is on the line $m_1 + m_3 = M - 1$ (one particle has jumped to site 2), and $S_1(t)$ can be absorbed by both the line $m_1 + m_3 = M$ (site 2 is empty again) and the origin (merge on site 2). At each state (m_1, m_3) within this region, the jump rates of $S_1(t)$

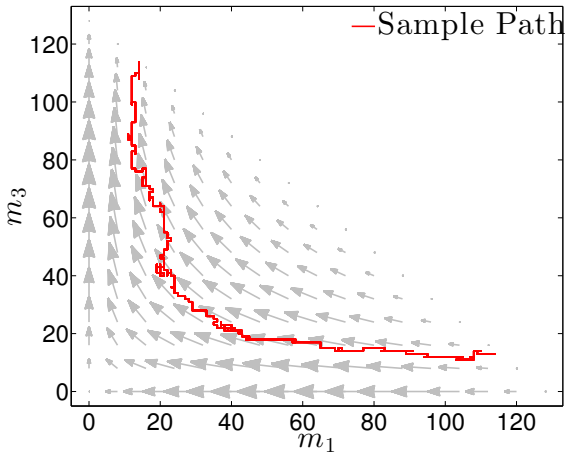

Figure 4.7: A sample path (in the up-left direction) of the interaction in the effective jump field of the interaction $M = 128$, $p = 0.75$. Sizes of arrows are proportional to effective jump rates, which is calculated as the vector norm of rates in Table (4.1) as $\sqrt{(R_1^+ - R_1^-)^2 + (R_3^+ - R_3^-)^2}$.

in the four directions are shown in Table 4.1.

Transition	Rate
$(m_1, m_3) \to (m_1 + 1, m_3)$	$R_1^+ = qm_2(d + m_1)$
$(m_1, m_3) \to (m_1 - 1, m_3)$	$R_1^- = pm_1(d + m_2)$
$(m_1, m_3) \to (m_1, m_3 + 1)$	$R_3^+ = pm_2(d + m_3)$
$(m_1, m_3) \to (m_1, m_3 - 1)$	$R_3^- = qm_3(d + m_2)$

Table 4.1: Transition rates of two-dimensional random walk equivalent to interaction between two clusters in the PASIP.

For a fixed M we can construct a vector field in D_S according to the average drift and an interaction event can be represented by a fluctuating path of $S_1(t)$ in this field (see Figure 4.7). In most cases, $S_1(t)$ is absorbed close to $(m_1(0), m_3(0))$. For the exchange events in $p > 0.5$ models, $S_1(t)$ walks to a site around $(m_3(0), m_1(0))$, i.e. the symmetric position of $S_1(0)$ with respect to the main diagonal. Notice, for the TASIP $S_1(t)$ can only move left or up while for the PASIP it can move in all four directions even if it has a left-up drift. Therefore, a typical interaction path in the PASIP accumulates more fluctuations than in the TASIP. The full distribution of the path is complicated and hard to predict. Here we only approximate the order of this additional fluctuation through a projection of $S_1(t)$ on the $-\boldsymbol{e}_{m_1} + \boldsymbol{e}_{m_3}$ direction, i.e. the anti-diagonal, where we only consider the interactions leading to the exchange

of clusters. After normalising the jump rates by $(m_1m_2 + m_2m_3)$, the projection is equivalent to a one-dimensional random walk of step size 1 defined on a finite lattice of size $\Theta(M)$ with jump rates p and q, and the initial state is determined by $S_1(0)$. Two clusters have exchanged positions when this random walk successfully travels to the other end of this lattice, with the drift $(p-q)$. The accumulated variance per step along the path is

$$\text{Var} = p \cdot 1^2 + q \cdot (-1)^2 - (p-q)^2 = 4pq. \tag{4.15}$$

The drift $(p-q)$ leads to $\Theta(M/(p-q))$ steps. Hence the accumulated fluctuation along the 1-dimensional walk is approximately of the order $\sqrt{4pqM/(p-q)}$. Therefore, we approximate the fluctuations of interactions between two clusters in the PASIP by

$$E_2 \simeq \Theta\left(\sqrt{\left(C_1 + \frac{4pq}{p-q}\right)m}\right), \tag{4.16}$$

where C_1 (as for $p = 1$) is a constant representing the inherent fluctuations as in the TASIP, and the rest is the fluctuations caused by partial asymmetry. Notice here we use notation m instead of M to indicate the typical size of a cluster, which under the mean-field assumption is of the same order as M and will be used in later analysis of the coarsening dynamics in Section 4.4. This result agrees with the linear relationship between E_2^2 and M shown in Figure 4.6, as well as the slope's dependence of p. The fitted numerical values of the fluctuation's pre-factor in Figure 4.6 are slightly different from our prediction (4.16), since in (4.16) we only considered the partial asymmetry's influences on $-\boldsymbol{e}_{m_1} + \boldsymbol{e}_{m_3}$ direction. But the argument used to derive (4.16) is valid and we will use this prediction to investigate coarsening regime later in Section 4.4.

Notice Equation (4.15) is derived under the condition that two clusters exchange positions. To compute the probability of such exchange event in one interaction, one could project $S_1(t)$ to the direction $-\boldsymbol{e}_{m_1} - \boldsymbol{e}_{m_3}$ and look at a 1-dimensional random walk with only one absorbing state. This is the subject of the following subsection.

Further analysis: probability of swap

During a single interaction, there is a possibility that two clusters remain at their positions rather than swap, and this is dominated by the event that the first particle jumping to site 2 is absorbed immediately by one of the clusters. This event can be mapped to the two dimensional random walk model where the walker starting from

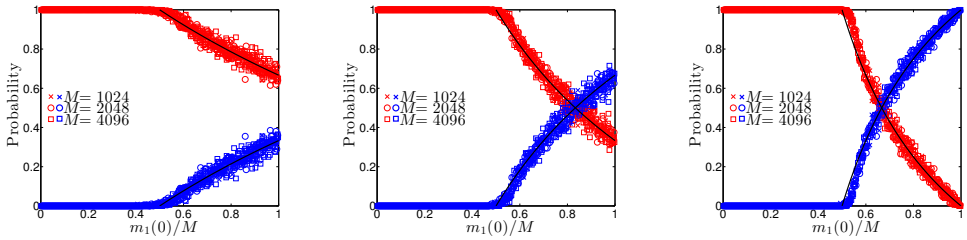

(a) $p = 0.6$ (b) $p = 0.75$ (c) $p = 1.0$

Figure 4.8: Probability of two clusters remaining in the same positions (red) or swapping/merging (blue) in the PASIP and the TASIP. Predictions (4.18) are shown as full lines. Each data point is the empirical probability over 200 realisations with fixed M and $m_1(0)/M$.

$m_1(0) + m_3(0) = M - 1$ jumps one step to the absorbing boundary, rather than travelling to the mirror point with respect to the main diagonal. To estimate this probability, we can project the two dimensional random walk on the $-\boldsymbol{e}_{m_1} - \boldsymbol{e}_{m_3}$ direction (main diagonal). Then the projection is a one dimensional random walk $S_2(t)$ with jump rate

$$\alpha = pm_1 + qm_3 \quad \text{and} \quad \beta = pm_3 + qm_1. \tag{4.17}$$

Since we are only interested in the probability of $S_2(t)$ returning to the absorbing boundary $m_1(t) + m_3(t) = M$, we can approximate α, β to be constants only depending on initial values $m_1(0)$ and $m_3(0)$ because this re-absorption happens relatively quickly. Define

$$P_k = \mathbb{P}\left[S_2(0) = k, S_2(T) = 0\right],$$

then the probability that the first particle on site 2 is absorbed immediately is given by P_1, with boundary condition $P_0 = 1$. The solution is simply $P_k = (\beta/\alpha)^k$ (see (B.3) Appendix B) and with (4.17) writing $x = m_1/(m_1 + m_3)$ we get

$$P_1 = \frac{p(1-x) + qx}{px + q(1-x)} \quad \text{and} \quad 1 - P_1 = \frac{(p-q)(2x-1)}{px + q(1-x)}. \tag{4.18}$$

Due to the positive drift $(p - q)$ in the interaction, the exchange event can only happen when $m_1(0)$ is larger or of similar size to $m_3(0)$ and therefore the above equations only holds for $x \in [1/2, 1]$. Simulations with different p are shown in Figure 4.8 and show a very good agreement with the prediction in (4.18). If clusters do not swap position in an interaction event, they will start interacting again after

a very short time until they finally swap. Since the probability of swapping is of order 1 as long as $m_1 > m_3$, a swap will occur after a finite number of interactions, the expectation of which is given by $1/(1 - P_1)$. Initial interaction before swapping decreases the size of the larger cluster m_1, but this does not create a significant bias in the interaction. After the swap, an analogous amount of small particle exchange takes place in the other direction increasing again the size of the larger cluster, before it eventually moves away from the smaller one. We see that the probability of swapping in a given interaction increases with p and is highest in the TASIP. This only affects the duration of the cluster interaction and not the number of particles exchanged, which is the main characteristic that determines the coarsening dynamics, as explained in the next section.

4.4 Coarsening and saturation

The previous section shows that the microscopic dynamics of clusters in the PASIP is similar to the TASIP. Recall the probabilities given in (4.3) (4.4) of an isolated cluster move one step successfully to the right and left respectively, the effective jumping rate to the right is then $(1 - \frac{q}{p})p\eta_x$ and proportional to its size, and clusters step to the left with a vanishing rate except for very small ones. When a larger cluster catches up with a smaller one, they only exchange a small number of particles given by (4.16) in an unbiased way. Compared with the TASIP, the speed of clusters is reduced but the fluctuations during each interaction are enhanced, and they have opposite effects on the coarsening process. In this section, we extend the arguments in Section 3.5 and give descriptions of coarsening and saturation dynamics of the PASIP in a heuristic way with mean-field approximations.

4.4.1 Dynamics in the coarsening regime

Let $m(t)$ denotes the typical size of a cluster in the coarsening regime, and $n(t)$ the typical number of clusters per unit volume, so $n(t)m(t) = \rho$. From (4.3), the effective speed of a cluster is $v(t) = (p - q)d_L m(t)$ where we omitted the small correction $(q/p)^m$ and the typical distance of two clusters is $s(t) = m(t)/\rho$. Then two clusters meet at rate

$$v(t)/s(t) = (p - q)\rho d_L. \tag{4.19}$$

We denote the unbiased exchange of particles in the TASIP as $\sqrt{C_1 m}$, where C_1 (for $p = 1$) is a constant and has been approximated as $C_1 \approx 2$ in Section 3.5. Considering the additional randomness caused by partial asymmetry (4.15), the

number of particles exchanged in the PASIP is of order $\sqrt{(C_1 + 4pq/(p-q))\, m(t)}$ and is unbiased. Thus if k is the number of exchanges required for one cluster to lose all of its particles, the accumulated variance should be equal to $m(t)^2$, i.e. $k(C_1 + 4pq/(p-q))m(t) = m(t)^2$, which implies $k = (C_1 + 4pq/(p-q))^{-1}m(t)$. Therefore, each cluster independently dissolves with rate $\frac{C_1+4pq/(p-q)}{m(t)}(p-q)\rho d_L$, which typically happens after a time Δt per unit volume given by the inverse of this expression. These death events effectively increase $m(t)$ by $\Delta m(t) = \frac{m(t)}{n(t)-1} - \frac{m(t)}{n(t)} \sim m(t)$ per unit volume due to the conserved total number of particles. This leads to

$$\frac{d}{dt}m(t) = \frac{\Delta m(t)}{\Delta t} = \left(C_1 + \frac{4pq}{p-q}\right)(p-q)\rho d_L \quad . \tag{4.20}$$

With initial condition $m(0) = \rho/n(0) = \rho/r$, where r (3.3) is the expected ratio of occupied sites after the nucleation regime which we fitted from data, the solution is simply

$$m(t) = \left(C_1 + \frac{4pq}{p-q}\right)(p-q)\rho d_L t + \frac{\rho}{r}, \tag{4.21}$$

and with $s(t) = m(t)/\rho$ we have

$$\frac{\sigma^2}{\rho^2} = \frac{m^2(t)}{s(t)\rho^2} = \left(C_1 + \frac{4pq}{p-q}\right)(p-q)d_L t + \frac{1}{r} \quad . \tag{4.22}$$

The right hand side above converges to (3.32) as $p \to 1$, and we keep the $(p-q)$ terms to emphasise that this equation does not hold for $p = q$ and the dynamics of SIP are fundamentally different from asymmetric cases. Similar to the TASIP, this analysis applies to infinite systems, given a fixed small parameter d, since there is no explicit system size dependence. For finite systems, it only applies for a certain scaling window (see Figure 4.9, 4.10) after which the system convergences exponentially to the stationary regime. This is shown in Figure 4.9 and 4.10, with agreements of data and theoretical predictions. Due to the competing effects of decreased cluster speed but increased interaction strength, the coarsening scaling laws look very similar (see Figure 4.10(a)), and the subtle differences are explained well by our theory (see Figure 4.10(b)).

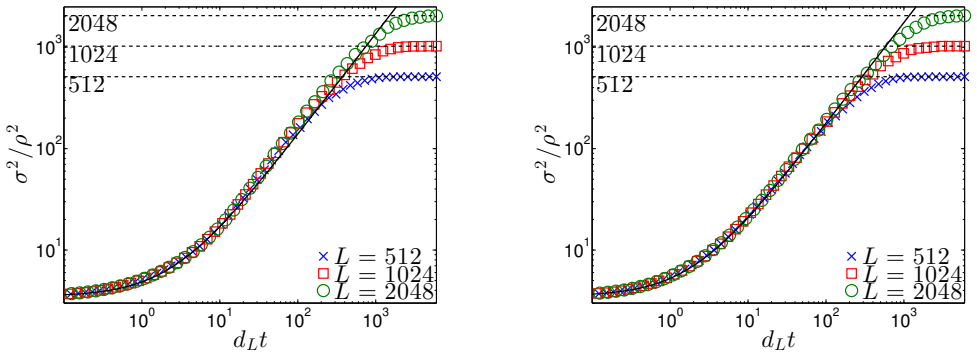

Figure 4.9: Coarsening dynamics in PASIP. (a): Data of PASIP with fixed $p = 0.6$, $\rho = 2$ compared to the prediction (4.22) shown as a full line with constants $C_1 = 2$ and initial condition $r = 0.2851$. (b): Data for PASIP with fixed $p = 0.75$, $\rho = 2$ compared to the prediction (4.22) shown as a full line with constants $C_1 = 2$ and initial condition $r = 0.2856$. Data points are averaged over 200 realisations. Errors are bounded by the size of symbols.

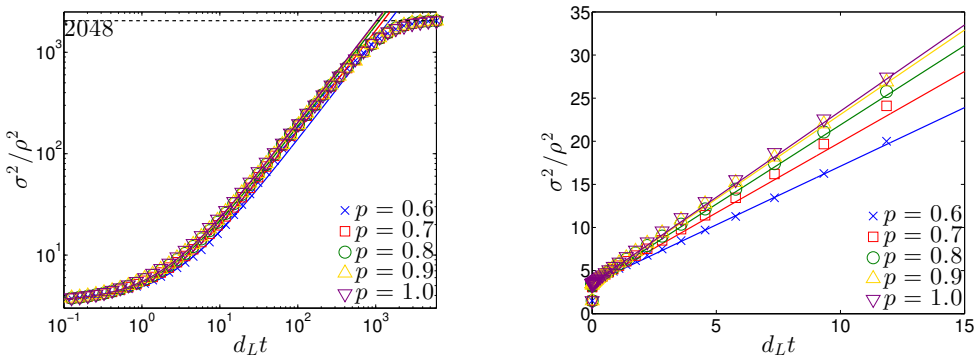

Figure 4.10: Data of a PASIP with fixed $L = 2048$, $\rho = 2$ compared to prediction (4.22). Predictions with different p are shown as full lines with the same colour of corresponding data, and $C_1 = 2$, $r = 0.2851$. (a): Data and prediction for full simulations. (b): Data and predictions in coarsening regime window. Data points are averaged over 200 realisations. Errors are bounded by the size of symbols.

Comparison with SIP

Recall the coarsening dynamics of SIP derived in Section 3.5

$$\frac{\sigma^2(t)}{\rho^2} = \sqrt{2C_s d_L t + \left(3 + \frac{1}{\rho}\right)^2}. \qquad \text{(3.34 revisited)}$$

Compared to (4.22), one can see the different scaling behaviour in the coarsening regimes for the SIP and the PASIP. Indeed, the asymptotic linear scaling in (4.21) holds even for p relatively close to $1/2$, as confirmed in Figure 4.11. However, simulations in this figure also indicate that in an early time window the scaled second moment σ^2/ρ^2 in the PASIP and the SIP follow the same function, which implies that the early coarsening dynamics in both models have similar behaviour. The reason is that for early stages in the coarsening regime, the typical size of a cluster $m(t)$ is small so the diffusion effects cannot be neglected. Indeed, the rate of two clusters meeting in the PASIP can be written as $d_L/s(t)^2 + v(t)/s(t)$, with an additional diffusive contribution $d_L/s(t)^2$. Note that in the beginning of the coarsening regime $m \simeq \rho/r$ and $s \simeq 1/r$, so with (4.19) $d_L/s(t)^2$ and $v(t)/s(t)$ are of the same order if $\rho \simeq \Theta(1)$. After some time, the typical distance $s(t)$ grows and the cluster meeting rate is only dominated by $v(t)/s(t)$ term. So there exists a critical value s^* below which the dynamics in the PASIP are highly affected by the diffusive contribution and thus similar to the SIP, and we can estimate the corresponding critical $\sigma^{*2}(t)$ as follows,

$$\frac{d_L}{s^{*2}} = \frac{v(t)}{s^*} \Rightarrow s^* = \frac{1}{\sqrt{\rho(p-q)}}.$$

Then with $\rho s^* = m^*$ and $n^* = \frac{\rho}{m^*}$ we have the (scaled) critical observable

$$\frac{\sigma^{*2}}{\rho^2} \simeq \frac{1}{\sqrt{\rho(p-q)}}. \qquad (4.23)$$

Figure 4.11 shows the numerical results that confirm this prediction.

4.4.2 Saturation and stationarity

Relaxation time scale

The coarsening and saturation regimes can be described through a relaxation time scale. Recall the derivation of the relaxation time scale $\tau_L^a = L/d_L$ for the TASIP (3.28) and $\tau_L^s = L^2/d_L$ for the SIP (3.29) in Section 3.4. One can apply the same

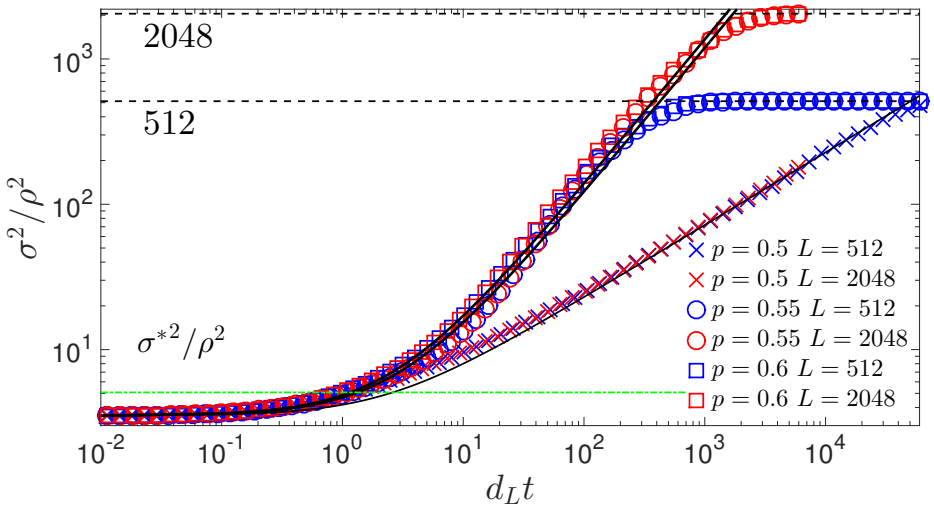

Figure 4.11: Data of PASIP and SIP with fixed $\rho = 2$. The two full lines above are prediction (4.22) with corresponding p and fitted $r = 0.2858$ for $p = 0.55$ and $r = 0.2866$ for $p = 0.6$ respectively. The full line below is prediction (3.34) with $r = 0.2857$ (c.f. (3.15)) and fitted constant $C_s = 2.5888$. The dashed horizontal line in green is the prediction of critical value σ^{*2}/ρ^2 (4.23) for $p = 0.6$, above which the PASIP and the SIP perform different dynamics. Data points are averaged over 200 realisations. Errors are bounded by the size of symbols.

method to derive τ_L^p for partially asymmetric systems as follows. Consider the situation where only two clusters with size of order ρL interact on the lattice. The previous section indicates that the relative speed of them is of order $d_L(p-q)\rho L$, which leads to the average time between two encounters being of order $L/(d_L(p-q)\rho L) \sim 1/(\rho d_L(p-q))$. And since every interaction leads to an unbiased exchange of order $\sqrt{\rho L(C_1 + 4pq/(p-q))}$ particles, it typically takes $\rho L/(C_1 + 4pq/(p-q))$ encounters to achieve a macroscopic change. Therefore, the relaxation time scale of the PASIP is

$$\tau_L^p = \frac{L}{C_p d_L} \simeq \frac{L}{(p-q+2pq)d_L}, \tag{4.24}$$

where the parameter C_p is the pre-factor in partially asymmetric dynamics (4.21) (with a constant 2 difference in order to agree $\tau_L^p \to \tau_L^a$ as $p \to 1$),

$$C_p = \frac{1}{2}(p-q)\left(C_1 + \frac{4pq}{p-q}\right) \simeq p - q + 2pq. \tag{4.25}$$

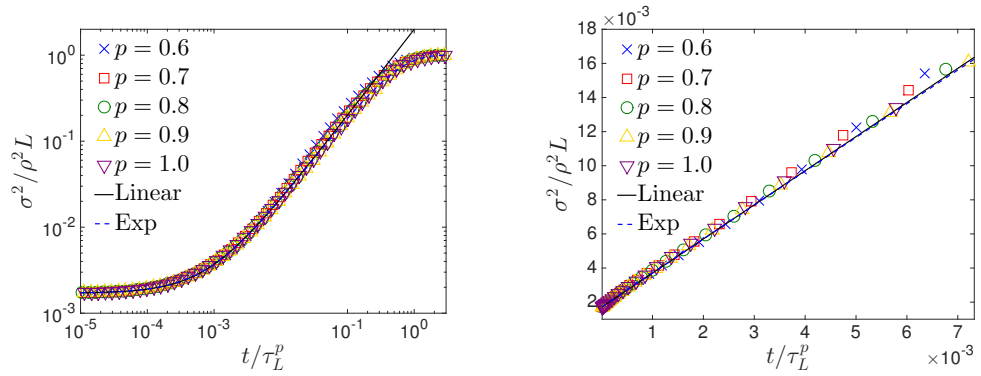

(a) (b)

Figure 4.12: Data of PASIP with fixed $L = 2048$, $\rho = 2$ compared to linear prediction (4.26) shown as full lines with fitted initial condition $r = 0.2851$. Exponential convergence function (3.35) for finite systems are shown as dashed lines (with constant $C' = 2$) for comparison. (a): Data and prediction for full simulations. (b): Data and predictions in coarsening regime window. Data points are averaged over 200 realisations. Errors are bounded by the size of symbols.

Indeed, τ_L^p is essentially the same time scale that a typical cluster needs to grow to size ρL following (4.21). With τ_L^p and $C_1 = 2$, we can rewrite (4.22) as

$$\frac{\sigma^2}{\rho^2 L} = 2\frac{t}{\tau_L^p} + \frac{1}{rL}, \tag{4.26}$$

which holds for the coarsening window (see Figure 4.12).

Exponential convergence

Similar to TASIP and SIP dynamics, the derivation of the linear scaling law (4.22) does not involve explicitly a system size dependence, therefore it also holds on infinite lattices with a fixed small parameter d_L. On a finite lattice, the systems will saturate after the coarsening time window and converge to stationarity exponentially. Recall the exponential saturation of systems discussed in Section 3.5.2, where the behaviour of the observable $\sigma^2(t)/(\rho^2 L)$ can be described by equation (3.35):

$$\frac{\sigma^2(t)}{\rho^2 L} \simeq 1 - e^{-C't/\tau_L} \quad \text{as } t \to \infty\ , \tag{3.35 revisited}$$

where C' is a constant with estimates $C'_s \approx 10$ for the SIP and $C'_a \approx 2$ for the TASIP. Indeed, C'/τ_L is the spectral gap of the generator of the system, which describes the exponential convergence to equilibrium of a finite system according to (3.35).

Since the exact form of a spectral gap in an interacting particle systems

is generally difficult to derive and the finite size effect is not our main interest, here we only give numerical results of the exponential convergence with a heuristic understanding of the p-independence of the dynamics. Recall the derivation of the scaling law in the coarsening regime (4.22), where we started from studying a typical cluster. One major differences between the saturation regime and the coarsening regime is that in the coarsening regime, there are $n(t) \gg 1$ clusters on the lattice, and they provide enough encounters for a cluster to grow. However, in the saturation regime there are only a few clusters and the dynamics are typically dominated by competitions between two clusters of similar size. Consider the situation where only two clusters m_1, m_2 are left on the lattice and both contain order ρL particles, and denote $\delta m(t) = |m_1(t) - m_2(t)|$ as the difference of two clusters, which is now $\delta m(t) \simeq \Theta(1)$. Then the rate of encounters is of the order

$$\frac{v}{s} = \frac{d_L(p-q)(|m_1 - m_2|)}{L} \simeq \frac{d_L(p-q)\delta m(t)}{L}, \tag{4.27}$$

where v is the relative speed of m_1, m_2 and this rate is order L slower than the rate (4.19) in the coarsening regime. We used (4.16) to estimate the fluctuations of two clusters' interactions in the coarsening regime, where this fluctuation consists of two parts, one is inherent and the other is caused by the partial asymmetry,

$$E_2 \simeq \Theta\left(\sqrt{\left(C_1 + \frac{4pq}{p-q}\right) m}\right). \tag{4.16 revisited}$$

Indeed, the term m in this prediction should be understood as the differences between the sizes of the two interacting clusters, i.e. $\delta m(t)$. In the coarsening regime, we can replace it with the size of a typical cluster m since there is enough encounters and interactions between different clusters. However, when only two similar size clusters remain, this argument is not valid since the size difference between the two clusters is of order 1 and much smaller than either m_1 or m_2. Therefore in (4.16) the order of fluctuation should be adapted to $\sqrt{(C_1 + 4pq/(p-q))\,\delta m(t)}$, which can be approximated as $\sqrt{C'\delta m(t)}$ compared with m_1, m_2, both of which are order ρL. In other words, the two similar size clusters not only meet less frequently, but also exchange fewer particles when they meet, compared to the coarsening dynamics. This scenario dominates the saturation regime and will only be broken if the fluctuations leads to an significant difference between the sizes of the clusters, i.e. where $\delta m(t)$ grows to the order of $1/(p-q)$. This scenario can be studied following the coarsening dynamics, and the only difference is now the death event is no longer the dissolution of a cluster but just the growth of $\delta m(t)$ from order 1 to

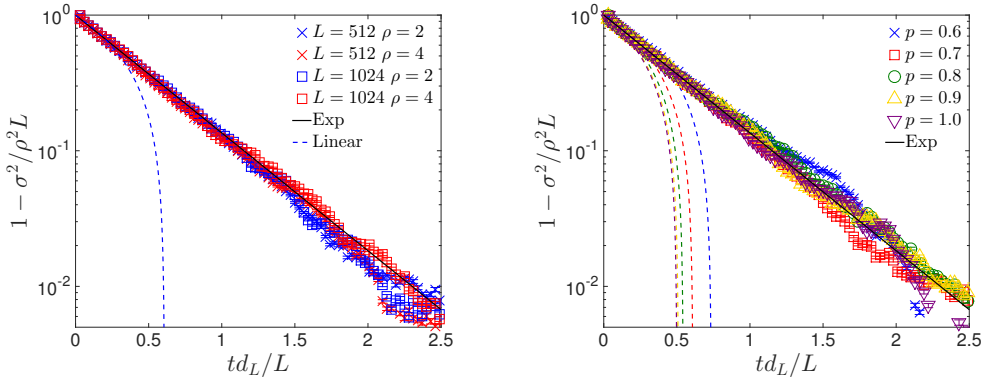

(a) (b)

Figure 4.13: Exponential relaxation in the saturation regime for PASIP with (a) fixed $p = 0.7$ in different system sizes, and (b) fixed $L = 512$ with different p. The predictions (3.35) are shown as full lines with constant $C' = 2$. The dashed lines are the linear coarsening scaling law (4.26) for comparison. Data points are averaged over 200 realisations. Errors are bounded by the size of symbols.

order $1/(p-q)$. Analogously to the derivation of (4.20), the number of encounters required is $\delta m(t)/C'$ and the time Δt of such an event is then $\frac{\delta m(t)}{C'}\frac{s(t)}{v(t)}$. Until $\delta m(t)$ grows to the order $1/(p-q)$ we have the following differential equation

$$\frac{dm}{dt} = \frac{\delta m(t)}{\Delta t} = \delta m(t)\frac{C'}{\delta m(t)}\frac{d_L(p-q)\delta m(t)}{L} \simeq C'\frac{d_L}{L},$$

where we used $\delta m(t) \simeq 1/(p-q)$. The above changing rate of $m(t)$ is much slower than that of (4.20) in the coarsening regime and only depends on p very weakly though the constant C'. Since such dynamics dominate the saturation regime, we predict the exponential convergence is independent of p in the PASIP, which agrees well with simulation results as shown in Figure 4.13 where the simulation data strongly suggests $C' = 2$ independently of p. Notice the time scale used in Figure 4.13 is the p-independent scale L/d_L instead of τ_L^p (4.24).

So far the above analysis only considers the dominating dynamics of two clusters of the same size, which is not enough to give a precise description of the exact spectral gap C'/τ_L. Investigating the exact form of spectral gaps of the inclusion process itself is an interesting question, but as far as we know there are no rigorous results yet. Spectral gap and exponential convergence on nearest neighbour particle systems was first studied by Liggett in [111]. Recently there has been a series of results on certain classes of zero-range processes [112, 113, 114, 115] and exclusion processes [116], which can be a starting point for studies on the inclusion processes.

4.5 Further study and summary

4.5.1 Weakly asymmetric inclusion process

An interesting aspect of the PASIP we have not covered in this chapter is the case when p and q are close such that $p-q = \Theta(1/L)$, namely the weakly asymmetric inclusion process (WASIP). Numerical results in Figure 4.14 illustrate that dynamics in WASIP contain features of both the SIP and the PASIP/TASIP models. Comparing Figure 4.14(a) and Figure 4.3 one can see that interactions of the WASIP are very similar to the SIP, where no cluster swap is observed except for very late times. Figure 4.14(b) shows the coarsening dynamics of the WASIP follows the SIP in the coarsening window, then converging to stationarity following a similar dynamics as in the PASIP. Intuitively, we can understand this through the movement of isolated clusters. Recall the effective speed of isolated clusters in the PASIP is $d_L(p-q)m$. In the WASIP, this speed is slowed down to the order of d_L/L, and so drift and diffusion of clusters are on the same scale. Therefore, in the coarsening regime, where encounters of clusters is rich, the dynamical behaviour of the WASIP is similar to those in the SIP. However, after this coarsening regime, there are only a few clusters left on lattice cannot provide enough encounters through diffusion, and the asymmetry $p-q$ leads to a drift of cluster movement. Therefore, the interaction events are more evenly distributed over time as compared to the SIP due to the weak drift, which leads to more frequent encounters of clusters. Thus, the WASIP switches to the PASIP-like behaviour in the late stages of the coarsening regime and then saturates into the stationary state exponentially as discussed in the previous section.

There has been a large volume of publications studying weakly asymmetric exclusion process (WASEP) (e.g. [101, 102, 105, 106, 107, 117]), where the weak asymmetry was shown to provide a crossover between asymmetric and symmetric dynamics, and provides an insight into further study on the WASIP and its relationship with the PASIP and the SIP.

4.5.2 Cluster size distribution

A recent study in [118] has considered a coarsening process on a one-dimensional cell complex, where cells grow with a speed proportional to the size difference of neighbouring cells. In this paper, the authors predict the system has an exponential convergence to the stationary state as e^{-2t}, which could be another approach to further understanding the saturation regime in the inclusion process. We apply the idea of this paper to our model and find that at least the numerical simulation shows

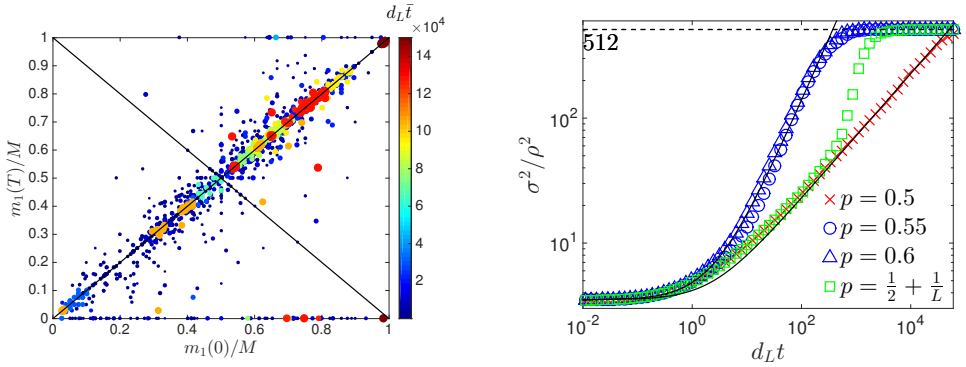

(a) (b)

Figure 4.14: Data from simulations of the Weakly Asymmetric Inclusion Process (WASIP) with fixed $L = 512$, $\rho = 2$. (a): Scatter plot of normalised $m_1(0)/M$ and $m_1(T)/M$ in a single realisation of a full trajectory until a complete condensate is formed. Data are generated by one full simulation. M may differ for each interaction event. Size of data points scales with M, the total number of particles involved in the interaction. Colour of data indicates the time of observation. Two diagonals are shown as full lines. See Figure 4.3 for data on the PASIP and the SIP. (b): Coarsening dynamics of the WASIP (data points in green), where data and predictions for the PASIP (4.22) and for the SIP (3.34) are shown as full lines for comparison. Data points are averaged over 200 realisations. Errors are bounded by the size of symbols.

very similar results. In Figure 4.15 we measured the histograms of the normalised cluster sizes when the system first saturates to n clusters, and the cluster size shows an exponential distribution. This corresponds to a uniform split of the total mass into n clusters, which is the simplest possible ansatz and turns out to be a good approximation. Therefore, when the system first reaches a state with n clusters, we can construct the typical cluster as the following: first generate $n-1$ uniformly i.i.d random variables x_1, x_2,...,x_{n-1} on the interval $[0, N]$ to separate the total particles into n clusters, and we take the first one as the typical cluster and its size is given by $X := \min\{x_1, x_2, ..., x_{n-1}\}$. It is easy to show that $\mathbb{P}(X \leq x) = 1 - \left(\frac{L-x}{L}\right)^{n-1}$, which leads to the following equation with normalised $x \mapsto x/L$

$$\mathbb{P}(X > x) = (1-x)^{n-1}, \tag{4.28}$$

and is supported by simulation results in Figure 4.15. It would be interesting to study this further, in particular to understand the exact form of the saturation dynamics in finite systems.

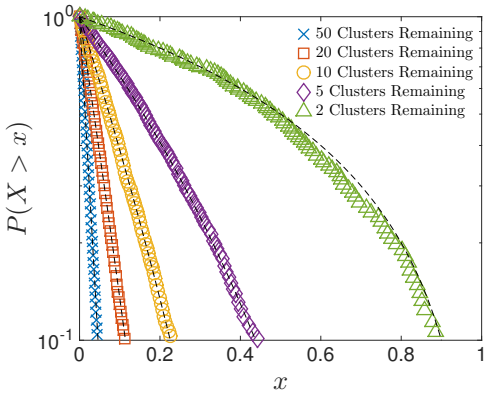

Figure 4.15: Histogram of cluster sizes in a TASIP model when the number of clusters left on the lattice are $n = 50, 20, 10, 5, 2$. The black dashed lines are predictions (4.28) with $n = 50, 20, 10, 5, 2$ respectively.

4.5.3 Summary

In this Chapter we extended results in Chapter 3 to partially asymmetric dynamics in the thermodynamic limit. Due to the partial asymmetry, dynamics of isolated clusters are similar to the TASIP but with slowed average speed (4.3). The interaction in the PASIP is complicated since particles are allowed to move against the drift. We study it through a detailed numerical approach and derive an approximation of the exchanged number of particles during an interaction (4.16). As a result, the second moment $\sigma^2(t)$ follows a p-dependent scaling law (4.22) in the coarsening window, and then convergences to stationarity exponentially with respect to the same p-independent function (3.35) as in the TASIP. As in Chapter 3, our heuristic description has been confirmed by extensive simulations and is based on the analysis of the dynamics of a typical cluster and interaction with others under a mean-field approximation.

Chapter 5

Inclusion Processes in Higher Dimensions

5.1 Introduction

In this chapter, we apply the analysis from previous chapters to inclusion processes defined on two dimensional lattices, with focus on the dynamics of condensation in the thermodynamic limit. Results of inclusion processes in the stationary states as we reviewed in Chapter 2 are independent of dimension and therefore guarantee the condensation in the two-dimensional models under certain conditions. However, almost all recent results on non-equilibrium inclusion processes and related models [31] focus on one-dimensional systems, particularly for the dynamics of condensation (see review in Section 2.3.2). A few other two-dimensional lattice gas models have been studied extensively, for example the asymptotic behaviour of the simple exclusion process has been investigated rigorously (see [119, 120] and references therein); a generalised stationary product measure result of ZRP defined in two and three dimensional spaces is studied in [121]; the super-diffusivity of a two-dimensional energy model, which is the dual process to the inclusion process, has been studied in [122] as well. In this chapter we will show that the heuristic method based on a typical cluster as discussed in previous chapters still applies for inclusion processes defined on two-dimensional lattices, and we will also show the symmetric inclusion process is closely related to the classic coalescing random walk model, in particular for the high dimensional cases.

In the rest of this chapter, we define the inclusion process $(\boldsymbol{\eta}(t) : t \geq 0)$ on a two-dimensional square lattice Λ_L of L sites with periodic boundary conditions, i.e. a two-dimensional torus of $K \times K = L \subset \mathbb{N}$ sites, where K is the number of sites

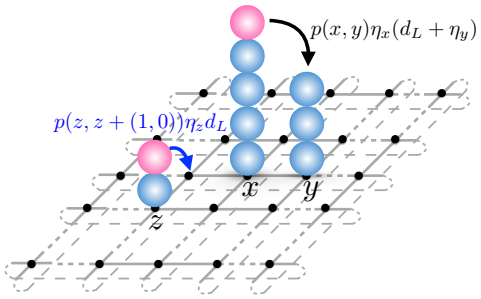

Figure 5.1: Illustration of the dynamics of two-dimensional inclusion process defined on a 2D torus.

on each side. The total number of particles is denoted by N, and configurations are still $\boldsymbol{\eta} = (\eta_x : x \in \Lambda_L) \in X_L$ where $\eta_x \in \mathbb{N}$ is the number of particles at site $x \in \Lambda_L$ and the state space is $X_L = \mathbb{N}^L$. The dynamics are still defined by generator (2.27) acting on bounded test functions $f \in C^b(X)$,

$$\mathcal{L}_L f(\boldsymbol{\eta}) = \sum_{x,y\in\Lambda_L} p(x,y)\eta_x(d+\eta_y)(f(\boldsymbol{\eta}^{x,y}) - f(\boldsymbol{\eta}))\,, \qquad \text{(2.27 revisited)}$$

where $\boldsymbol{\eta}^{x,y}$ is the configuration after moving one particle from site x to site y and we scale the diffusion parameter $d = d_L$ with system size. Analogously to one-dimensional inclusion processes, we define three types of nearest-neighbour dynamics on two dimensional lattice :

(i) Two-dimensional Symmetric (2DSIP): $p(x,y) = \frac{1}{4}(\delta_{y,x+(1,0)}+\delta_{y,x-(1,0)}+\delta_{y,x+(0,1)}+\delta_{y,x-(0,1)})$.

(ii) Two-dimensional Partially Asymmetric (2DPASIP): $p(x,y) = p_1\delta_{y,x+(0,1)} + p_2\delta_{y,x-(0,1)} + p_3\delta_{y,x-(1,0)} + p_4\delta_{y,x+(1,0)}$, where $p_i \in [0,1)\ \forall i = 1,2,3,4$, and $\sum_{i=1}^4 p_i = 1$.

(iii) Two-dimensional Totally asymmetric (2DTASIP): $p(x,y) = \delta_{y,x+z}$, for some fixed $z \in \{(1,0),(0,1),(-1,0),(0,-1)\}$.

Throughout this chapter we focus on the 2DSIP, since the 2DTASIP is just K parallel one-dimensional TASIP. For 2DPASIP, it also has a drift in the direction $(p_4 - p_3, p_1 - p_2)$ which is determined by the differences of jump rates in both horizontal and vertical directions. Though particles are restricted to move on the lattice for each jump, macroscopically they will follow the drifted direction, in particular for the coarsening regime where clusters are dispersed, and therefore the 2DPASIP

is merely parallel one-dimensional PASIP in the drifted direction where particles can jump between these parallel orbits with small probabilities. This chapter is organised as follows. In Section 5.2 we introduce the stationary measures and the dynamical regimes, then look at the dynamics in the nucleation regime. In Section 5.3 we investigate the coarsening regime following the heuristic method used in one-dimensional models, and then discuss the link between the two-dimensional inclusion process and the coalescing random walk model. In Section 5.4 we summarise both methods used and introduce the potential aspects for further study of inclusion process in higher dimensions.

5.2 Condensation and nucleation dynamics

5.2.1 Stationary distribution, condensation and dynamics

Recall the general results of stationary distributions reviewed in Section 2.3.2, we can apply them to the two-dimensional inclusion processes and get the same formula. In [74, Theorem 2.1] it was proved that for an inclusion process defined on a spatial homogeneous lattice (including the 2-dimensional torus defined above), the product measure in the form

$$\nu_\phi^L[d\boldsymbol{\eta}] = \prod_{x\in\Lambda_L} \bar{\nu}_\phi(\eta_x)d\boldsymbol{\eta} \qquad \text{with } \bar{\nu}_\phi(n) = \frac{1}{z(\phi)}w(n)\phi^n \ ,$$

where

$$w(n) = \frac{\Gamma(d_L+n)}{n!\Gamma(d_L)} \ , \ \text{ and } \ z(\phi) = \sum_{k=0}^{\infty} w(k)\phi^k = (1-\phi)^{-d_L}$$

is a stationary measure if $p(x,y)$ is doubly stochastic modulo a constant,

$$\sum_{j\in\Lambda_L} (p(i,j)-p(j,k)) = 0 \quad \text{for all } \ i,k\in\Lambda_L.$$

Obviously $p(x,y)$ defined in this chapter fulfils this condition, and therefore we can apply results reviewed in Section 2.3.2 to two-dimensional inclusion processes.

Analogous to the one-dimensional inclusion process, the condensation phenomenon can be observed in two-dimensional models under the condition of weak diffusion, where a rigorous proof has been given in [74, Theorem 4.1] for homogeneous systems. Recall the asymptotic behaviour of the partition function $Z_{L,N}$ reviewed in Section 2.3.3 which is independent of the dimension. In addition, the rigorous results in [42] based on one-dimensional models can be easily extended to two-dimensional cases since the stationary measures are of the same form. We

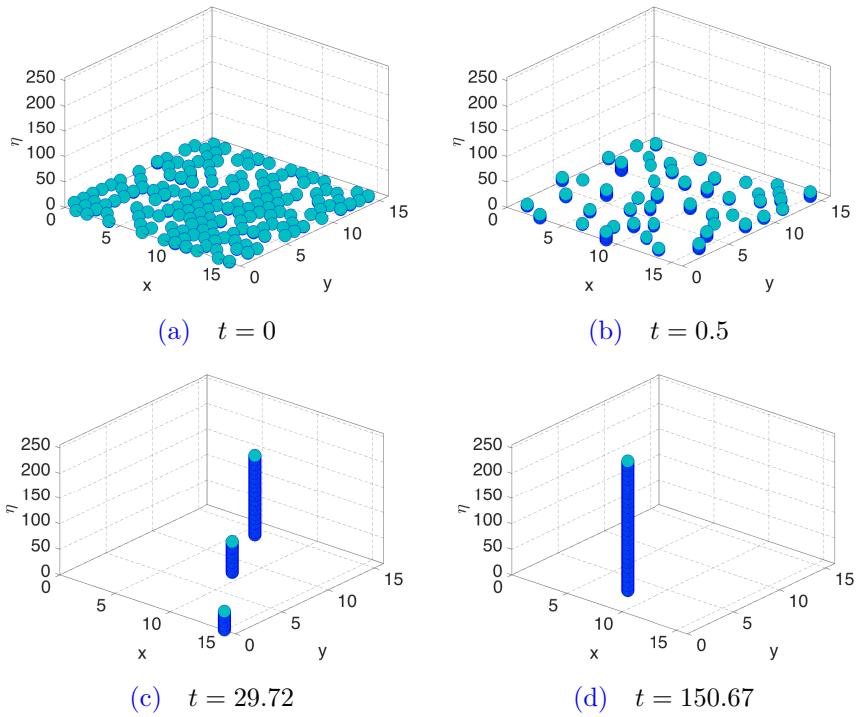

(a) $t = 0$ (b) $t = 0.5$

(c) $t = 29.72$ (d) $t = 150.67$

Figure 5.2: Snapshots of 2DSIP with $L = 256$, $\rho = 1$ for (a) $t = 0$, (b) $t = 0.5$, (c) $t = 29.72$, (d) $t = 150.67$. After the fast nucleation regime, clusters slowly merge to a few condensates and finally saturate to the single complete condensate.

conclude that in a finite two-dimensional inclusion process a complete condensation can be observed if the diffusion rate is weak enough as $d_L \ll 1/L$ (see snapshots of an example system in Figure 5.2). To keep consistency with previous chapters, we consider the thermodynamic limit (2.32) for two-dimensional inclusion process

$$L, N \to \infty \ , \ d_L \to 0 \quad \text{such that} \quad \frac{N}{L} \to \rho > 0, \quad \text{and} \quad d_L L \to 0, \quad \text{(2.32 revisited)}$$

where we scale $d_L = L^{-\gamma}$ with $\gamma > 1$. And in the simulations we use $d_L = \frac{1}{L^2}$ as in the one-dimensional models but have checked the validity of our results also for other scaling of d_L.

Our interests again focus on the dynamics of the formation of the complete condensation in the two-dimensional model from a translation invariant initial condition in the above thermodynamic limit. In higher dimensions we expect the asymmetric and the symmetric systems to have the same scaling, as is discussed later in more details. The generator of the 2DSIP with nearest jumps can be written

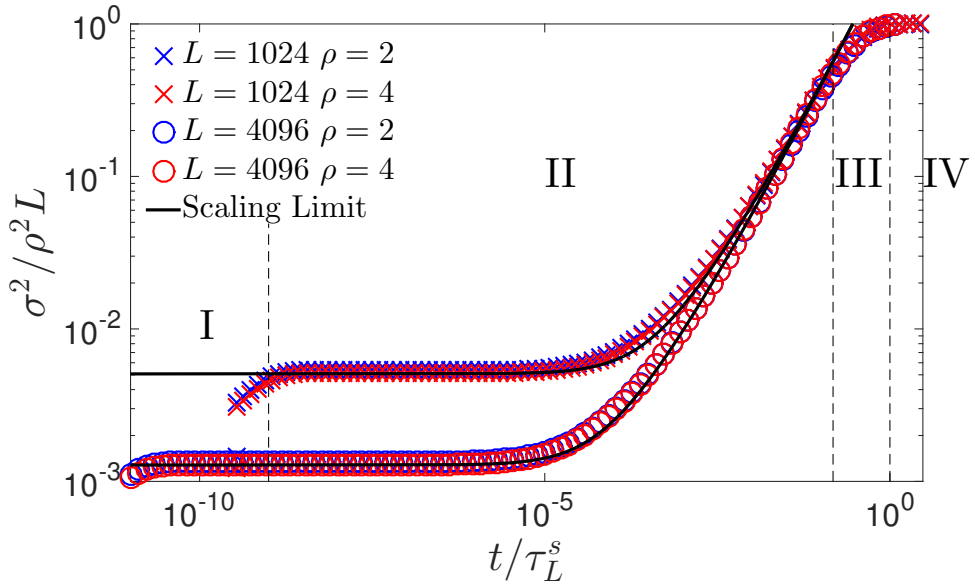

Figure 5.3: Illustration of dynamical regimes of 2DSIP in different systems. I. Nucleation Regime. II. Coarsening Regime. III. Saturation Regime. IV. Stationary Regime. The normalised observable $\sigma^2(t)/\rho^2 L$ is plotted against scaled time t/τ_L^s with $\tau_L^s = L\log(L)/d_L$ (5.11) and $d_L = 1/L^2$. Full lines are prediction (5.18) (see details later in Section 5.3.3) with fitted parameter $C_{s2} \approx 6.9040$ for $L = 1024$ and $C_{s2} \approx 7.0837$ for $L = 4096$, respectively. Data points are averaged over 200 simulations and errors are bounded by the size of symbols.

explicitly as

$$\begin{aligned}\mathcal{L}_L f(\boldsymbol{\eta}) &= \sum_{x\in\Lambda_L} \frac{1}{4}\eta_x(d_L + \eta_{x+(1,0)})(f(\boldsymbol{\eta}^{x,x+(1,0)}) - f(\boldsymbol{\eta})) \\ &+ \frac{1}{4}\eta_x(d_L + \eta_{x+(-1,0)})(f(\boldsymbol{\eta}^{x,x+(-1,0)}) - f(\boldsymbol{\eta})) \\ &+ \frac{1}{4}\eta_x(d_L + \eta_{x+(0,1)})(f(\boldsymbol{\eta}^{x,x+(0,1)}) - f(\boldsymbol{\eta})) \\ &+ \frac{1}{4}\eta_x(d_L + \eta_{x+(0,-1)})(f(\boldsymbol{\eta}^{x,x+(0,-1)}) - f(\boldsymbol{\eta})),\end{aligned} \tag{5.1}$$

for any test function $f \in C^b(X)$. Following the idea in previous chapters, we again qualitatively divide the whole condensation formation process into four different regimes: the nucleation regime, the coarsening regime, the saturation regime and the stationary regime (See Figure 5.3). To keep consistency with previous chapters, we again choose $\sigma(t)^2 = \mathbb{E}[\eta_x^2(t)](2.4)$ as the observable to capture the time evolution of the condensed phase and assume translation invariant initial condi-

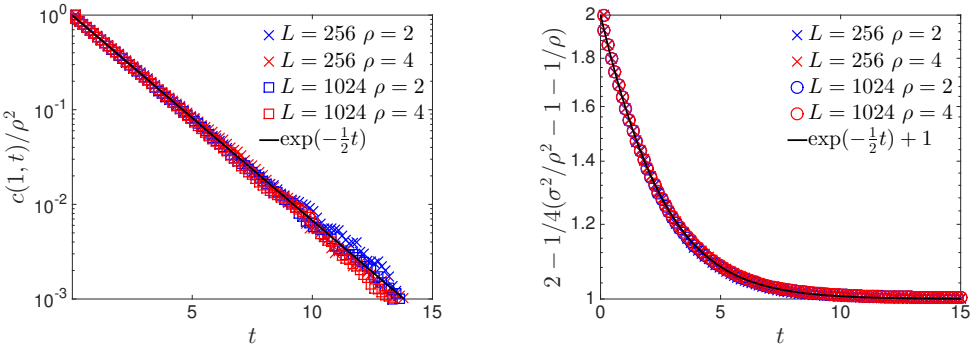

(a) (b)

Figure 5.4: Exponential behaviour of $c(1,t)$ (5.5) and $\sigma^2(t)$ (2.4) for the 2DSIP in the nucleation regime. (a) Exponential decay of $c(1,t)/\rho^2$ as given in (5.6). (b) Exponential convergence of $\sigma^2(t)/\rho^2$ as given in (5.9). Since the fluctuations of σ^2/ρ^2 around its limit could be negative and explore in a log-plot, we plot an equivalent form of (5.9), $2 - \frac{1}{4}\left(\frac{\sigma^2}{\rho^2} - 1 - \frac{1}{\rho}\right) = \exp(-\frac{1}{2}t) + 1$, to avoid this computational error. Data points are averaged over 200 realisations. Errors are of the order 10^{-4}.

tions. In numerical results in this chapter we measure $\sigma^2(t)$ with the spatial average $\left\langle 1/L \sum_{x=1}^{L} \eta_x^2(t) \right\rangle$ as usual, where the $\langle \cdot \rangle$ denotes averaging over a large number of realisations. We also consider initial condition where N particles are placed uniformly and independently on the lattice, which gives $\boldsymbol{\eta}(0)$ a symmetric multinomial distribution with N trials and success probability $1/L$. Then for $N/L \to \rho$ the occupation numbers are asymptotically independent Poisson random variables $\eta_x(0) \sim \text{Poi}(\rho)$, with the second moment $\sigma^2(0) \simeq \rho(1+\rho)$.

5.2.2 Nucleation regime

The nucleation regime starts from the initial distribution, which we take to be a uniform multinomial distribution for simplicity, and it ends when no particles reside on neighbouring sites. Recall the study of the nucleation regime in the SIP model in Section 3.3.2 where we gave equations in closed form to describe the exponential behaviour of observable $\sigma^2(t)$. As indicated in Section 3.3.2, the reason behind the closed equations is that the symmetric inclusion process is a self-dual process (see more details in Chapter 6). This also holds for the 2DSIP and therefore we can apply the same ideas as in Section 3.3.2 to analyse the dynamics in this regime. For the simplicity of notation, in the rest of this chapter we denote the nearest neighbours

of a given site on the lattice as

$$A_x := \{x + (1,0), x + (-1,0), x + (0,1), x + (0,-1)\}, \quad \forall x \in \Lambda_L, \tag{5.2}$$

and then we can characterise the nucleation regime through the hitting time

$$T := \inf \left\{ t > 0 \ : \ \sum_{x \in \Lambda_L} \sum_{y \in A_x} \eta_x(t)\eta_y(t) = 0 \right\}. \tag{5.3}$$

Under the condition of weak diffusion $d_L \ll 1/L$, this regime is dominated by the inclusion rate and finishes in a very short time compared with coarsening or saturation regimes. Therefore, we focus on the dynamics rather than the specific time scales of this stopping time. Similar to the nearest-neighbour product $c(1,t)$ defined in (2.5) for one-dimensional models, we use $c(1,t)$ with a slight abuse of notation in this chapter to denote the product of η_x with one of its neighbours as

$$c(1,t) := \mathbb{E}[\eta_x(t)\eta_y(t)], \quad \text{for some} \quad x \in \Lambda_L,\, y \in A_x, \tag{5.4}$$

which is x-independent and also y-independent due to the homogeneity of the initial distributions and the symmetric dynamics. It is equivalent to choose $c(1,t) = \frac{1}{4}\sum_{y \in A_x} \mathbb{E}[\eta_x(t)\eta_y(t)]$ but we keep the above definition for simplicity. Therefore, under our nearest-neighbour setting we write (5.4) as

$$c(1,t) := \mathbb{E}[\eta_x(t)\eta_{x+(1,0)}(t)], \quad \text{for some} \quad x \in \Lambda_L, \tag{5.5}$$

without loss of generality and the uniform initial condition implies $c(1,0) = \rho^2$ and $c(1,t) \to 0$ with increasing time in the nucleation regime. We then can apply the generator (5.1) to the test function $f(\boldsymbol{\eta}) = \eta_x\eta_{x+(1,0)}$ for some $x \in \Lambda_L$ and get

$$\mathcal{L}(\eta_x\eta_{x+(1,0)}) = -\frac{1}{2}\eta_x\eta_{x+(1,0)} + \Theta(d_L),$$

where we used $d_L \ll 1/L$ and within the nucleation regime η_x is of order ρ. Then by standard evolution equation we have

$$\frac{d}{dt}c(1,t) = \mathbb{E}[\mathcal{L}(\eta_x\eta_{x+(1,0)})] = -\frac{1}{2}c(1,t) + \Theta(d_L),$$

and for large system we can omit d_L and solve the ODE with $c(1,0) = \rho^2$ to get

$$c(1,t) = \rho^2 e^{-\frac{1}{2}t}, \tag{5.6}$$

which is confirmed by simulation results in Figure 5.4. This prediction is same as the one for the one-dimensional SIP (3.8) with only a constant pre-factor $1/2$ in front of t, which is due to our definition of $c(1,t)$. Technically, in the 2DSIP the equivalent variable to the nearest neighbour product used in the SIP is the sum of the two nearest-neighbour products in two directions on the lattice, e.g. $\hat{c}(1,t) = \mathbb{E}[\eta_x\eta_{x+(1,0)} + \eta_x\eta_{x+(0,1)}]$, but due to the symmetry both in the dynamics and the lattice, it is the same as the sum of two $c(1,t)$. Therefore we stick to our definition of $c(1,t)$ for simplicity, which gives the $1/2$ in the convergence rate in (5.6). Notice, $c(1,t)$ cannot reach precisely 0 in a finite system, particularly in the simulation where we measure $c(1,t)$ by averaging a finite number of realisations. The reason is that attempted motion of clusters to neighbouring empty sites with slower rate d_L leads to finite size fluctuations of the asymptotic values of $c(1,t)$, which will vanish with increasing system sizes. The details of this fluctuations is the same as in the SIP model we analysed in Section 3.3.2, since for any particle within a cluster in the 2DSIP to jump to a neighbouring empty site the underlying dynamics is exactly the same as in a one-dimensional SIP model.
We can then further investigate the evolution of our observable $\sigma^2(t)$ with (5.6). Applying the generator (5.1) to the test function $f(\boldsymbol{\eta}) = \eta_x^2$ for some $x \in \Lambda_L$, we have

$$\mathcal{L}(\eta_x^2) \;=\; \frac{1}{2}\sum_{y\in A_x}\eta_x\eta_y + \Theta(d_L), \tag{5.7}$$

and we take expectation and notice $c(1,t) = \mathbb{E}[\eta_x\eta_y]$, $\forall y \in A_x$ to get

$$\frac{d}{dt}\sigma^2(t) = \mathbb{E}[\mathcal{L}(\eta_x^2)] = 2c(1,t) + \Theta(d_L). \tag{5.8}$$

Ignoring d_L terms for large systems and considering initial condition $\sigma^2(0) = \rho(1+\rho)$ and prediction (5.6), we have

$$\sigma^2(t) = 4\rho^2\left(1 - e^{-\frac{1}{2}t}\right) + \rho^2 + \rho, \tag{5.9}$$

and

$$\frac{\sigma^2(t)}{\rho^2} \to 5 + \frac{1}{\rho}, \quad \text{as} \quad t \to \infty. \tag{5.10}$$

This gives the value of the second moment after the nucleation regime in large systems which we take as the initial condition of the coarsening regime as discussed in Section 5.3.2.

5.3 Condensate interaction and coarsening dynamics

In this section we briefly introduce the dynamics of isolated clusters and the interactions between two clusters, which are similar to one-dimensional models. Then we study the dynamics in the coarsening regime following the same idea as in the SIP, as well as a new approximation method from the results of coalescing random walks on two-dimensional lattices.

5.3.1 Condensate motion and interaction

The dynamics of an isolated clusters moving to an empty site on the lattice are analogous to those in the SIP for sufficiently large clusters. Consider a cluster of size m residing on $x \in \Lambda_L$ and all its four neighbour sites are empty, i.e. $\sum_{y\in A_x} \eta_y = 0$. Then one of the particles could jump to one of the neighbouring sites $y \in A_x$ by diffusion with rate $d_L m$, after which the particles on site x could follow it by inclusion or jump to a different neighbouring site $z \neq y$ and in the meantime particles on y could jump back to x by inclusion or to other neighbouring sites in $A_y \setminus \{x\}$ by diffusion. Since we assume the diffusion rate d_L is very small compared with the inclusion rate, this process is dominated by inclusion and the probability of any particle escapes during the interaction vanishes for large m. Therefore, the motion of an isolated cluster is essentially the same as in the SIP which we discussed in Section 3.4.1 except the cluster can move in four directions rather than two. The expected time of one cluster move to any neighbour site is then the same as (3.21) $\mathbb{E}[T_{\text{step}}] \simeq \frac{1}{d_L m} + \Theta(d_L)$ and the cluster performs a symmetric random walk with effective jump rate d_L. The stationary regime is then dominated by a complete condensate containing all the particles and moving as a simple symmetric random walk with speed d_L.

The interactions of clusters in the 2DSIP is slightly more complicated than in the one-dimensional models, particularly in the early time. Theoretically, there could be more than three sites involved in one interaction, even if we ignore the escaping event. But for coarsening regime where clusters are dispersed, the probability of an interaction involving more than three sites are negligible as discussed below. As illustrated in Figure 5.5, we divided the interactions into three types according to the number of sites involved as

- Type A: Three sites interaction or two clusters exchange particles through the intermediate site.
- Type B: Four sites interaction or three clusters exchange particles through the

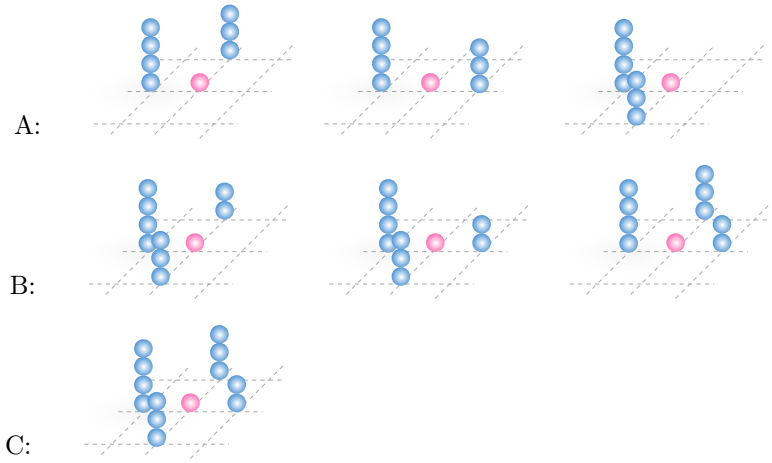

Figure 5.5: Illustration of multiple cluster interactions in the 2DSIP where the red particle is the one just jumped from one of the blue clusters. Row 1: type A interaction between 2 clusters. Row 2: Type B interaction between 3 clusters. Row 3: Type C interaction between 4 clusters. After interaction all the particles will redistribute on one (all particles merge) or more sites which are not directly linked.

intermediate site.

- Type C: Five sites interaction or four clusters exchange particles through the intermediate site.

Type A interaction is the same as one-dimensional case which we have discussed in detail in Section 3.4.2 and Section 4.3.2. If the two clusters are residing on the sites sharing two neighbouring sites, i.e. two diagonal sites of a size-1 lattice square, they have 1/2 probability to interact. And if the two clusters share only one neighbouring site, i.e. they are on the same vertical or horizontal line with one empty site in between, they have 1/4 probability to interact. Recall previous discussion in Section 4.3.2 that a typical 'catch up and swap' interaction scenario of two clusters on the lattice consists of order m sub-interaction processes, which start when the first particle jumps to the intermediate site and finishes when this site becomes empty again or two clusters merge on it. As the discussion and numerical results given in Section 4.3.2, during one such sub-interaction process two clusters merge with a probability of the order $1/m$ or keep their original sizes, where m is the typical size of the clusters. Therefore in an interaction event, until the first time one of the clusters moves away, the particles will coalesce or redistribute in an unbiased fashion with a probability of order 1 and the number of particles which are exchanged is of the order m. Type B interaction is much more complicated since the mechanism also depends on the initial sizes of the clusters and it can transfer

to type A interaction, e.g. one cluster is absorbed by one of the others during the interaction, but the inverse transfer is negligible due to the tiny escaping probability. However, the merge probability in a sub-interaction process is still of the order $1/m$ and an interaction event leads to order m particles exchanged. We do not cover the details of this type of interaction here. For further study, one potential approach is to apply the similar method as used in the PASIP (see Section 4.3.2) but here one needs to map type B interaction to a random walk in a three-dimensional space (rather than two-dimensional space in the PASIP) with absorbing surfaces (rather than absorbing lines). Similarly, results of a type C interaction include merge or redistribution with order m particles exchanged, and also it can transfer to type B or type A interaction. One can also map it to a random walk in a four-dimensional space with absorbing volumes. In fact, theoretically in the 2DSIP type B and type C interactions only occur in a short time after the nucleation regime where no neighbouring sites are occupied but there are sufficiently many clusters left on the lattice. After clusters started to merge through interactions, the probabilities of type B or type C interactions vanish for large systems since one (or two) cluster have to join two interacting clusters and the inclusion-dominated interactions happens in a much smaller time scale than the diffusion of any isolated cluster. In fact, due to a well known effect in coalescing random walks in two-dimensional space the walkers are anti-correlated (see, e.g., [123, 124] and references therein), which means the probability of type B and type C interactions is even less than multiple independent random walk models. Therefore in the rest of this chapter we only consider type A interaction which is essentially the same as in the SIP.

Derivation of time scales

The time scale of the coarsening and relaxation of the system can be estimated through previous arguments of the motion of isolated clusters and their interactions. The total relaxation time is dominated by the dynamics of two similar sized clusters of the order L. Before these two clusters move to a close enough position where they share one (or two) neighbouring sites, they perform symmetric simple random walks on the lattice with diffusivity d_L. It is well known result (see, e.g., [125]) that for two simple random walks to meet on a two-dimensional lattice of size L, it takes order $L\log(L)$ steps, which is different from order L^2 steps in a one-dimensional lattice, and the same scaling as partially asymmetric models, except for the log corrections. Therefore the two clusters encounter with an effective rate $d_L/(L\log(L))$ and exchange order L particles when they meet. Thus, one of the cluster will be absorbed after order 1 encounters and we have the relaxation time

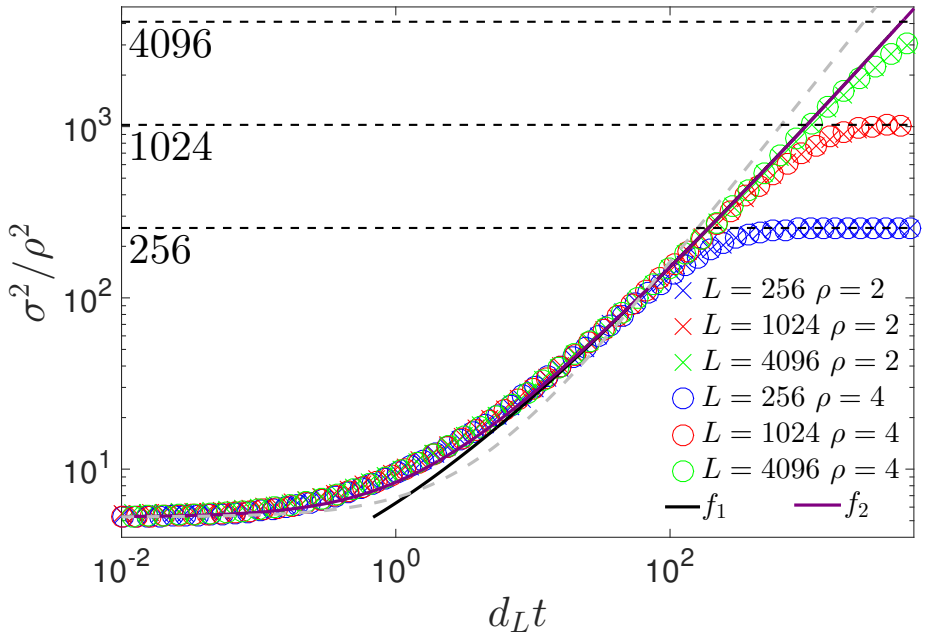

Figure 5.6: Scaling of σ^2/ρ^2 in the 2DSIP. Prediction f_1 (black full line) is the numerical solution of (5.14) with fitted constant $C_{s1} \approx 6.1146$ for $L = 4096$. Prediction f_2 (purple full line) is (5.18) with fitted constant $C_{s2} \approx 7.0824$ for $L = 4096$. The grey dashed line is the prediction (5.14) without log part. Data points are averaged over 200 realisations and errors are bounded by the size of the symbols.

scale as

$$\tau_L^s = \frac{L \log(L)}{d_L}, \tag{5.11}$$

which is used in Figure 5.3 and is confirmed by the collapse of the simulation data in it.

5.3.2 Coarsening and saturation regime

Coarsening dynamics

We follow the ideas of typical clusters used in previous chapters and give heuristic arguments of the coarsening dynamics. As usual we define $m(t)$ as the size of a typical cluster on the lattice and the number of clusters per unit volume is denoted by $n(t)$, and we have $m(t)n(t) = \rho$. The diffusivity of clusters is $D = d_L$ and we denote the typical volume (area as in two-dimensional space) per cluster as $a(t)$. Then the rates of interactions are of the order $D/(a(t)\log(a(t)))$ in a two-dimensional lattice, and each interaction leads to exchange of order $m(t)$ particles. Therefore,

the growth of typical cluster size can be described by the ODE

$$\frac{dm(t)}{dt} = C\frac{d_L}{a(t)\log(a(t))}m(t), \tag{5.12}$$

where C is some constant. We also denote the expected ratio of occupied sites after the nucleation regime as r, and the initial value of $m(t)$ is given by $m(0) = \rho/r$. Notice the simple relation $a(t) = m(t)/\rho$, we can integrate (5.12) from 0 to t and get

$$m(t)(\log(m(t)) - 1 - \log\rho) = C\rho d_L t - \frac{\rho}{r}(\log r + 1). \tag{5.13}$$

This equation does not give an explicit solution for $m(t)$, but we can see that the time scale of $m(t)$ satisfies $m(t)\log(m(t)) \sim d_L t$. Comparing this time scale with $m(t) \sim d_L t$ in the TASIP and the PASIP and $m^2(t) \sim d_L t$ in the SIP, we can see the coarsening process is slower than the TASIP or the PASIP by only a logarithmic factor but faster than the SIP. This is closely related to the different behaviour of random walk in one and two dimensional lattices, which is natural since the random walk can be seen as a basic component constructing the inclusion processes, since we define $p(x, y)$ in the generator (2.27) as the transition rates of random walks.

Notice the equation $\sigma^2(t) = \rho m(t)$ still holds in the 2DSIP and we can substitute it into (5.13) to get an equation of $\sigma^2(t)/\rho^2$ as

$$\frac{\sigma^2(t)}{\rho^2}\left(\log\frac{\sigma^2(t)}{\rho^2} - 1\right) = C_{s1}d_L t - \frac{1}{r}(\log r + 1). \tag{5.14}$$

We can solve this equation numerically and fit C_{s1} from data, and it agrees well with the simulation data in the coarsening window as shown in Figure 5.6. In the figure we also show the prediction ignoring the log term, i.e. the same linear prediction as in one-dimensional systems. And the numerical results suggest the log term is not negligible, as a consequence of the interaction rate between clusters. In addition, taking $m(\tau_L^s) \to \Theta(\rho L)$ in (5.13) we can approximate the order of the relaxation time scale as

$$\tau_L^s \simeq \frac{L\log L}{d_L},$$

which agrees with our previous prediction (5.11) and is confirmed by the simulation in Figure 5.3. The above analysis does not have explicit system size dependence and therefore also holds on infinite lattices with a given small diffusion parameter d. In a finite system, the scaling only holds in a certain window after which the system saturate due to finite size effects.

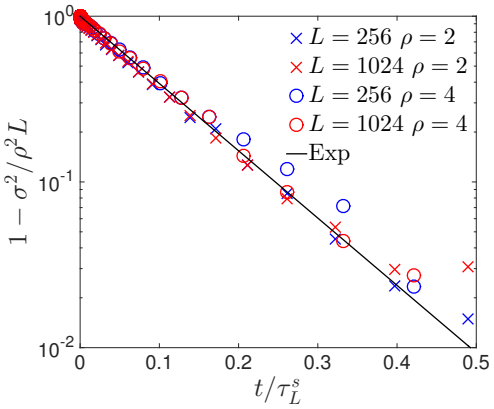

Figure 5.7: Exponential relaxation in the saturation regime in 2DSIP. The prediction (5.15) is shown as the full line with best fit constant $C' \approx 9.3496$. Data points are averaged over 200 realisations. Errors are bounded by the size of symbols.

Saturation dynamics

After the coarsening window, we expect the system to converge exponentially to the single condensate state due to the finite system size. Similar to the discussion in Section 3.5.2 for the one-dimensional model, we predict our observable follows

$$\frac{\sigma^2(t)}{\rho^2 L} \simeq 1 - e^{-C't/\tau_L^s}, \tag{5.15}$$

where τ_L^s is the time scale of coarsening and relaxation in the system as shown in (5.11), and C' is a constant. A non-rigorous analysis based on two equal size clusters similar to the one used in Section 3.5.2 can be applied here, but cannot give satisfactory estimations of C' or the convergence rate. This is because the exact dynamics in the 2DSIP is also spatially dependent, as seen in Section 5.3.1 that even the two-cluster interaction has different merge probabilities. Therefore, here we only give prediction from simulation that $C' \approx 9.3496$ as shown in Figure 5.7. As in the one-dimensional inclusion processes, C'/τ_L^s in (5.15) can be treated as the spectral gap of the generator of the system and a starting point to further study the precise behaviour for dynamics in the saturation regime.

5.3.3 Connection with coalescing random walk

The analysis in the previous subsection is analogous to the one-dimensional models studied in previous chapters, and the agreements with simulations confirm that our method is accurate and has the potential to extend to other similar models. We

also find the symmetric inclusion process shares some common aspects with the classic coalescing random walk model, and here we briefly give another approach to approximate the coarsening behaviour in the 2DSIP based on some known properties of coalescing random walk. In a **coalescing random walk** model, a set of particles perform independent random walks on a undirected connected graph and when two or more particles meet at one site they unite to form a single particle and continue to make a random walk through the graph. If we start this model from all sites occupied and denote $\rho^{\mathrm{CRW}}(t)$ as the probability of a given site x occupied at time t, or equivalently the particle density of walkers in the system at time t, it is easy to show $\rho^{\mathrm{CRW}}(t) \to 0$ as $t \to \infty$. And the large time behaviour has been well studied in a series of papers [126, 127, 128, 129] in which it was shown

$$\rho^{\mathrm{CRW}}(t) \sim \begin{cases} \frac{1}{\sqrt{\pi t}} & \text{if } \hat{d} = 1 \\ \frac{\log(t)}{\pi t} & \text{if } \hat{d} = 2 \\ \frac{1}{\gamma_{\hat{d}} t} & \text{if } \hat{d} > 2 \end{cases} , \quad \text{as} \quad t \to \infty \tag{5.16}$$

where $\hat{d}$ is the dimension of the graph and $\gamma_{\hat{d}}$ is the probability a $\hat{d}$-dimensional random walk returns to the origin. This model is closely related to the classic voter model [6], where the connections between these two models in two dimensional spaces have been studied in [130, 131].

Since in a sub-interaction process of the 2DSIP two cluster merge with a probability of the order $1/m$ and an interaction event typically consists of order m such sub-interaction processes, the merge probability of an interaction event is of the order 1. However, the probability that any cluster splits is small and vanishes for large clusters, therefore we can approximate a 2DSIP in coarsening regime as a coalescing random walk on the same two-dimensional lattice. Take a 2DSIP on a finite lattice Λ_L and approximate it as a coalescing random walk with effective speed d_L, then we can approximate the number of occupied sites per unit volume $n(t)$ by $\rho^{\mathrm{CRM}}(d_L t)$. Notice that the above asymptotic behaviour of ρ^{CRW} only holds for large time, and for 2DSIP we have the boundary conditions $n(0) = r$ and $n(t) \to 1/L$. Thus, we introduce a constant (assumed to be 1) in the log term and two constant parameters C_1' and C_2' in the following prediction in order to accord with boundary conditions,

$$n(t) \simeq C_1' \frac{\log(d_L t + 1)}{d_L t} + C_2' \,. \tag{5.17}$$

And the equation $\sigma^2(t) = \rho m(t) = \rho^2/n(t)$ gives

$$\frac{\sigma^2(t)}{\rho^2} = \frac{1}{n(t)} \simeq C_1 \frac{d_L t}{\log(1 + d_L t)} + C_2,$$

where C_1 and C_2 are constants. The initial value of σ^2/ρ^2 can be considered as the asymptotic limit of the same variable in the nucleation regime, which we derived in Section 5.2.2 as $\sigma^2/\rho^2 = 5 + 1/\rho$ (5.10). With this initial condition we can simplify the above equation slightly as

$$\frac{\sigma^2(t)}{\rho^2} = C_{s2} \left(\frac{d_L t}{\log(1 + d_L t)} - 1 \right) + 5 + \frac{1}{\rho}, \tag{5.18}$$

which agrees well with simulation data in Figure 5.6.

It is also interesting to see that the analogous analysis can also be applied to one-dimensional model where $\rho^{\mathrm{CRW}} \sim 1/\sqrt{t}$ which then gives the approximation

$$\frac{\sigma^2(t)}{\rho^2} \simeq C_1 \sqrt{d_L t} + C_2,$$

which shows the same time scaling as our previous prediction (3.34) derived in Section 3.5.1. And therefore we expect the same approximation could be extended to symmetric inclusion processes in higher dimensions with $\rho^{\mathrm{CRW}} \sim 1/\gamma_{\hat{d}} t$.

5.4 Further study and summary

5.4.1 Inclusion process in higher dimensions

After extending results from one-dimensional systems to two-dimensional systems, it would be interesting to investigate higher dimensional systems. The general definition of inclusion process is easy to adapt to a $\hat{d}$-dimensional torus $\Lambda_L = \mathbb{N}^{\hat{d}}$, $\hat{d} > 2$, and the dynamics is described by generator (2.27). Similarly one can define symmetric, partially asymmetric and totally asymmetric versions by defining $p(x, y)$ to be the transition rates of the corresponding type of $\hat{d}$ dimension random walk. Similar to the two dimensional cases, the only interesting model would be the symmetric one since the totally asymmetric one is multiple parallel one-dimensional TASIP and partially asymmetric model is also parallel one-dimensional PASIP in the drifted direction with small probability to merge, therefore should behave like the symmetric one.

The general results of stationary distributions we reviewed in Chapter 2 are independent of the dimension, particularly the product form of the stationary

measures under some restrictions of $p(x, y)$. In addition, under the condition of weak diffusion a complete condensation also exists and one can study the same thermodynamic limit (2.32). It is then natural to apply the analogous analysis in this chapter to investigate the dynamics of the condensation formation process in a higher dimensional SIP model, where $\sigma^2(t)$ (2.4) is still an appropriate observable to capture the temporal evolution in the system and converges to $\rho^2 L$ when a complete condensate is constructed. And if we start with a uniform initial condition and only consider nearest-neighbour jumps, one can expect a fast nucleation regime dominated by inclusion and a slower coarsening regime driven by diffusion. The nucleation regime has the same absorbing condition where no neighbouring sites on the lattice are occupied as shown in (5.3), and the set of all nearest-neighbour A_x contains $2\hat{d}$ sites. Then one can apply the analogous analysis as in one and two dimensional models using generator and test functions $f(\boldsymbol{\eta}) = \eta_x^2$, for some $x \in \Lambda$ to study the behaviour of $\sigma^2(t)$ in this regime.

For the coarsening dynamics, one has two approaches to predict the scaling law of $\sigma^2(t)$. The first one is based on the motion of a typical cluster and interactions between two clusters, where now the expected number of steps of two clusters to meet is of the order $v(t)$ ([125]), where $v(t)$ is the typical volume of each cluster occupied. The second approach is to approximate the model as a coalescing random walk where $\rho^{\mathrm{CRM}} = 1/\gamma_{\hat{d}} t$ as shown in (5.16), and then fit the prediction

$$\frac{\sigma^2}{\rho^2} \simeq C_1 \gamma_{\hat{d}} d_L t + C_2,$$

where C_1 and C_2 are constants.

5.4.2 Summary

In this chapter we extended previous results to inclusion processes defined on two-dimensional lattices, particularly the symmetric version (2DSIP). The similar dynamical regimes as in the one-dimensional models can still be observed in the 2DSIP, and we show that the method we used in previous chapters can be applied analogously, in particular the analysis of the coarsening regime based on motion of a single typical cluster. Due to the properties of random walk in two dimensional lattices, the coarsening dynamics exhibits a different time scaling $\tau_L^s \sim L \log(L)/d_L$ (5.11). We also show that the symmetric inclusion process shares many common features with the coalescing random walk model, and use the results in this model to predict the coarsening behaviour in the 2DSIP, which is a promising method to investigate inclusion processes in higher dimensions.

For further study, it would also be interesting to see the model defined on more general two-dimensional graphs such as a lattice with open boundary conditions, and then the specific structure of the graph could be vital to the dynamics. The one-dimensional inclusion processes with boundary driven generators and closed finite lattices have been discussed in [16, 65] and [74] respectively, which could be a starting point for general two-dimensional models. One can also further investigate the dynamics of the 2DSIP in different thermodynamic limits, for example such as the one studied in [41] for one-dimensional model: L fixed, $N \to \infty$, and $d_N \to 0$.

Chapter 6

Preliminary Results on Symmetric Systems with Duality

6.1 Introduction

Duality of Markov processes with respect to a duality function was firstly introduced in the literature in late 1940s [132, 133, 134], and has been further investigated in a series of papers [135, 136, 137, 138, 139, 140, 141]. The method has been applied in many fields, including interacting particle systems, interacting diffusions, queueing theories and mathematical population genetics. However, so far there is no complete and systematic theory for the duality of Markov process with respect to a function, even some basic questions such as giving necessary and sufficient conditions for the existence of a dual process of a given Markov process have not yet been fully resolved. For the general theories we refer to a recent review [142] where the authors studied the existence and uniqueness of dual processes through a functional analytic language. Notice, duality of Markov processes with respect to a *measure*, which is a different but related topic, has been well studied and developed a rather complete theory (see [143, 144] for recent reviews), but in this thesis we only consider duality of Markov processes with respect to a duality function and will simply call it duality in the rest of this chapter. Applications of duality generally focus on certain aspects or applications of particular fields [43, 138, 145, 146, 147, 148, 149], and the presentations of the duality are closely related to the fundamental structures or properties of the specific Markov processes, such as time reversal, symmetries or conserved quantities. In this thesis, we only focus on duality theory in the field

of interacting particle systems with particular emphasis on the symmetric inclusion process.

Duality has been a key tool in the study of inclusion processes since the first appearance of this process was as a dual of the Brownian energy process in [15]. Then the self-duality of the symmetric inclusion process was proved in [65] and further studied in [16, 142]. It is also studied in [47] with several other classic interacting particle systems with generalised settings of boundary driven lattices. Recent studies also illustrate how powerful the duality is to investigate further properties of the inclusion process, such as the local equilibrium property of the non-equilibrium steady state [93] and the ergodic measures with finite moments [150]. The study on the inclusion process also provides a cornerstone for the duality theory of more general Markov process in [151, 152], where the authors used a deep connection with symmetries and representations of Lie algebras with a quantum mechanics formalisms. The study also includes the self-duality of a special version of asymmetric inclusion process *different* to the one we have studied in previous chapters. The duality of the inclusion processes has also been applied to other areas, such as the kinetic wealth exchange models in econophycs [153] and a wide class of population dynamic models [154]. In this chapter, we first briefly review some of the results of duality in the inclusion process, then give some exact computations of the correlations in the symmetric inclusion process with the usage of self-duality, which leads to a more detailed understanding of the dynamics of condensation.

This chapter is organised as follows. In Section 6.2 we give basic definitions of duality and review some relevant results. In Section 6.3 we compute the covariances with a dual process containing only two particles. And in Section 6.4 we compute exact results of the simple two-particle dual process and recover some results in previous chapters.

6.2 Duality

6.2.1 Definitions and relevant results

Definition 6.1. Let $(\boldsymbol{\eta}(t), t \geq 0)$, $(\boldsymbol{\zeta}(t), t \geq 0)$ be two interacting particle systems defined on state spaces X, X^{dual}, respectively. We say they are **dual with respect to the duality function** $D : X \times X^{\mathrm{dual}} \to \mathbb{R}$, if

$$\mathbb{E}^{\boldsymbol{\eta}} \left[D(\boldsymbol{\eta}(t), \boldsymbol{\zeta}) \right] = \mathbb{E}^{\boldsymbol{\zeta}} \left[D(\boldsymbol{\eta}, \boldsymbol{\zeta}(t)) \right], \quad \text{for any} \quad t \geq 0, \tag{6.1}$$

where $\mathbb{E}^{\boldsymbol{\eta}}$ denotes the expectation of the process $(\boldsymbol{\eta}(t), t \geq 0)$ starting from configuration $\boldsymbol{\eta}$, and $\mathbb{E}^{\boldsymbol{\zeta}}$ denotes the expectation in the process $(\boldsymbol{\zeta}(t), t \geq 0)$ starting from configuration $\boldsymbol{\zeta}$.

Remark: Here and in the rest of this thesis we assume boundedness of the duality function D for the sake of simplicity of the expression, but in principle duality can be defined for unbounded functions as well.

The duality relationship (6.1) implies that expectations of certain functions for a process of interest $(\boldsymbol{\eta}(t), t \geq 0)$ can be computed in terms of expectations of a second, auxiliary process $(\boldsymbol{\zeta(t)}, t \geq 0)$. Often the process $(\boldsymbol{\zeta(t)}, t \geq 0)$ is considerably simpler than the process of interest, for example it can be the same process as $(\boldsymbol{\eta}(t), t \geq 0)$ but only with a small number (e.g. 1 or 2) of particles, for which explicit computations are possible. Also, the duality functions often have a polynomial structure and can be related to correlation functions of the process $(\boldsymbol{\eta}(t), t \geq 0)$, as is shown in detail below in Subsection 6.2.2.

The duality relationship can be equivalently presented by semigroups (Definition 2.3) or generators (Definition 2.4) of the corresponding processes as well. Let $\{S^{\boldsymbol{\eta}}(t), t \geq 0\}$ and $\{S^{\boldsymbol{\zeta}}(t), t \geq 0\}$ be the semigroups of interacting particle systems $(\boldsymbol{\eta}(t), t \geq 0)$ and $(\boldsymbol{\zeta}(t), t \geq 0)$, respectively. Then the duality formula is equivalent to

$$S^{\boldsymbol{\eta}}(t)D(\cdot, \boldsymbol{\zeta})(\boldsymbol{\eta}) = S^{\boldsymbol{\zeta}}(t)D(\boldsymbol{\eta}, \cdot)(\boldsymbol{\zeta}), \quad \boldsymbol{\eta} \in X, \ \boldsymbol{\zeta} \in X^{\text{dual}}.$$

If $(\boldsymbol{\eta}(t), t \geq 0)$ and $(\boldsymbol{\zeta}(t), t \geq 0)$ have generators $\mathcal{L}^{\boldsymbol{\eta}}$ and $\mathcal{L}^{\boldsymbol{\zeta}}$ with domain $\mathcal{D}_{\mathcal{L}^{\boldsymbol{\eta}}}$ and $\mathcal{D}_{\mathcal{L}^{\boldsymbol{\zeta}}}$ respectively, and we assume $D(\boldsymbol{\eta}, \cdot) \in \mathcal{D}_{\mathcal{L}^{\boldsymbol{\zeta}}}$, $D(\cdot, \boldsymbol{\zeta}) \in \mathcal{D}_{\mathcal{L}^{\boldsymbol{\eta}}}$, the above equation then implies

$$\mathcal{L}^{\boldsymbol{\eta}}D(\cdot, \boldsymbol{\zeta})(\boldsymbol{\eta}) = \mathcal{L}^{\boldsymbol{\zeta}}D(\boldsymbol{\eta}, \cdot)(\boldsymbol{\zeta}) \quad \forall \boldsymbol{\eta} \in X, \ \boldsymbol{\zeta} \in X^{\text{dual}}.$$

And the converse is true as well, under certain conditions:

Proposition 6.1. *Let $(\boldsymbol{\eta}(t), t \geq 0)$, $(\boldsymbol{\zeta}(t), t \geq 0)$ be interacting particle systems with generators $\mathcal{L}^{\boldsymbol{\eta}}$, $\mathcal{L}^{\boldsymbol{\zeta}}$, let $D : X \times X^{dual} \to \mathbb{R}$ be bounded and continuous. If $D(\boldsymbol{\eta}, \cdot)$, $S^{\boldsymbol{\eta}}(t)D(\boldsymbol{\eta}, \cdot) \in \mathcal{D}_{\mathcal{L}^{\boldsymbol{\zeta}}}$ for all $\boldsymbol{\eta} \in X$, $t \geq 0$ and $D(\cdot, \boldsymbol{\zeta}), S^{\boldsymbol{\zeta}}(t)D(\cdot, \boldsymbol{\zeta}) \in \mathcal{D}_{\mathcal{L}^{\boldsymbol{\eta}}}$ for all $\boldsymbol{\zeta} \in X^{dual}$, $t \geq 0$, and if*

$$\mathcal{L}^{\boldsymbol{\eta}}D(\cdot, \boldsymbol{\zeta})(\boldsymbol{\eta}) = \mathcal{L}^{\boldsymbol{\zeta}}D(\boldsymbol{\eta}, \cdot)(\boldsymbol{\zeta}) \quad \forall \boldsymbol{\eta} \in X, \ \boldsymbol{\zeta} \in X^{dual},$$

then $(\boldsymbol{\eta}(t), t \geq 0)$ and $(\boldsymbol{\zeta}(t), t \geq 0)$ are dual with respect to D.

Proof. See [142, Proposition 1.2]. □

An interacting particle system is called **self-dual** with respect to a duality function D if for any two versions of the process $(\boldsymbol{\eta}(t), t \geq 0)$ and $(\boldsymbol{\zeta}(t), t \geq 0)$, equation (6.1) or its equivalent form hold with this function D. Here 'version' denotes processes that are defined on the same state space and governed by the same dynamics, for example an inclusion process defined on a fixed lattice with only two particles is a different version of an inclusion process defined on the same lattice containing an arbitrary number of particles. The duality functions are model specific, but it has been shown that many classic interacting particle system are self-dual under certain conditions, such as the symmetric inclusion process, the symmetric exclusion process and a system of independent random walks (see [47] for more details).

6.2.2 Self-duality of the symmetric inclusion process

In the rest of this chapter, we consider the symmetric inclusion process defined on a one-dimensional lattice, which can be infinite $\Lambda = \mathbb{Z}$ or finite with periodic boundary condition $\Lambda_L = \mathbb{Z}/(L\mathbb{Z})$. The dynamics are described by the generator (2.27) with a more explicit form

$$\mathcal{L}f(\boldsymbol{\eta}) = \sum_{x\in\Lambda}\sum_{\epsilon=\pm 1}\frac{1}{2}\eta_x(d+\eta_{x+\epsilon})\left(f(\boldsymbol{\eta}^{x,x+\epsilon}) - f(\boldsymbol{\eta})\right)$$

for test functions $f \in C^b(X)$. The SIP is self-dual with the duality function constructed in the following way. Define the polynomial

$$d(k,n) = \frac{n!}{(n-k)!}\frac{\Gamma(d)}{\Gamma(d+k)}$$

for $k, n \in \mathbb{N}$. By definition $d(k,n) = 0$ when $k > n$, i.e., negative factorials are interpreted as $+\infty$. In particular, we have

$$d(1,n) = \frac{n}{d}, \tag{6.2}$$

$$d(2,n) = \frac{n(n-1)}{d(d+1)}, \tag{6.3}$$

and $d(0,n) = 1$, for all $n \geq 0$. Then for $\boldsymbol{\zeta} \in X$ a configuration with a finite number of particles, i.e., such that $\sum_x \zeta_x < \infty$, and $\boldsymbol{\eta} \in X$ we define

$$D(\boldsymbol{\zeta}, \boldsymbol{\eta}) = \prod_{x\in\mathbb{Z}} d(\zeta_x, \eta_x). \tag{6.4}$$

The self-duality of the SIP is then given by

$$\mathbb{E}_{\boldsymbol{\eta}}\left[D(\boldsymbol{\zeta},\boldsymbol{\eta}(t))\right] = \mathbb{E}_{\boldsymbol{\zeta}}\left[D(\boldsymbol{\zeta}(t),\boldsymbol{\eta})\right], \tag{6.5}$$

which was first proved in [65], see also [16, 142] for more details on the self-duality of the SIP.

6.3 Time dependent covariances

As discussed in previous chapters, in the limit $d \to 0$ a condensation phenomena occurs in the SIP. In this section, we show some preliminary work in order to understand how coarsening arises, starting from a homogeneous product measure. More precisely, we are interested in the variances and covariances of the occupation numbers, i.e.,

$$C_{xy}(t) := \mathbb{E}_{\nu_\rho}(\eta_x(t)\eta_y(t)) \ . \tag{6.6}$$

Here $C_{xx}(t) \equiv \sigma^2(t)$ is independent of x and in general C_{xy} is only a function of $|x-y|$ due to translation invariance. Here the initial distribution ν_ρ is a translation invariant product measure with density ρ and second moment σ_0^2. For a Poisson distribution with density ρ we have $\sigma_0^2 = \rho(1+\rho)$.

With slight abuse of notation, for a configuration $\boldsymbol{\eta}(t) = \sum_{i=1}^n \delta_{x_i}$ with particles at positions $x_1, \ldots, x_n$, we denote by $\mathbb{E}_{x_1,\ldots,x_n}$ and $\mathbb{P}_{x_1,\ldots,x_n}$ the expectation and probability in the SIP with starting configuration $\boldsymbol{\eta}$ respectively. For $n = 2$, i.e., two SIP-particles, we denote the corresponding particle positions by X_t, Y_t. The following easy consequence of self-duality is then the starting point of our computations.

Proposition 6.2. *For $x \neq y \in \Lambda$, and for every initial product measure ν_ρ with density ρ and second moment σ_0^2 we have*

$$C_{xx}(t) = \sigma_0^2 \mathbb{P}_{x,x}[X_t = Y_t] + \left(\frac{d\rho(1+\rho)+\rho^2}{d}\right)\mathbb{P}_{x,x}[X_t \neq Y_t] \tag{6.7}$$

$$C_{xy}(t) = \left(\frac{d(\sigma_0^2 - \rho(1+\rho)) - \rho^2}{d+1}\right)\mathbb{P}_{x,y}[X_t = Y_t] + \rho^2 \ . \tag{6.8}$$

Proof. Consider two SIP processes: a general one $(\boldsymbol{\eta}(t), t > 0)$ starting with initial state $\boldsymbol{\eta}$; another one with only two particles with initial positions $x, y \in \Lambda$ and the particle positions are denoted by X_t, Y_t. We first compute the second moment $C_{xx}(t)$ by considering the initial condition for the two-particle SIP to be $x = y$ (two particles are on the same site). Due to the self-duality of SIP, (6.5) holds for these

two specific processes and can be written as

$$\mathbb{E}_{\boldsymbol{\eta}}\left[D(2\delta_x, \boldsymbol{\eta}(t))\right] = \mathbb{E}_{x,x}\left[D(\delta_{X_t} + \delta_{Y_t}, \boldsymbol{\eta})\right] ,$$

and the two particles lead to a simple form of the duality function as

$$D(2\delta_x, \boldsymbol{\eta}(t)) = \frac{\eta_x(t)(\eta_x(t)-1)}{d(d+1)},$$

according to (6.3). Then we consider the variable $\eta_x(t)(\eta_x(t)-1)$ and use the duality relation to get

$$\begin{aligned} & \mathbb{E}_{\boldsymbol{\eta}}\left[\eta_x(t)(\eta_x(t)-1)\right] \\ = \;& d(d+1)\mathbb{E}_{\boldsymbol{\eta}}\left[D(2\delta_x, \boldsymbol{\eta}(t))\right] \\ = \;& d(d+1)\mathbb{E}_{x,x}\left[D(\delta_{X_t} + \delta_{Y_t}, \boldsymbol{\eta})\right] \\ = \;& \mathbb{E}_{x,x}\left[\eta_{X_t}(\eta_{X_t}-1)\mathbb{I}\{X_t = Y_t\}\right] \\ + \;& \mathbb{E}_{x,x}\left[\frac{d+1}{d}\eta_{X_t}\eta_{Y_t}\mathbb{I}\{X_t \neq Y_t\}\right], \end{aligned}$$

which holds for general $\boldsymbol{\eta}$. Now we take the initial distribution to be translation invariant with density ρ and second moment σ_0^2, then the above relationship implies

$$\begin{aligned} & \mathbb{E}_{\nu_\rho}\left[\eta_x(t)^2\right] - \rho \\ = \;& (\sigma_0^2 - \rho)\mathbb{P}_{x,x}(X_t = Y_t) + \frac{d+1}{d}\rho^2\mathbb{P}_{x,x}\left(X_t \neq Y_t\right), \end{aligned}$$

which is equivalent to (6.7) after moving the ρ on the left hand side to the right.

The correlation $C_{x,y}(t)$ can be derived analogously. Taking $x \neq y$ and using the duality equation

$$\mathbb{E}_{\boldsymbol{\eta}}\left[D(\delta_x + \delta_y, \boldsymbol{\eta}(t))\right] = \mathbb{E}_{x,y}\left[D(\delta_{X_t} + \delta_{Y_t}, \boldsymbol{\eta})\right],$$

and the specific form of $D(\delta_x + \delta_y, \boldsymbol{\eta}) = \eta_x\eta_y/d^2$, we get

$$\begin{aligned} & \mathbb{E}_{\boldsymbol{\eta}}\left[\eta_x(t)\eta_y(t)\right] \\ = \;& d^2\mathbb{E}_{\boldsymbol{\eta}}\left[D(\delta_x + \delta_y, \boldsymbol{\eta}(t))\right] \\ = \;& d^2\mathbb{E}_{x,y}\left[D(\delta_{X_t} + \delta_{Y_t}, \boldsymbol{\eta})\right] \\ = \;& d^2\mathbb{E}_{x,y}\left[\frac{\eta_{X_t}(\eta_{X_t}-1)}{d(d+1)}\mathbb{I}\left\{X_t = Y_t\right\}\right] \\ + \;& d^2\mathbb{E}_{x,y}\left[\frac{\eta_{X_t}\eta_{Y_t}}{d^2}\mathbb{I}\left\{X_t \neq Y_t\right\}\right]. \end{aligned}$$

Averaging η again over the initial distribution ν_ρ, we have

$$\mathbb{E}_{\nu_\rho}\left[\eta_x(t)\eta_y(t)\right] = \frac{d}{d+1}(\sigma_0^2-\rho)\mathbb{P}_{x,y}\left(X_t = Y_t\right) + \rho^2\mathbb{P}_{x,y}\left(X_t \neq Y_t\right),$$

which is equivalent to (6.8) with $\mathbb{P}_{x,y}\left(X_t \neq Y_t\right) = 1 - \mathbb{P}_{x,y}\left(X_t = Y_t\right)$.

□

6.4 Exact computations for two dual particles

6.4.1 Finite systems

In this section we study the probabilities $\mathbb{P}_{x,x}[X_t = Y_t]$ and $\mathbb{P}_{x,y}[X_t = Y_t]$ for two dual SIP particles. Their relative position $(Z_t := |X_t - Y_t|,\ t \geq 0)$ is a continuous-time birth-death chain on the state space $X = \mathbb{N}_0$ for $\Lambda = \mathbb{Z}$ or $X_L = \{0, \ldots, L/2\}$ for finite $\Lambda_L = \mathbb{Z}/(L\mathbb{Z})$ with L even. The generator on X_L is given by

$$\begin{aligned}
\mathcal{L}_L f(z) &= d_L \mathbb{I}\{z=0\}(f(1)-f(0)) \\
&+ d_L \mathbb{I}\{z+1 \in X_L\}(f(z+1)-f(z)) \\
&+ d_L \mathbb{I}\{z-1 \in X_L\}(f(z-1)-f(z)) + d_L \mathbb{I}\{z=\frac{L}{2}\}(f(\frac{L}{2}-1)-f(\frac{L}{2})) \\
&+ \mathbb{I}\{z=1\}(f(0)-f(1)),
\end{aligned} \tag{6.9}$$

where we assume d_L decays with increasing L. The terms proportional to d_L in the above generator correspond to a simple random walk on X with reflecting boundaries and rate d_L, and the last term results from the inclusion attraction with an order 1 rate from the distance 1 to 0. With the initial position $z = |x-y|$ we then have $\mathbb{P}_{x,y}[X_t = Y_t] = \mathbb{P}_z[Z_t = 0]$ for the expressions in Proposition 6.2. In the rest of this section we focus on finite systems Λ_L and assume L is even.

$(Z_t : t \geq 0)$ is a birth-death chain and the rates can be read from the above generator as

$$\begin{aligned}
&\text{Birth rates:} && \alpha_0 = 2d_L, \quad \alpha_i = d_L \ \text{ for } i = 1, 2, ..., \frac{L}{2} - 1, \\
&\text{Death rates:} && \beta_1 = 1 + d_L, \quad \beta_i = d_L \ \text{ for } i = 2, 3, ..., \frac{L}{2} - 1, \ \ \beta_{\frac{L}{2}} = 2d_L \ .
\end{aligned}$$

For such a birth-death chain one can compute its stationary distribution μ following

a standard recursive method (see for example [94, Section 6.11]), which are

$$\mu_0 = \left(1+\sum_{n=1}^{L/2}\frac{\alpha_0\alpha_1...\alpha_{L/2-1}}{\beta_1\beta_2...\beta_{L/2}}\right)^{-1} = \frac{1+d_L}{1+d_LL}\,, \tag{6.10}$$

$$\mu_n = \left(\prod_{i=1}^{n}\frac{\alpha_{i-1}}{\beta_i}\right)\mu_0 = \frac{2d_L}{1+d_LL}, \quad \text{for } 1\le n\le\frac{L}{2}-1, \tag{6.11}$$

$$\mu_{L/2} = \left(\prod_{i=1}^{L/2}\frac{\alpha_{i-1}}{\beta_i}\right)\mu_0 = \frac{d_L}{1+d_LL}\,. \tag{6.12}$$

The stationary distribution implies that in the limit $t\to\infty$ we have

$$\begin{aligned}\mathbb{P}_{x,y}\left[X_t=Y_t\right] &\to \mu(0)=\frac{1+d_L}{1+d_LL}\\ \mathbb{P}_{x,y}\left[X_t\neq Y_t\right] &\to \sum_{n=1}^{L/2}\mu(n)=\frac{d_L(L-1)}{1+d_LL}.\end{aligned}$$

Substituting above equations into (6.7) we can get the asymptotic values of the second moment as

$$\begin{aligned}\sigma^2_\infty &= \lim_{t\to\infty}C_{xx}(t)=\sigma_0^2\frac{1+d_L}{1+d_LL}+\left(\frac{d_L\rho(1+\rho)+\rho^2}{d_L}\frac{d_L(L-1)}{1+d_LL}\right) \\ &= \sigma_0^2\frac{1+d_L}{1+d_LL}+\rho^2\frac{L-1}{1+d_LL}+d_L\rho(1+\rho)\frac{L-1}{1+d_LL}\\ &\simeq \sigma_0^2+\rho^2(L-1)+\Theta(d_LL),\end{aligned} \tag{6.13}$$

as $L\to\infty$ with $d_L\ll 1/L$. The initial condition σ_0^2 still enters this expression since it determines the total number of particles which is conserved, and the leading order is given by $\rho^2(L-1)$. If we start with deterministic initial conditions with $\sigma_0^2=\rho^2$ we get ρ^2L, for Poisson initial condition it is then $\rho^2L+\rho$. In any case, we have

$$\sigma^2_\infty\simeq\rho^2L+\Theta(1),$$

which is consistent with the normalisation ρ^2L we used in previous chapters.

Analogously, substituting $\mathbb{P}_{x,y}[X_t=Y_t]$ and $\mathbb{P}_{x,y}[X_t\neq Y_t]$ into (6.8), the correlation is given by

$$\begin{aligned}\sigma^{xy}_\infty &= \lim_{t\to\infty}C_{xy}(t)=\frac{d_L(\sigma_0^2-\rho(1+\rho))-\rho^2}{1+d_LL}+\rho^2,\\ &\simeq \rho^2\frac{d_LL}{1+d_LL}+\Theta(d_L),\end{aligned}$$

as $L \to \infty$ with $d_L \ll 1/L$. The asymptotic behaviour only weakly depend on the initial condition (terms of the order d_L), and the second moment given above vanishes in the limit $L \to \infty$, indicating that occupation numbers are strongly anti-correlated, due to the presence of a complete condensate.

Starting the process Z_t from $z = 0$ on a time scale of order 1 and letting the diffusion decay with the system as $d_L = L^{-\gamma}$, $\gamma > 1$, we have $\mathbb{P}[Z_t = 0] \simeq 1 - e^{-2d_L t} \simeq 2d_L t$ due to the exponentially distributed waiting time. After a time of order $1/d_L$ the process is still restricted on the first two sites $\{0, 1\}$ due to the high jump rate from 1 to 0. It will reach an intermediate distribution μ', where $\mu'_0 = (1+d_L)/(1+3d_L)$, $\mu'_1 = 2d_L/(1+3d_L)$ are determined by detailed balance. In fact, this time scale corresponds to the nucleation dynamical regime as we discussed in Section 3.3.2, where particles residing on neighbouring sites merge by the strong inclusion interaction. The intermediate distribution μ'_0, μ'_1 can be interpreted as the absorbing state of the nucleation regime where no neighbouring sites are occupied on the lattice. Substituting μ'_0 and μ'_1 into (6.7), we have

$$\sigma^2(t) \simeq \sigma_0^2 \frac{1+d_L}{1+3d_L} + \frac{2(d_L\rho(1+\rho)+\rho^2)}{1+3d_L} \simeq 3\rho^2 + \rho,$$

if we assume a Poisson initial distribution with $\sigma_0^2 = \rho(1+\rho)$ and it agrees with our previous result (3.15).

Since the analysis based on order 1 time scale above can only describe the nucleation regime and provides little information of the dynamics after one particle escape from these two sites, next we consider the dynamics of a higher time scale $1/d_L$, under which Z_t tries to escape from the first two sites and to reach the stationary distribution μ. The expected time of this event can be estimated from the hitting time of the site $L/2$ starting the chain from 0. In Appendix B, the hitting time of such a chain on a finite state space $X = \{0, 1, ..., n\}$ with initial position $k \in X$ is derived as

$$\tau_k^n = \sum_{i=k}^{n-1} \lambda_i^n = \sum_{i=k}^{n-1} \frac{1}{\alpha_i \mu_i} \sum_{j=0}^{i} \mu_j, \tag{B.1}$$

where μ_i, $0 \le i \le n$ is the stationary distribution of the chain. Notice, under the time scale $1/d_L$, the birth and death rates are all scaled by $1/d_L$ but $\mu[Z_t]$ stays the same. Therefore, taking $k = 0$, $n = L/2$ and substituting (6.10) and (6.11) into the above equation, we can get the expected hitting time as

$$\tau_0^{L/2} = \frac{1}{\alpha_0} + \sum_{i=1}^{L/2-1} \frac{1+d_L+2id_L}{2d_L} = \frac{L^2}{8} + \frac{L-2}{4d_L}, \tag{6.14}$$

which depends on L and d_L. We then rescale above hitting time back to real time by multiplying above equation by $1/d_L$. Its inverse is then the rate of any two clusters meet on the lattice, which is dominated by the term of the order d_L/L^2, same as the rate $v(t)/s^2(t) = d_L/L^2$ used in previous derivation of (3.33).

To estimate the coarsening scaling law, we first write (6.7) as

$$C_{xx}(t) = \frac{d_L(\rho(1+\rho) - \sigma_0^2) + \rho^2}{d_L} \mathbb{P}_{z=0}\left[Z_t \neq 0\right] + \sigma_0^2,$$

then we assume the Poisson initial distribution and take the time derivative to get

$$\frac{dC_{xx}(t)}{dt} = \frac{\rho^2}{d_L} p_{z=0}\left(Z_t \neq 0\right), \tag{6.15}$$

where $p_{z=0}\left(Z_t \neq 0\right)$ is the probability density function of Z_t starting from 0 and not returning to 0 at time t. Notice, the exit rate of Z_t from site 1 to the right is $d_L/(1+2d_L)$ and the intermediate distribution of site 1 is $\mu'[1] = 2d_L/(1+3d_L)$, the total rate of Z_t escaping the first two site is $2d_L^2/(1+5d_L+6d_L^2)$, which is of the order d_L^2. After Z_t moving to site 2, it is then a simple symmetric random walk on the state space $\bar{X} = \{2, ..., L/2\} \subset X$ and reflecting at the right boundary. Therefore, we consider the time scale t/d_L^2, under which Z_t starting from site 2 is equivalent to a simple random walk with jump rate $1/d_L$ on a finite lattice $X^{\text{SRW}} = \{0, 1, 2, ..., L/2-1\}$, starting from site 1 with reflecting barrier $L/2-1$ and absorbing barrier 0. And Z_t starting from 2 and not returning to the two site $\{0, 1\}$ is equivalent to the simple random walk on X^{SRW} starting from 1 and not being absorbed by 0 at time t. For sufficiently large system, it is well known that the probability density of such random walk not being absorbed by the origin at time t decays as $\sqrt{d_L/t}$ (see, e.g., [126]) where d_L is the step size of the random walk. Therefore, we can take $\bar{t} = t/d_L^2$ and approximate $p_{z=0}\left(Z_{\bar{t}} \neq 0\right) \sim \sqrt{d_L/\bar{t}}$ in (6.15), and the solution of which is then

$$C_{xx}(t) \simeq C\rho^2\sqrt{d_L t} + \Theta(1), \tag{6.16}$$

where C is some constant and we assume the initial condition $C_{xx}(0) = \sigma_0^2 = \Theta(1)$. This approximation is based on large systems and confirms the same scaling law as our previous result (3.34) derived in Section 3.5.

6.4.2 Infinite systems

Next, we extend the above results to the SIP defined on an infinite lattice $\Lambda = \mathbb{Z}$. On an infinite lattice, we fix the average particle density to be ρ and a small diffusion

parameter d, which is now independent of the system size and plays the role of the scaling parameter. The system does not reach a fully condensed state as the finite systems, but we can still study the coarsening dynamics which stops after a window that now depends on d. Recall the time dependent variance $C_{xx}(t)$ (6.7) which also holds for infinite systems, and as $t \to \infty$ we have $\mathbb{P}_{x,x}[X_t = Y_t] \to 0$ and $\mathbb{P}_{x,x}[X_t \neq Y_t] \to 1$, which leads to

$$\sigma^2_\infty = \lim_{t\to\infty} C_{xx}(t) = \rho(1+\rho) + \frac{\rho^2}{d}, \quad \text{for a fixed } d. \tag{6.17}$$

The asymptotic behaviour is now independent of the initial second moment σ_0^2 and has a leading order of ρ^2/d, which depends on d in contrast to the finite system. We can also write the equivalent limit ρ^2/d_L in a finite system, but it cannot be reached if d_L is sufficiently small since the finite size effect will force the system to converge to a state where $C_{xx}(t) \simeq \rho^2 L$ as discussed in (6.13). It also confirms we need $d_L \ll 1/L$ to see the complete condensation in a finite system, otherwise $\rho^2/d_L \leq \rho^2 L$ and the system will stay in the state with $C_{xx}(t) \simeq \rho^2/d_L$ and does not reach complete condensation with a higher value of $C_{xx}(t) \simeq \rho^2 L$. Now we move back to the infinite case and look at the covariance $C_{xy}(t)$, which has a simple limit as

$$\sigma^{xy}_\infty = \lim_{t\to\infty} C_{xx}(t) = \rho^2.$$

In contrast to finite systems this is independent of d and is consistent with the limiting distribution being a product measure with density ρ, so that covariances $\sigma^{xy}_\infty - \rho^2$ vanish. Still, we see that the second moment of this measure increases with decreasing d, leading to rough configurations. Indeed, the distribution reached here as $t \to \infty$ is actually the grand-canonical stationary distribution with ϕ chosen to fix the density ρ. Recalling the average particle density derived in (2.30) as

$$R(\phi) = \phi\partial_\phi \log z(\phi) = \frac{d_L\phi}{1-\phi}\,, \tag{2.30 revisited}$$

and using the relation

$$\phi\partial_\phi R(\phi) = \sigma^2(\phi) - R^2(\phi),$$

with $\phi = \frac{\rho}{d_L+\rho}$, we have the following expression of the second moment under the grand-canonical distribution

$$\begin{aligned}\sigma^2(\phi) &= R^2(\phi) + \phi\partial_\phi R(\phi) \\ &= \rho^2 + \frac{\rho}{d_L+\rho}\frac{d_L(d_L+\rho)^2}{(d_L+\rho)^2 - 2\rho(d_L\rho) + \rho^2} \\ &= \rho(\rho+1) + \frac{\rho^2}{d_L},\end{aligned}$$

which is the same as (6.17) if we assume d_L to be fixed.

Now we look at the coarsening dynamics before the system reaches the stationary state $\nu_\phi(\rho)$ following the above computation with $C_{xx}(t) \simeq \rho^2/d$. We can apply the analogous analysis as in the finite system and consider the process $(Z_t := |X_t - Y_t|,\ t \geq 0)$, where the generator needs to be adapted as

$$\mathcal{L}f(z) = d(f(z+1)-f(z))+d(f(z-1)-f(z))+\mathbb{I}\{z=1\}(f(0)-f(1)),\ z \in \mathbb{N}_0. \quad (6.18)$$

Indeed, the argument we used in finite systems to derive the coarsening scaling law (6.16) can also be applied, since in the previous approximation we assume L to be sufficiently large. Therefore, the same method leads to the same scaling law as

$$C_{xx}(t) \simeq C\rho^2\sqrt{dt} + \Theta(1),$$

which holds until $C_{xx}(t)$ reaches the d-dependent limit (6.17).

6.5 Further study and summary

In this chapter we computed time dependent covariances of the symmetric inclusion process using the self-duality. Then we recovered heuristic results derived in previous chapters on nucleation and coarsening dynamics and relevant time scales, which we expect to turn into rigorous results with this approach in future work. The self-duality approach we used in this chapter also allows us to treat coarsening dynamics on infinite lattices directly, and reveals an interesting connection to the dynamics of two dual particles.

For further study, it would be interesting to investigate the rigorous forms of different dynamical regimes as well as symmetric systems in higher dimensions, where we expect the results derived in Chapter 5 could be recovered as well. The self-duality in inclusion processes introduced in this chapter relies on the symmetry of the dynamics, and cannot be directly applied to the asymmetric cases we discussed

in previous chapters. However, in a recent study [152] the authors constructed a different asymmetric inclusion process on finite lattice with Lie algebra and proved it is self-dual with a non-local self-duality function. This provides insights to construct self-duality for our asymmetric systems, with which we can further extend results in this chapter. In addition, it is interesting to apply our approach in previous chapters to the special asymmetric system and investigate the corresponding dynamics.

Chapter 7

Conclusion and Outlook

In this chapter we summarise the main results of this thesis and give an outlook of further research, supplementing the summaries and outlook provided at the end of each chapter in a more general perspective.

In this thesis we introduced several stochastic models that exhibit a condensation phenomenon, in particular models with stationary product measures, including the recently introduced inclusion process. We focused on the dynamics of condensation in the stochastic models under certain conditions, with particular emphasis on the inclusion process with vanishing diffusion rates. We generalised previous results on the symmetric inclusion process on finite lattices to more general asymmetric and higher dimensional cases in the thermodynamic limit. We identified all dynamic regimes during the formation of the condensate, with main focus on deriving the coarsening scaling law. Our predictions have been confirmed by extensive simulations and describe the actual dynamics very well, in particular in the asymmetric case. In the first part of this thesis we established a heuristic approach based on the analysis of the dynamics of a typical cluster and interactions with others in a mean-field approximation, which is justified by observations of the typical time evolution of the system. Besides this non-rigorous approach, we also give exact results of symmetric inclusion process in the sense of the nucleation dynamics and time scales of all dynamical regimes, where we used the self-duality and revealed an interesting connection to a two-particle dual process. The exact results also confirmed our predictions with the heuristic approach.

We considered the simple totally asymmetric inclusion process (TASIP) in Chapter 3 and compared to exact solutions for symmetric systems. We first identified the initial nucleation regime where neighbouring clusters from the initial distribution merge by the strong inclusion interaction. The nearest-neighbour product is

a suitable observable to describe this regime, where it exhibits a super-exponential decay due to the asymmetry, in contrast to the exact exponential decay in symmetric case. We then focused on the coarsening regime where clusters move on the lattice with a speed proportional to their sizes and exchange a small number of particles unbiasedly when they meet, leading to a growing average cluster size. The second moment of the occupation number is then a suitable observable here to characterise the transition, and it exhibits a power law scaling in this regime before saturating to stationarity following an exponential law depending on the system size. The interaction between two clusters is similar to the 'slinky' motion in the explosive condensate model as studied in [31, 32], but the approach we established in this thesis does not work for that model, where the full dynamics is dominated by a single large cluster and leads to a relaxation time scale that is decreasing with the system size. Our approach has been used in a recent paper on a symmetric version of the explosive condensation model, which also exhibits a regime of a coarsening scaling law with several clusters competing for particles [155].

In Chapter 4 we extended previous results to more general partially asymmetric inclusion processes (PASIP). Due to the partial asymmetry, particles in the system can move against the drifted direction, but due to the large size of clusters they effectively follow a totally asymmetric motion like in the TASIP, only with a slower speed. The interactions between two clusters are more complicated since the particles can 'jump back' as opposed to the TASIP. To investigate this mechanism, we mapped it to two-dimensional random walks with site-dependent rates and we revealed that a higher number of particles are exchanged when two cluster meet. Macroscopically, the clusters move slower but exchange more particles during interactions, which result in a very similar coarsening behaviour as in the TASIP, where the second moment exhibits a similar scaling law with a pre-factor depending on the intensity of the asymmetry in the system. We also studied the weakly asymmetric inclusion process (WASIP) where the asymmetry decays with the system size, and we found that it exhibits the features of both the SIP and the PASIP. This is similar to the classic and simpler results of the weakly asymmetric simple exclusion process, which has been shown to be a crossover between the symmetric and asymmetric versions of the simple exclusion process.

In Chapter 5 we looked at inclusion processes in two-dimensional lattices, with particular emphasis on the symmetric case (2DSIP). We first followed the heuristic approach used in previous chapters with the analysis of a typical cluster. We found that the interaction mechanism stayed the same while the rates of clusters meeting to interact were changed due to the high dimensionality, which we adapted

according to the underlying two-dimensional simple random walk. Therefore, the scaling law of the coarsening regime is different to the one-dimensional model and the second moment exhibits a logarithmic correction to the scaling. We also found that the coarsening regime in the 2DSIP is closely related to the classic two-dimensional coalescing random walk since the merge rates in the 2DSIP are high, and that the results for coalescing random walk provide satisfying approximations of the coarsening laws. The results in this chapter can also be easily generalised for inclusion processes defined on higher dimensional lattices, in particular the approximation of coarsening laws through the coalescing random walk. Due to transience of symmetric random walks in higher dimensions, symmetric and asymmetric systems in fact show the same scaling law as opposed to the results in one dimension.

In Chapter 6 we derived some preliminary exact results on symmetric systems through duality. We gave exact computations of the time dependent covariance using the self-duality of symmetric inclusion processes and a two-particle dual process. By considering this covariance under different time scales, we were able to recover previous results on the coarsening regime. With this approach, we expected the heuristic results in previous chapters can be turned into rigorous results in future work. More importantly, this approach also allows us to treat coarsening in the infinite lattice directly within a window depending on the fixed diffusion parameter, and reveal the relevant time scales of the nucleation and coarsening in the inclusion process.

A number of interesting and important open questions follow directly from the work in this thesis. Firstly, it would be interesting to derive the exact formula of the spectral gap of the generator in finite systems, which will also provide a rigorous description of the exponential dynamics in the saturation regime. Secondly, as we have shown numerically the WASIP stands as a crossover between the SIP and the PASIP, and one can further study this crossover in a more comprehensive way, where a reasonable starting point is to find the exact crossover scale. The analysis with duality also provided insights into the understanding of the inclusion process, and it posed significant challenges to give rigorous proofs of the dynamics, in particular for the asymmetric systems.

It is also interesting to further explore the potential applications of this work. For example, the Moran model in evolutionary genetics describes the competition between two alleles in a fixed population and is essentially the same as a symmetric inclusion process defined on a two-site lattice. The inclusion process studied in this thesis is equivalent to a multi-allele version Moran model with mutation, where the lattice site represents a phenotype and particles on the site denotes the individuals

has that phenotype. The pre-factor of transition rate can be understood as the fitness of the alleles controls that phenotype and the small diffusion rate represents mutation rate. The condensation is then equivalent to the genetic fixation of one certain allele, or the distinction of other alleles. In this case, the work within this thesis can be applied to investigate some multi-allelic biological systems such as the self-incompatibility loci in plants and the major histocompatibility complex (MHC) loci in vertebrates. Another potential application of inclusion process studied in this thesis is the kinetic wealth distribution in econophysics, which represented simplified models of an economy, where at random instances agents exchange wealth and the total wealth is preserved. In this case, the particles can be represented as wealth or money, and lattice sites are agents. One can the further investigate the wealth concentration through the condensation in inclusion processes, as well as more general properties such as stationary distribution and time dependent correlation functions.

Appendix A

Mathematical Definitions and Related Results

A.1 Interacting particle system, Markov semigroup and generator

In this appendix, we introduce the definitions and results of interacting particle systems, Markov semigroups and generators in a more mathematical sense. Even the introduction in Section 2.1 provides enough theoretical foundation for the results of this thesis, we extend these definitions and theories slightly here for completeness. Comparing with introduction in Section 2.1, we introduce the definition of Feller process and extend the definition of semigroups to more general continuous functions, and then introduce the Hille-Yosida theorem which presents the one-to-one correspondence of a Markov semigroup and a Markov generator.

The **state space** of an interacting particle system is the set of all possible configurations $X = E^{\Lambda}$, where E is the countable local state space and Λ is the lattice (a countable set). Throughout this thesis we restrict to $E = \mathbb{N}$ and Λ to be a subset of $\mathbb{Z}^d$ and denote a lattice of L sites as Λ_L. Configurations are denoted by $\boldsymbol{\eta} = (\eta_x : x \in \Lambda) \in X$, where η_x is the number of particles on site $x \in \Lambda$. X is then a metric space with measurable structure given by the σ-algebra of Borel sets. Let $D([0, +\infty), X)$ be the set of all functions $\boldsymbol{\eta}(\cdot)$ on $[0, +\infty)$ with values in X which are right continuous and have left limits. $t \mapsto \boldsymbol{\eta}(t)$ is a sample path for a Markov process with state space X. For $s \in [0, +\infty)$, the evaluation mapping π_s from $D([0, +\infty), X)$ to X is defined by $\pi_s(\boldsymbol{\eta}(\cdot)) = \boldsymbol{\eta}(s)$. Let $\mathcal{F}$ be the smallest σ-algebra on $D([0, +\infty), X)$ relative to which all the mappings π_s are measurable. For $t \in [0, +\infty)$, let $\mathcal{F}_t$ be the smallest σ-algebra on $D([0, +\infty), X)$ relative to which

all the mappings π_s for $s \leq t$ are measurable. Then $\Omega = (D([0,+\infty), X), \mathcal{F}, \mathcal{F}_t)$ is the filtered probability space of the process.

Definition A.1. A **Markov Process** on X is a collection $\{\mathbb{P}^n, \boldsymbol{\eta} \in X\}$ of probability measures on $D[0,+\infty)$ indexed by X with the following properties:

(a) $\mathbb{P}^{\boldsymbol{\eta}}[\boldsymbol{\zeta}(\cdot) \in D[0,+\infty) : \boldsymbol{\zeta}(0) = \boldsymbol{\eta}] = 1$, for all $\boldsymbol{\eta} \in X$.

(b) The mapping $\boldsymbol{\eta} \mapsto \mathbb{P}^{\boldsymbol{\eta}}[A]$ from X to $[0,1]$ is measurable for every $A \in \mathcal{F}$.

(c) $\mathbb{P}^{\boldsymbol{\eta}}[\boldsymbol{\eta}(s+\cdot) \in A | \mathcal{F}_s] = \mathbb{P}^{\boldsymbol{\eta}(s)}[A]$ a.s. $(P^{\boldsymbol{\eta}})$ for every $\boldsymbol{\eta} \in X$ and $A \in \mathcal{F}$ (Markov property).

The expectation with respect to $\mathbb{P}^{\boldsymbol{\eta}}$ is denoted by

$$\mathbb{E}^{\boldsymbol{\eta}}[F] = \int_{D[0,+\infty)} F \, d\mathbb{P}^{\boldsymbol{\eta}} \tag{A.1}$$

for any measurable function F on $D[0,+\infty)$ which is integrable relative to $\mathbb{P}^{\boldsymbol{\eta}}$.

Let $C(X)$ denote the collection of continuous functions on X, regarded as a Banach space with

$$\|f\|_\infty = \sup_{\boldsymbol{\eta} \in X} |f(\boldsymbol{\eta})| \, .$$

For $f \in C(X)$, write the operator $S(t) : C(X) \to C(X)$ as

$$S(t)f(\boldsymbol{\eta}) = \mathbb{E}^{\boldsymbol{\eta}}[f(\boldsymbol{\eta}(t))]. \tag{A.2}$$

Definition A.2. A Markov process $\{\mathbb{P}^{\boldsymbol{\eta}}, \boldsymbol{\eta} \in X\}$ is said to be a **Feller process** if $S(t)f \in C(X)$ for every $t \geq 0$ and $f \in C(X)$.

Definition A.3. A family $\{S(t), t \geq 0\}$ of linear operators on $C(X)$ is called a **Markov semigroup** if it satisfies the following properties:

(a) $S(0) = I$, the identity operator on $C(X)$.

(b) The mapping $t \mapsto S(t)f$ from $[0,+\infty)$ to $C(X)$ is right continuous for every $f \in C(X)$.

(c) $S(t+s)f = S(t)S(s)f$ for all $f \in C(X)$ and all $s, t \geq 0$.

(d) $S(t)1 = 1$ for all $t \geq 0$.

(e) $S(t)f \geq 0$ for all nonnegative $f \in C(X)$.

Remark. (a) is equivalent to (a) in Definition 2.3 and (b) follows the right continuity of $\boldsymbol{\eta}$ and f. (c) is also the Markov property which is equivalent to (c) in Definition 2.3.

The importance of Markov semigroups lies in the fact there is a one-to-one correspondence between Markov semigroups and Markov processes, as stated in the following theorems.

Theorem A.1. *For a Feller Markov process* $\{\mathbb{P}^{\boldsymbol{\eta}}, \boldsymbol{\eta} \in X\}$ *on* X*, the family of linear operators* $\{S(t), t \geq 0\}$ *defined in Definition A.3 is a Markov semigroup.*

Theorem A.2. *For a Markov semigroup* $\{S(t), t \neq 0\}$ *as given in Definition A.3, there exists a unique Feller Markov process* $\{\mathbb{P}^{\boldsymbol{\eta}}, \boldsymbol{\eta} \in X\}$ *such that (A.2) holds for all* $t \geq 0$*.*

Proof. The proofs of above two theorems can be found in many textbooks, for example [43, Section 1.1]. □

For a given Markov process, the corresponding semigroup fully describes the time evolution of expected values of observables $f \in C(X)$. The expectation of an observable at time $t \neq 0$ with respect to initial distribution μ is given by

$$\mathbb{E}^{\mu}\left[f(\boldsymbol{\eta}(t))\right] = \int_X \left(S(t)f\right)(\boldsymbol{\zeta})\mu[d\boldsymbol{\zeta}] = \int_X S(t)f \, d\mu \quad \text{for all} \quad f \in C(X).$$

It is then natural to introduce Markov generator, which can be intuitively thought of as the time derivative of semigroup.

Definition A.4. The **Markov generator** of a Markov semigroup $(S(t), t \geq 0)$ defined on $C(X)$ is a linear operator $\mathcal{L}$ defined on its domain $D_{\mathcal{L}} \subseteq C(X)$ as $\mathcal{L} : D_{\mathcal{L}} \to C(X)$,

$$\mathcal{L}f = \lim_{t \searrow 0} \frac{1}{t}\left(S(t)f - f\right), \quad \text{for every} \quad f \in D_{\mathcal{L}}\,. \tag{A.3}$$

The **resolvent set** of a linear operator $\mathcal{L}$ is the set of all complex number $\lambda \in \mathbb{C}$ for which $(\lambda I - \mathcal{L})^{-1}$ is bounded. The following theorem illustrates the one-to-one correspondence of a Markov generator and a Markov semigroup.

Theorem A.3 (Hille-Yosida)**.** *A linear operator* $\mathcal{L}$ *defined on a linear subspace* $D_{\mathcal{L}}$ *of* $C(X)$ *generates a Markov semigroup if and only if*

(a) $D_{\mathcal{L}}$ *is dense in* $C(X)$ *and ,*

(b) every real $\lambda > 0$ *belongs to the resolvent set and for such* λ

$$\left\|(\lambda I - \mathcal{L})^{-1}\right\| \leq \frac{1}{\lambda}.$$

For lattice gases with compact local state space, we restrict $\mathcal{L} : C_0(X) \to C(X)$ and $u(t) = S(t)f \in C(X)$ is the unique solution to the backward equation

$$\frac{d}{dt}u(t) = \mathcal{L}u(t), \quad u(0) = f.$$

Here $C_0(X) \subset C(X)$ denotes the set of cylinder functions, which depend only on the configuration on finitely many lattice sites. The Markov generator is then given by

$$\mathcal{L}f(\boldsymbol{\eta}) = \sum_{\boldsymbol{\eta}' \in X} c(\boldsymbol{\eta}, \boldsymbol{\eta}') \left[f(\boldsymbol{\eta}') - f(\boldsymbol{\eta}) \right]. \tag{A.4}$$

The restriction to cylinder functions is necessary for convergence of the sum of $c(\boldsymbol{\eta}, \boldsymbol{\eta}')$.

Appendix B

Results on Birth-Death Chains and Random Walks

In the following we derive the mean first-passage time of a special birth-death process with site-dependent rates which was used to calculate the expected time of a single cluster's movement in Section 4.3.1. It is essentially equivalent to the discussion in [87, Section 4.5] and a continuous version of results in [156]. We then state relevant results of a simplified version which was used to calculate the expected number of jumps of an interaction in Section 3.4.1 and Section 4.3.1. For detailed discussion of more general birth-death processes see, e.g., [45, 94].

Consider a birth-death process $(S(t), t \geq 0)$ as a continuous-time Markov chain on a finite state space $X = \{0, 1, 2, ..., n\} \in \mathbb{N}$ with site-dependent birth rates α_i and death rates β_i, $i \in X$, and with boundary conditions $\alpha_n = 0$, $\beta_0 = 0$.

Denoting the expectation of $(S(t), t \geq 0)$ with initial condition $S(0) = k \in X$ as $\mathbb{E}_k$, the mean first-passage time of $S(t)$ is defined as

$$\tau_k^n = \mathbb{E}_k \left[\inf\{t > 0 : S(t) = n\}\right], \quad \forall k \in X = \{0, 1, 2, ..., n\}.$$

Then we have the recursion equation

$$\tau_k^n = \frac{\alpha_k}{\alpha_k + \beta_k}\tau_{k+1}^n + \frac{\beta_k}{\alpha_k + \beta_k}\tau_{k-1}^n + \frac{1}{\alpha_k + \beta_k}, \quad \text{for} \quad k = 0, 1, 2, ..., n-1,$$

with $\tau_n^n = 0$ and $\frac{1}{\alpha_k + \beta_k}$ is the mean waiting time on site k. Rearranging this equation we have

$$\left(\tau_k^n - \tau_{k+1}^n\right)\frac{\alpha_k}{\alpha_k + \beta_k} = \left(\tau_{k-1}^n - \tau_k^n\right)\frac{\beta_k}{\alpha_k + \beta_k} + \frac{1}{\alpha_k + \beta_k}, \quad \text{for } k = 1, 2, 3, ..., n-1.$$

Denoting $\lambda_k^n = \tau_k^n - \tau_{k+1}^n$, we have

$$\alpha_k \lambda_k^n = \beta_k \lambda_{k-1}^n + 1,$$

with $\lambda_0^n = \tau_0^n - \tau_1^n = \frac{1}{\alpha_0}$. Denoting the stationary measure for this process $\boldsymbol{\mu} = (\mu_0, \mu_1, ..., \mu_n)$, the detailed balance of stationary measures (Proposition 2.2) is then $\mu_k \alpha_k = \mu_{k+1} \beta_{k+1}$, which leads to

$$\mu_k = \left(\prod_{i=1}^{k} \frac{\alpha_{i-1}}{\beta_i} \right) \mu_0, \quad \text{for } k = 1, 2, ..., n.$$

Now we have

$$\begin{aligned} \lambda_1^n &= \frac{\beta_1}{\alpha_1} \lambda_0^n + \frac{1}{\alpha_1} = \frac{1}{\alpha_1} \left(\frac{\beta_1}{\alpha_0} + 1 \right) = \frac{1}{\alpha_1} \left(\frac{\mu_0}{\mu_1} + \frac{\mu_1}{\mu_1} \right), \\ \lambda_2^n &= \frac{\beta_2}{\alpha_2} \lambda_1^n + \frac{1}{\alpha_2} = \frac{1}{\alpha_2} \left(\frac{\mu_0}{\mu_2} + \frac{\mu_1}{\mu_2} + \frac{\mu_2}{\mu_2} \right). \end{aligned}$$

It is then easy to show by induction that

$$\lambda_k^n = \frac{1}{\alpha_k \mu_k} \sum_{i=0}^{k} \mu_i \,.$$

Therefore, with $\tau_n^n = 0$ we have

$$\tau_k^n = \sum_{i=k}^{n-1} \lambda_i^n = \sum_{i=k}^{n-1} \frac{1}{\alpha_i \mu_i} \sum_{j=0}^{i} \mu_j. \tag{B.1}$$

We only discuss birth-death chains on a finite state space here since in the thesis we always consider interactions of a finite number of particles. For such birth-death chains defined on infinite space with $X = \{0, 1, 2, ...\}$, one can also find a closed form for the hitting time of the origin, see, e.g., [45, Theorem 1.3.5]. For transient or null recurrent chains expectations of hitting times can also be infinite. In the case of $k > n$ for a birth-death chain restricted on the finite state space $0, .., N$ with $N > k$, we can simply invert the states i by mapping $i \mapsto N - i$, $\alpha_i \mapsto \beta_{N-i}$ and $\beta_i \mapsto \alpha_{N-i}$, and obtain the formula $\tau_k^n = \tau'^{N-n}_{N-k}$ where τ' is given by the formula (B.1).

In Section 3.4.1 and 4.3.1 in this thesis we also used results from a simplified version of above process with $\alpha_i = p$, $\beta_i = q$, for $i = 1, 2, 3, ..., n-1$, where $p + q = 1$ are constants and absorption condition $\alpha_0 = \beta_0 = \alpha_n = \beta_n = 0$. This is indeed the classic simple asymmetric random walk on a finite lattice with absorption at the

boundaries, which is also called the gambler's ruin problem. We briefly introduce relevant results for completeness here, and more general discussion can be found in many textbooks, e.g. [45, 94].

For a given random walk $(S(t), t \geq 0)$ on X, define the hitting time of a set $A \in X$ as

$$T^A := \inf \{t \geq 0, S(t) \in A\},$$

then the hitting time of either boundaries is given by

$$T^* := T^{\{0,n\}} = \inf \{t \geq 0, S(t) \in \{0, n\}\}.$$

We also define the probability of the random walker starting from site k and being absorbed at boundary n as

$$h_k := \mathbb{P}_{S(0)=k} [S(T^*) = n].$$

First, we consider h_k, which satisfies the recursion equation

$$h_k = ph_{k+1} + qh_{k-1},$$

with $h_0 = 0$, $h_n = 1$. The characteristic function of the above equation is

$$s = ps^2 + q$$

with roots $s_1 = 1$, $s_2 = q/p$. Therefore, if $p \neq q$, the general form of h_k is

$$h_k = As_1^k + Bs_2^k = A + B\left(\frac{q}{p}\right)^k,$$

and with boundary conditions we have

$$h_k = \frac{1 - \left(\frac{q}{p}\right)^k}{1 - \left(\frac{q}{p}\right)^n}. \tag{B.2}$$

If $p = q$, then $s = s_1 = s_2 = 1$ and the general solution is

$$h_k = As^k + Bks^k = A + Bk,$$

with boundary conditions we have

$$h_k = \frac{k}{n}. \tag{B.3}$$

In Section 4.3.1, we use (B.2) to derive the effective jump rates (4.3) and (4.4) of a single cluster in the PASIP.

Now we consider the expectation of the hitting time $\delta_k = \mathbb{E}_k[T^*]$ with initial position $S(0) = k$. δ_k fulfils the recursion

$$\delta_k = p\delta_{k+1} + q\delta_{k-1} + 1, \quad k = 1, 2, ..., n-1\,, \tag{B.4}$$

and terminal condition $\delta_0 = \delta_n = 0$. Similar to h_k, we can find the characteristic equation of the above difference equation to be

$$s = ps^2 + q$$

with roots $s_1 = 1$ and $s_2 = q/p$.

Therefore, if $p \neq q$, the general solution of the homogeneous version of (B.4) is

$$As_1^k + Bs_2^k = A + B\left(\frac{q}{p}\right)^k.$$

To obtain a particular solution we try ck, where c is some constant to be determined. Plugging it into (B.4) we get

$$ck = pc(k+1) + qc(k-1) + 1,$$

which implies $c = \frac{1}{q-p}$. Then the solution follows as

$$\delta_k = A + B\left(\frac{q}{p}\right)^k + \frac{k}{q-p}.$$

And using the boundary conditions we get

$$\delta_k = \frac{k}{q-p} - \frac{n}{q-p}\frac{1-(q/p)^k}{1-(q/p)^n}. \tag{B.5}$$

If $p = q = 1/2$, $s = s_1 = s_2 = 1$ and the general solution to the homogeneous equation is

$$As^k + Bks^k = A + Bk.$$

To obtain a particular solution we try ck^2, and get

$$ck^2 = \frac{1}{2}c(k+1)^2 + \frac{1}{2}c(k-1)^2 + 1,$$

which implies $c = -1$. It follows that

$$\delta_k = A + Bk - k^2,$$

and with boundary conditions we have

$$\delta_k = k(n-k). \tag{B.6}$$

Expression (B.5) is used in Section 4.3.1 to derive the waiting time of a single cluster's movement in the PASIP, and (B.6) is used in Section 3.4.1 for the SIP. For the above asymmetric random walk problem, one can also use a different approach which defines a martingale $Y_n := (q/p)^{S(n)}$. This approach is called De Moivre's martingale and details can be found in textbooks, e.g. [94, Section 12.1].

Appendix C

Numerical Methods

C.1 Canonical measures and current

We summarise some properties of the canonical measures which we use in Chapter 2 to calculate the canonical current following ideas in [87]. The calculations are possible due to the product form of the reference measures.

Consider an interacting particle system $(\boldsymbol{\eta}(t),\, t \geq 0)$ with product measures defined on a finite lattice Λ_L with L sites (see detailed definitions in Section 2.2). Choosing fugacity $\phi = 1$, the reference measures are given by the product of L single site marginals as

$$\nu^L[d\boldsymbol{\eta}] = \prod_{x=1}^{L} \bar{\nu}[\eta_x] d\boldsymbol{\eta}.$$

The canonical measures are defined by conditioning on the total number of particles N in the system (see details in Section 2.2). And we write the canonical measure as

$$\pi_{L,N}[d\boldsymbol{\eta}] = \nu^L \left[d\boldsymbol{\eta} \middle| \sum_{x=1}^{L} \eta_x = N \right] = \frac{1}{Z_{L,N}} \prod_{x \in \Lambda} w(\eta_x) d\boldsymbol{\eta},$$

where $Z_{L,N} = \nu^L \left[\sum_{x=1}^{L} \eta_x = N \right]$. The product form of ν^L leads to

$$\begin{aligned} Z_{L,N} &= \sum_{k=0}^{N} \nu^L \left[\sum_{x=1}^{L} \eta_x = N, \sum_{x=1}^{L-1} \eta_x = (N-k) \right] \\ &= \sum_{k=0}^{N} \bar{\nu}[k] Z_{L-1,N-k}, \end{aligned}$$

which can be used to calculate $Z_{L,N}$ recursively with initial condition $Z_{1,k} = \bar{\nu}[k]$. One can also divide $Z_{L,N}$ into any sub-system in the same way, and for large system $L = 2^n$ for some $n \in \mathbb{N}$ we use a more efficient form as

$$Z_{L,N} = \sum_{k=0}^{N} Z_{L/2,k} Z_{L/2,N-k} \ . \tag{C.1}$$

For the zero-range process (2.23) we have

$$\nu[n] \propto \prod_{k=1}^{n} \frac{1}{g(k)},$$

and thus $g(k)\nu[k] = \nu[k-1]$. Therefore the current, defined as the average jump rate of a single site, can be calculated as

$$\begin{aligned} \pi_{L,N}(g(\eta_1)) &= \frac{1}{Z_{L,N}} \sum_{\boldsymbol{\eta}} g(\eta_1) \nu^L[\boldsymbol{\eta}] \delta \left(\sum_{x=1}^{L} \eta_x - N \right) \\ &= \frac{1}{Z_{L,N}} \sum_{\boldsymbol{\eta}'} \nu^L[\boldsymbol{\eta}'] \delta \left(\sum_{x=1}^{L} \eta'_x - (N-1) \right) \\ &= \frac{Z_{L,N-1}}{Z_{L,N}}. \end{aligned}$$

For the inclusion process, we do not have the simple formula as for the zero-range process and we use the following recursive method to calculate the canonical current for a fixed system. For a given system size $L+2$, we first fix the diffusion parameter $d_{L+2} = (L+2)^{-\gamma}$, $\gamma > 1$. Then calculate $Z_{L,n}$ as in (C.1) with $w(n) = \frac{\Gamma(d_{L+2}+n)}{n!\Gamma(d_{L+2})}$ for $n = 0, 1, ..., N$. Then we have

$$Z_{L+2,n} = \sum_{k=0}^{n} Z_{L,k} Z_{2,n-k}, \quad \text{for } \ k = 0, 1, ..., N,$$

and

$$J_{L+2,n} = \sum_{k=0}^{n} Z_{L,k} \sum_{i=0}^{n-k} w(i) w(n-k-i) i(d_{L+2} + n - k - i) \, ,$$

and the canonical current is given by

$$j_{L+2,n} = \frac{J_{L+2,n}}{Z_{L+2,n}} \, .$$

Notice during the approximation d_{L+2} is a fixed value and therefore for different

sized system the whole calculation needs to be done from scratch.

C.2 Simulation methods of Inclusion Process

Throughout this thesis the simulation results for the inclusion processes are produced using a Gillespie type update algorithm[157, 158] described in this section, extended in [87] to more general systems. This algorithm is also known as the Bortz-Kalos-Lebowitz algorithm [159], and mathematically is a variety of a dynamic Monte Carlo method. It is an exact algorithm giving statistically correct trajectories of the Markov process.

All the pseudo random numbers in the simulations results were generated using the Fast Mersenne Twister [160], an improved version of the classic Mersenne Twister [161].

C.2.1 Exact Algorithm

We first introduce the exact algorithm to simulate inclusion processes as described by the generator (2.27). The simulation is applied to a system with N particles on a finite lattice Λ_L of L sites with periodic boundary conditions. The state of the process at time t is denoted by $\boldsymbol{\eta}(t) = (\eta_x(t))_{x\in\Lambda_L}$ and the diffusion parameter is a fixed constant as $d_L = L^{-\gamma}$, $\gamma > 1$. The jump rate of the underlying homogeneous random walk is $q(x)$ (2.24) with a finite range B. The initial state is uniformly distributed.

Algorithm 1 Main algorithm for the Inclusion process.

Input: L, N, d_L and the stopping criteria.

{**Initialise the system uniformly**}
$t \leftarrow 0$
for $x = 1$ to N **do**
  Select $x \in \{1, 2, ..., L\}$ uniformly
  $\eta_x \leftarrow \eta_x + 1$
end for
Calculate and store the L jump rates off each site in the current state $c_x = \sum_y q(y)\eta_x(d_L + \eta_y)$, $x = 1, 2, ..., L$.
Calculate and store the partial rate sums $C_n = \sum_{x=1}^{n} c_x$, for $n = 1, 2, ..., L$ and $C_0 = 0$.
{**The main update loop**}
while The stopping criteria is not satisfied **do**
  Update state $\boldsymbol{\eta}(t)$ according to Algorithm 2
end while

Algorithm 2 Update algorithm for the Inclusion Process

Input: Current jump rates off each site $(c_x)_{x=1}^{L}$,
Input: Current partial rate sums $(C_n)_{n=0}^{L}$.
{ **Sample time increment from** $\exp(C_L)$ }
$dt \leftarrow$ Exponentially distributed random number with mean $1/C_L$
$t \leftarrow t + dt$
{ **Choose to move particle of site** x **with probability** c_x/C_L }
$r \leftarrow$ Uniform random number on $[0, C_L)$
Perform a binary search for x such that $C_{x-1} \leq r < C_x$
$\eta_x \leftarrow \eta_x - 1$
{ **Choose target site according to jump rates** }
Find all potential target sites $A := \{y \in \Lambda_L, |y - x| \leq R\}$, $M := |A|$
$S_0 = 0$
for $j = 1, 2, ..., M$ **do**
    $h_j = q(y)\eta_x(d_L + \eta_y)$
    $S_j = S_{j-1} + h_j$
    $j \leftarrow j + 1$
end for
$r \leftarrow$ Uniform random number on $[0, S_M)$
Perform a binary search for j such that $S_{k-1} \leq r < S_k$
and find the y such that $h_k = q(y)\eta_x(d_L + \eta_y)$
$\eta_y \leftarrow \eta_y + 1$
{ **Update transition rates and partial sums**}
Update rates for all c_y that contains η_x or η_y
Update C_n for $n \in \{\min\{y, c_y \text{ is influenced}\}, \ldots, L\}$

Remarks

(1) The stopping criteria in the main algorithm can be adapted to different aims of simulations. For example $t < t_{max}$ for running within a fixed time interval, $\sum_{x\in\Lambda_L} \mathbb{1}\{\eta_x\} = 1$ for reaching the stationary regime, and $\sum_{x\in\Lambda}\sum_{|y-x|\leq R}\eta_x\eta_y = 0$ for reaching the absorbing state of nucleation regime, etc.

(2) Since $\eta_x \in \mathbb{N}$ and $0 \leq \eta_x \leq N$, one way to optimise the algorithm is to construct a matrix of all possible (partial) transition rates $T_{i,j} = i(d_L + j)$, $\forall i, j \in \{0, 1, ..., N\}$, then look it up when calculating jump rates as $c_x = \sum_y q(y)T_{x,y}$ and $h_x = q(y)T_{x,y}$ in order to save repeated calculation. The expense of this optimisation is more memory usage since we have to store this $(N+1)\times(N+1)$ matrix for the whole simulation.

(3) The algorithms above can be applied to inclusion processes defined on general graphs. For the one-dimensional nearest-neighbour ones, $R = 1$ and choosing the target site y can be simplified as

- TASIP: $y = x + 1$,
- PASIP: $y = \begin{cases} x+1, & \text{with probability } p \\ x-1, & \text{with probability } q \end{cases}$,
- SIP: $y = \begin{cases} x+1, & \text{with probability } 1/2 \\ x-1, & \text{with probability } 1/2 \end{cases}$.

Also due to the simple spatial structure of a one-dimensional lattice, we can simplify the computation of C_x, with an expense of memory usage, by storing them in a binary tree. It is convenient to consider $L = 2^n$, $n \in \mathbb{N}$, then we can construct $C_{x,y} = C_{x-1,2y-1} + C_{x-1,2y}$ for $x \in \{0, 1, ..., n\}$ and $y \in \{1, 2, ..., 2^{n-x}\}$ with initial condition $C_{0,y} = c_y$ for $y \in \{1, 2, ..., L\}$. In this case the updates to the rates can be done by retracing the path followed down the binary tree by the binary search, which selects the transition to do and reduces the computation complexity for C_x from $O(L)$ to $O(\log L)$. For systems defined on higher dimensional lattices or more general graphs, this optimisation cannot be applied directly but one can follow the idea and find simplification methods adapted to the specific structure of the graph.

C.2.2 Effective Algorithm

In the coarsening regime of the inclusion process dynamics, the above algorithm is exact but inefficient particularly for the symmetric case, due to the large number

of attempted movement of particles to empty sites until successful cluster steps. In this sub-section we describe a more efficient algorithm to simulate the coarsening regime based on effective transition rates. We first simulate the system with the exact dynamics for a short time to reach the coarsening regime, then replace the exact dynamics by the effective dynamics depending on the neighbouring sites of the target site as follows: If the target site has no other occupied neighbouring site, we move the whole cluster with the effective rates derived in (4.3) or (4.4). And if the target site has an occupied neighbouring site, the jump triggers an interaction which we approximate with a random walk on a simplex with absorbing states (see details in Section 4.3.2). This is based on the strong separation of time scales resulting from the scaling $Ld_L \to 0$. The following is an example of this effective algorithm for one-dimensional PASIP (see details in Section 2.3.2).

Algorithm 3 Effective algorithm for PASIP.

Input: L, N, d_L, p, q and the stopping criteria.

{**Initialise the system uniformly**}
$t \leftarrow 0$
for $i = 1$ to N **do**
  Select $x \in \{1, 2, ..., L\}$ uniformly
  $\eta_x \leftarrow \eta_x + 1$
end for
Calculate and store the L jump rates off each site in the current state $c_x = p\eta_x(d_L + \eta_{x+1}) + q\eta_x(d_L + \eta_{x-1})$, $x = 1, 2, ..., L$.
Calculate and store the partial rate sums $C_n = \sum_{x=1}^{n} c_x$, for $n = 1, 2, ..., L$ and $C_0 = 0$.
{**Run exact dynamics for a short time**}
while $t < t_1$ **do**
  Update state $\boldsymbol{\eta}(t)$ with exact dynamics (Algorithm 2).
end while
{**Run effective dynamics for the rest**}
Update effective rates off a single site c'_x, for $x = 1, 2, ..., L$ (Algorithm5)
Update effective partial sums $C'_n = \sum_{x=1}^{n} c'_x$, for $n = 1, 2, ..., L$
while The stopping criteria is not satisfied **do**
  Update state $\boldsymbol{\eta}(t)$ with effective jump rates (Algorithm 4)
end while

Algorithm 4 Effective update algorithm for PASIP

Input: Current effective jump rates off each site $(c'_x)_{x=1}^L$,
Input: Current effective partial rate sums $(C'_n)_{n=0}^L$.
{ **Sample time increment from** $\exp(C'_L)$ }
$dt \leftarrow$ Exponentially distributed random number with mean $1/C'_L$
$t \leftarrow t + dt$
{ **Choose to move particle of site** x **with probability** c'_x/C'_L }
$r \leftarrow$ Uniform random number on $[0, C'_L)$
Perform a binary search for x such that $C'_{x-1} \leq r < C'_x$
$\eta_x \leftarrow \eta_x - 1$
{ **Choose target site according to jump rates** }
Compute effective jump rate to the right $c'_{x,R}$ and to the left $c'_{x,L}$
$r \leftarrow$ Uniform random number on $[0, c'_{x,R} + c'_{x,L})$
if $r > c'_{x,R}$ **then**
    Target site y is $x + 1$
else
    Target site y is $x - 1$
end if
if If y has no other occupied neighbour **then**
    $\eta_y \leftarrow \eta_x$
    $\eta_x \leftarrow 0$
else
    Run interaction (Algorithm 6) with η_x, η_y and the other neighbour η_z, $z = y + 1$ or $y - 1$
end if
{ **Update transition rates and partial sums**}
Update rates for all c'_y that contains η_x or η_y
Update C'_n for $n \in \{\min\{y, c'_y \text{ is influenced}\}, \ldots, L\}$

Algorithm 5 Effective rates update for PASIP.

Input: p, q, d_L, $\boldsymbol{\eta}$ and departure site x

{**Effective rate jump to the right**}
if $\eta_{x+2} = 0$ **then**
  $c'_{x,R} = \frac{1-q/p}{1-(q/p)^{\eta_x}} p d_L \eta_x$.
else
  $c'_{x,R} = p d_L \eta_x$
end if
{**Effective rate jump to the left**}
if $\eta_{x-2} = 0$ **then**
  $c'_{x,L} = \frac{1-p/q}{1-(p/q)^{\eta_x}} q d_L \eta_x$.
else
  $c'_{x,L} = q d_L \eta_x$
end if
{**Total jump rate off site** x}
$c'_x = c'_{x,L} + c'_{x,R}$

Algorithm 6 Two cluster interaction algorithm in PASIP

Input: Departure site η_x, intermediate site η_y the other neighbour site η_z

If $y = x + 1$, $p' = p$ and $q' = q$. If $y = x - 1$, $p' = q$, and $q' = p$.
$M = \eta_x + \eta_z$
$\eta_x \leftarrow \eta_x - 1$
$\eta_y \leftarrow 1$
{**Run a 2D random walk with site-dependent jump rates and absorbing boundary**}
while $0 < \eta_x + \eta_z < M$ **do**
{Update rates for all potential jump events}
  Event: $\eta_x \leftarrow \eta_x + 1$, $\eta_y \leftarrow \eta_y - 1$. Rate: $R_1 = q\eta_y(d_L + \eta_x)$
  Event: $\eta_x \leftarrow \eta_x - 1$, $\eta_y \leftarrow \eta_y + 1$. Rate: $R_2 = p\eta_x(d_L + \eta_y)$
  Event: $\eta_z \leftarrow \eta_z + 1$, $\eta_y \leftarrow \eta_y - 1$. Rate: $R_3 = p\eta_y(d_L + \eta_z)$
  Event: $\eta_z \leftarrow \eta_z + 1$, $\eta_y \leftarrow \eta_y - 1$. Rate: $R_4 = q\eta_z(d_L + \eta_y)$
  $R_s = R_1 + R_2 + R_3 + R_4$
  $r \leftarrow$ Uniform random number on $[0, R_s)$
  Search for i such that $\sum_{k=1}^{i-1} R_k < r < \sum_{k=1}^{i} R_k$
  Make the move corresponding to R_i
end while

Return: η_x, η_y, η_z

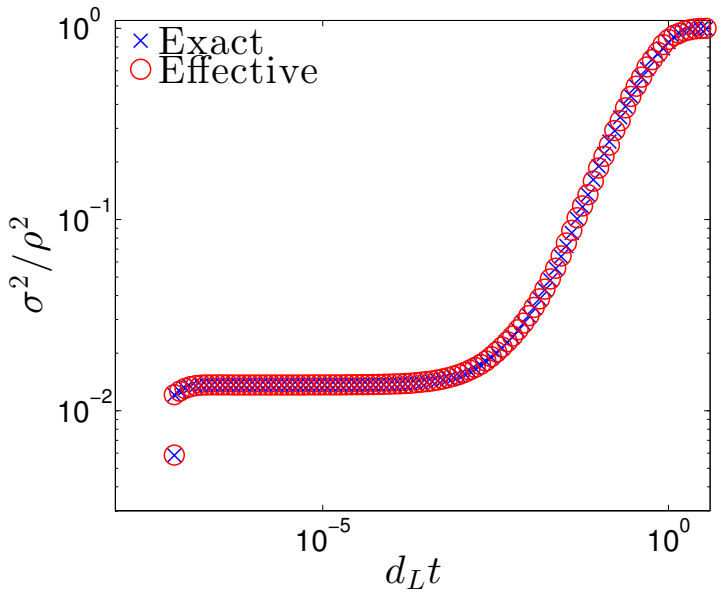

Figure C.1: Exact dynamics (Algorithm 1,2) and effective dynamics (Algorithm 3,4,5,6) for an PASIP model with $L = 256$, $\rho = 2$, $p = 0.75$. Data are averaged over 200 realisations. Errors are bounded by the size of symbols.

Remarks

(1) The only difference between the above effective algorithm and the exact algorithm is that the former omits the probabilities of the splitting of a cluster and any particle escaping during an interaction, or two or more interactions or steps occurring at the same time. But such probabilities decrease with the system size (see details in Section 3.4), therefore the effective algorithms are efficient and accurate for large systems comparing with the exact ones. Figure C.1 illustrates the agreement of the effective algorithms with the exact ones.

(2) Above algorithm for PASIP can be easily adapted to TASIP and SIP. For TASIP, simply take $p = 1$, $q = 0$ (or $p = 0$, $q = 1$) and restrict the single move direction of all particles. For the SIP, take $p = q = 1/2$ and also the effective jump rates to a site with no other occupied neighbour need to be computed as $\frac{1}{2}d_L$ due to the symmetry of the dynamics (see analysis in Section 3.4.1).

(3) The same effective algorithms can also be adapted to higher dimensional lattices. Taking two-dimensional lattices as we studied in Chapter 5 as an example, now for each departure site there are four potential target sites and to determine the effective transition rates for each of them we have to check if any of its other

three nearest-neighbour is occupied. Also the interaction algorithm would be more complicated since there are possible interactions between three and four clusters, and we need to map the interactions to site-dependent random walks in three and four dimensional spaces.

Bibliography

[1] J Cao, P Chleboun, and S Grosskinsky. Dynamics of condensation in the totally asymmetric inclusion process. *Journal of Statistical Physics*, 155(3):523–543, 2014.
1 citation(s) on 1 page(s): vii.

[2] D Ruelle. *Statistical Mechanics : Rigorous Results*. World Scientific Publishing Company Incorporated, 1999.
1 citation(s) on 1 page(s): 2.

[3] H Georgii. *Gibbs Measures and Phase Transitions*. Walter de Gruyter, 2nd edition, 2011.
2 citation(s) on 2 page(s): 2 and 14.

[4] F Spitzer. Interaction of Markov processes. *Advances in Mathematics*, 5:246–290 (1970), 1970.
9 citation(s) on 6 page(s): 2, 7, 13, 15, 17, and 22.

[5] C T MacDonald, J H Gibbs, and A C Pipkin. Kinetics of biopolymerization on nucleic acid templates. *Biopolymers*, 6(1):1–25, 1968.
1 citation(s) on 1 page(s): 3.

[6] T M Liggett. *Stochastic Interacting Systems: Contact, Voter and Exclusion Processes*. Springer, 1999.
4 citation(s) on 4 page(s): 3, 6, 22, and 99.

[7] L Bertini, A De Sole, D Gabrielli, G Jona-Lasinio, and C Landim. Stochastic interacting particle systems out of equilibrium. *Journal of Statistical Mechanics: Theory and Experiment*, 2007(07):P07014–P07014, 2007.
1 citation(s) on 1 page(s): 3.

[8] O Golinelli and K Mallick. The asymmetric simple exclusion process: an

integrable model for non-equilibrium statistical mechanics. *Journal of Physics A: Mathematical and Theoretical*, 39(4):12679–12705, 2006.
1 citation(s) on 1 page(s): 3.

[9] M R Evans. Phase transitions in one-dimensional nonequilibrium systems. *Brazilian Journal of Physics*, 30(1):42–57, 2000.
9 citation(s) on 6 page(s): 3, 4, 13, 22, 25, and 31.

[10] C Godrèche. Dynamics of condensation in zero-range processes. *Journal of Physics A: Mathematical and General*, 36(23):6313–6328, 2003.
6 citation(s) on 5 page(s): 3, 4, 22, 25, and 31.

[11] J-M Drouffe, C Godrèche, and F Camia. A simple stochastic model for the dynamics of condensation. *Journal of Physics A: Mathematical and General*, 31(1):L19–L25, 1998.
5 citation(s) on 5 page(s): 3, 4, 13, 22, and 31.

[12] S Grosskinsky, G M Schütz, and H Spohn. Condensation in the zero range process: stationary and dynamical properties. *Journal of Statistical Physics*, 113(3-4):389–410, 2003.
12 citation(s) on 9 page(s): 3, 4, 13, 19, 20, 21, 22, 25, and 31.

[13] M R Evans and T Hanney. Nonequilibrium statistical mechanics of the zero-range process and related models. *Journal of Physics A: Mathematical and General*, 38(19):R195–R240, 2005.
3 citation(s) on 3 page(s): 3, 4, and 31.

[14] C Godrèche and J M Luck. Condensation in the inhomogeneous zero-range process: an interplay between interaction and diffusion disorder. *Journal of Statistical Mechanics: Theory and Experiment*, 2012(12):P12013, 2012.
4 citation(s) on 4 page(s): 3, 4, 14, and 22.

[15] C Giardinà, J Kurchan, and F Redig. Duality and exact correlations for a model of heat conduction. *Journal of Mathematical Physics*, 48(3):033301, 2007.
4 citation(s) on 4 page(s): 3, 25, 26, and 104.

[16] C Giardinà, F Redig, and K Vafayi. Correlation inequalities for interacting particle systems with duality. *Journal of Statistical Physics*, 141(2):242–263, 2010.
7 citation(s) on 7 page(s): 3, 15, 25, 26, 102, 104, and 107.

[17] P A P Moran. *The Statistical Processes of Evolutionary Theory*. Clarendon Press; Oxford University Press., 1962.
2 citation(s) on 2 page(s): 3 and 26.

[18] J Kaupužs, R Mahnke, and R J Harris. Zero-range model of traffic flow. *Physical Review E*, 72(5):056125, 2005.
1 citation(s) on 1 page(s): 3.

[19] E Levine, G Ziv, L Gray, and D Mukamel. Phase transitions in traffic models. *Journal of Statistical Physics*, 117(5-6):819–830, 2004.
1 citation(s) on 1 page(s): 3.

[20] D Chowdhury, L Santen, and A Schadschneider. Statistical physics of vehicular traffic and some related systems. *Physics Reports*, 329(4):199–329, 2000.
1 citation(s) on 1 page(s): 3.

[21] O J O'loan, M R Evans, and M E Cates. Jamming transition in a homogeneous one-dimensional system: the bus route model. *Physical Review E*, 58(2):1404–1418, 1998.
1 citation(s) on 1 page(s): 3.

[22] Z Burda, D Johnston, J Jurkiewicz, M Kamiński, M A Nowak, G Papp, and I Zahed. Wealth condensation in pareto macroeconomies. *Physical Review E*, 65(2):026102, 2002.
1 citation(s) on 1 page(s): 3.

[23] A G Angel, M R Evans, E Levine, and D Mukamel. Critical phase in non-conserving zero-range processes and rewiring networks. *Physical Review E*, 72(4):046132, 2005.
1 citation(s) on 1 page(s): 3.

[24] P L Krapivsky, S Redner, and F Leyvraz. Connectivity of growing random networks. *Physical Review Letters*, 85(2):4629–4632, 2000.
1 citation(s) on 1 page(s): 3.

[25] I Jeon. Phase transition for perfect condensation and instability under the perturbations on jump rates of the zero-range process. *Journal of Physics A: Mathematical and Theoretical*, 43(2):235002, 2010.
1 citation(s) on 1 page(s): 4.

[26] I Jeon, P March, and B Pittel. Size of the largest cluster under zero-range invariant measures. *Annals of Probability*, 28(3):1162–1194, 2000.

4 citation(s) on 4 page(s): 4, 13, 20, and 25.

[27] Y Schwarzkopf, M R Evans, and D Mukamel. Zero-range processes with multiple condensates: statics and dynamics. *Journal of Physics A: Mathematical and Theoretical*, 41(2):205001, 2008.
1 citation(s) on 1 page(s): 4.

[28] A G Thompson, J Tailleur, M E Cates, and R A Blythe. Zero-range processes with saturated condensation: the steady state and dynamics. *Journal of Statistical Mechanics: Theory and Experiment*, 02(0):013, 2010.
1 citation(s) on 1 page(s): 4.

[29] B Waclaw, J Sopik, W Janke, and H Meyer-Ortmanns. Mass condensation in one dimension with pair-factorized steady states. *Journal of Statistical Mechanics: Theory and Experiment*, 2009(10):P10021, 2009.
2 citation(s) on 2 page(s): 4 and 14.

[30] R J Concannon and R A Blythe. Spatiotemporally complete condensation in a non-Poissonian exclusion process. *Physical Review Letters*, 112(5):050603, 2014.
1 citation(s) on 1 page(s): 4.

[31] M R Evans and B Waclaw. Condensation in stochastic mass transport models: beyond the zero-range process. *Journal of Physics A: Mathematical and Theoretical*, 47(9):095001, 2014.
8 citation(s) on 7 page(s): 4, 13, 31, 32, 53, 85, and 117.

[32] B Waclaw and M R Evans. Explosive condensation in a mass transport model. *Physical Review Letters*, 108(7):070601, 2012.
10 citation(s) on 9 page(s): 4, 13, 15, 17, 31, 32, 45, 53, and 117.

[33] S N Majumdar, S Krishnamurthy, and M Barma. Nonequilibrium phase transition in a model of diffusion, aggregation, and fragmentation. *Journal of Statistical Physics*, 99(1):1–29, 2000.
1 citation(s) on 1 page(s): 4.

[34] S N Majumdar, S Krishnamurthy, and M Barma. Nonequilibrium phase transitions in models of aggregation, adsorption, and dissociation. *Physical Review Letters*, 81(1):3691–3694, 1998.
1 citation(s) on 1 page(s): 4.

[35] O Hirschberg, D Mukamel, and G M Schütz. Motion of condensates in non-Markovian zero-range dynamics. *Journal of Statistical Mechanics: Theory and Experiment*, 2012(08):P08014, 2012.
3 citation(s) on 3 page(s): 4, 22, and 31.

[36] O Hirschberg, D Mukamel, and G M Schütz. Condensation in temporally correlated zero-range dynamics. *Physical Review Letters*, 103(9):090602, 2009.
1 citation(s) on 1 page(s): 4.

[37] C Godreche and J M Luck. Dynamics of the condensate in zero-range processes. *Journal of Physics A: Mathematical and General*, 38(33):7215–7237, 2005.
4 citation(s) on 4 page(s): 4, 22, 25, and 31.

[38] C Godrèche and J M Luck. Nonequilibrium dynamics of the zeta urn model. *The European Physical Journal B*, 23:473–486, 2001.
2 citation(s) on 2 page(s): 4 and 31.

[39] C Godreche. From urn models to zero-range processes: statics and dynamics. In *Ageing and the Glass Transition*, pages 261–294. Springer, 2007.
2 citation(s) on 2 page(s): 4 and 31.

[40] L Ferretti and G Bianconi. Dynamics of condensation in growing complex networks. *Physical Review E*, 78(5):056102, 2008.
2 citation(s) on 2 page(s): 4 and 31.

[41] S Grosskinsky, F Redig, and K Vafayi. Dynamics of condensation in the symmetric inclusion process. *Electronic Journal of Probability*, 18(0), 2013.
7 citation(s) on 7 page(s): 4, 30, 31, 32, 34, 47, and 102.

[42] P Chleboun and S Grosskinsky. Condensation in stochastic particle systems with stationary product measures. *Journal of Statistical Physics*, 154(1-2):432–465, 2014.
14 citation(s) on 13 page(s): 6, 14, 16, 17, 19, 20, 21, 22, 26, 27, 31, 32, and 87.

[43] T M Liggett. *Interacting Particle Systems*. Springer Verlag, Berlin, 1985.
11 citation(s) on 10 page(s): 6, 7, 8, 9, 11, 17, 18, 20, 103, and 122.

[44] D A Levin, Y Peres, and E L Wilmer. *Markov Chains and Mixing Times*. American Mathematical Soc., 2008.
1 citation(s) on 1 page(s): 6.

[45] J R Norris. *Markov Chains*. Cambridge University Press, 1998.
6 citation(s) on 6 page(s): 6, 8, 12, 124, 125, and 126.

[46] E D Andjel. Invariant measures for the zero range processes. *Annals of Probability*, 10(3):525–547, 1982.
5 citation(s) on 5 page(s): 8, 13, 17, 22, and 24.

[47] G Carinci, C Giardinà, C Giberti, and F Redig. Duality for stochastic models of transport. *Journal of Statistical Physics*, 152(4):657–697, 2013.
4 citation(s) on 4 page(s): 8, 13, 104, and 106.

[48] Walter Rudin. *Real and Complex Analysis*. McGraw-Hill international editions in mathematics. McGraw-Hill, New York, NY, 1987.
1 citation(s) on 1 page(s): 8.

[49] T M Liggett. An infinite particle system with zero range interactions. *Annals of Probability*, 1(2):240–253, 1973.
1 citation(s) on 1 page(s): 13.

[50] C Cocozza-Thivent. Processus des misanthropes. *Probability Theory and Related Fields*, 70(4):509–523, 1985.
4 citation(s) on 3 page(s): 13, 15, and 17.

[51] S N Majumdar, M R Evans, and R K P Zia. Nature of the condensate in mass transport models. *Physical Review Letters*, 94(18):180601, 2005.
1 citation(s) on 1 page(s): 13.

[52] E Levine, D Mukamel, and G M Schütz. Zero-range process with open boundaries. *Journal of Statistical Physics*, 120(516):759–778, 2005.
1 citation(s) on 1 page(s): 13.

[53] R J Harris, A Rákos, and G M Schütz. Current fluctuations in the zero-range process with open boundaries. *Journal of Statistical Mechanics: Theory and Experiment*, 08(0):003–P08003, 2005.
1 citation(s) on 1 page(s): 13.

[54] P A Ferrari, C Landim, and V V Sisko. Condensation for a fixed number of independent random variables. *Journal of Statistical Physics*, 128(5):1153–1158, 2007.
4 citation(s) on 4 page(s): 13, 19, 20, and 25.

[55] I Armendáriz and M Loulakis. Thermodynamic limit for the invariant measures in supercritical zero range processes. *Probability Theory and Related Fields*, 145(1-2):175–188, 2008.
3 citation(s) on 3 page(s): 13, 20, and 25.

[56] I Armendáriz, S Grosskinsky, and M Loulakis. Zero-range condensation at criticality. *Stochastic Processes and their Applications*, 123(9):3466–3496, 2013.
3 citation(s) on 3 page(s): 13, 20, and 25.

[57] M R Evans. Bose-Einstein condensation in disordered exclusion models and relation to traffic flow. *Europhysics Letters*, 36(1):13–18, 2007.
1 citation(s) on 1 page(s): 14.

[58] J Krug and P A Ferrari. Phase transitions in driven diffusive systems with random rates. *Journal of Physics A: Mathematical and General*, 29(18):L465–L471, 1999.
1 citation(s) on 1 page(s): 14.

[59] C Landim. Hydrodynamical limit for space inhomogeneous one-dimensional totally asymmetric zero-range processes. *Annals of Probability*, pages 599–638, 1996.
1 citation(s) on 1 page(s): 14.

[60] C Mailler, P Mörters, and D Ueltschi. Condensation and symmetry-breaking in the zero-range process with weak site disorder. *arXiv.org*, 2015.
1 citation(s) on 1 page(s): 14.

[61] P A Ferrari and V V Sisko. Escape of mass in zero-range processes with random rates. In *Asymptotics: Particles, Processes and Inverse Problems*, pages 108–120. Institute of Mathematical Statistics, Beachwood, Ohio, USA, 2007.
1 citation(s) on 1 page(s): 14.

[62] A G Angel, M R Evans, and D Mukamel. Condensation transitions in a one-dimensional zero-range process with a single defect site. *Journal of Statistical Mechanics: Theory and Experiment*, 2004(04):P04001–17, 2004.
1 citation(s) on 1 page(s): 14.

[63] S Grosskinsky, P Chleboun, and G M Schütz. Instability of condensation in the zero-range process with random interaction. *Physical Review E*, page 030101(R), 2008.

1 citation(s) on 1 page(s): 14.

[64] L C G del Molino, P Chleboun, and S Grosskinsky. Condensation in randomly perturbed zero-range processes. *Journal of Physics A: Mathematical and Theoretical*, 45(20):205001, 2012.
1 citation(s) on 1 page(s): 14.

[65] C Giardinà, J Kurchan, F Redig, and K Vafayi. Duality and hidden symmetries in interacting particle systems. *Journal of Statistical Physics*, 135(1):25–55, 2009.
8 citation(s) on 6 page(s): 14, 15, 26, 102, 104, and 107.

[66] M R Evans, S N Majumdar, and R K P Zia. Factorized steady states in mass transport models on an arbitrary graph. *Journal of Physics A: Mathematical and General*, 39(18):4859–4873, 2006.
1 citation(s) on 1 page(s): 14.

[67] T Hanney. Factorized steady states for multi-species mass transfer models. *Journal of Statistical Mechanics: Theory and Experiment*, 2006(12):P12006, 2006.
1 citation(s) on 1 page(s): 14.

[68] M R Evans, T Hanney, and S N Majumdar. Interaction-driven real-space condensation. *Physical Review Letters*, 97(1):010602, 2006.
1 citation(s) on 1 page(s): 14.

[69] J M Luck and C Godrèche. Structure of the stationary state of the asymmetric target process. *Journal of Statistical Mechanics: Theory and Experiment*, 2007(08):P08005–P08005, 2007.
2 citation(s) on 2 page(s): 15 and 17.

[70] T Gobron and E Saada. Couplings, attractiveness and hydrodynamics for conservative particle systems. *Annales de l'Institut Henri Poincaré, Probabilités et Statistiques*, 46(4):1132–1177, 2010.
1 citation(s) on 1 page(s): 15.

[71] T Rafferty, P Chleboun, and S Grosskinsky. Monotonicity and condensation in homogeneous stochastic particle systems. *arXiv.org*, 2015.
1 citation(s) on 1 page(s): 15.

[72] L Fajfrova, T Gobron, and E Saada. Invariant measures for mass migration processes. *arXiv.org*, 2015.

1 citation(s) on 1 page(s): 15.

[73] C Kipnis and C Landim. *Scaling Limits of Interacting Particle Systems*. Springer Science & Business Media, 1999.
4 citation(s) on 4 page(s): 17, 19, 20, and 22.

[74] S Grosskinsky, F Redig, and K Vafayi. Condensation in the inclusion process and related models. *Journal of Statistical Physics*, 142(5):952–974, 2011.
11 citation(s) on 8 page(s): 17, 22, 26, 27, 32, 57, 87, and 102.

[75] H Spohn. *Large Scale Dynamics of Interacting Particles*. Springer Verlag, 1991.
1 citation(s) on 1 page(s): 17.

[76] B Derrida, M R Evans, V Hakim, and V Pasquier. Exact solution of a 1d asymmetric exclusion model using a matrix formulation. *Journal of Physics A: Mathematical and General*, 26(7):1493–1517, 1993.
1 citation(s) on 1 page(s): 17.

[77] I Csiszar and J Körner. *Information Theory: Coding Theorems for Discrete Memoryless Systems*. Academic Press, 1981.
1 citation(s) on 1 page(s): 19.

[78] G M Schütz and R J Harris. Hydrodynamics of the zero-range process in the condensation regime. *Journal of Statistical Physics*, 127(2):419–430, 2007.
1 citation(s) on 1 page(s): 22.

[79] O Hirschberg, D Mukamel, and G M Schütz. Condensation in temporally correlated zero-range dynamics. *Physical Review Letters*, 103(9):090602, 2009.
1 citation(s) on 1 page(s): 22.

[80] J Beltrán and C Landim. Metastability of reversible condensed zero range processes on a finite set. *Probability Theory and Related Fields*, 152(3-4):781–807, 2011.
2 citation(s) on 2 page(s): 22 and 34.

[81] I Armendáriz, S Grosskinsky, and M Loulakis. Metastability in a condensing zero-range process in the thermodynamic limit. *arXiv.org*, 2015.
1 citation(s) on 1 page(s): 22.

[82] J Beltrán and C Landim. Tunneling and metastability of continuous time Markov chains II, the nonreversible case. *Journal of Statistical Physics*, 149(4):598–618, 2012.

1 citation(s) on 1 page(s): 22.

[83] C Landim. Metastability for a non-reversible dynamics: the evolution of the condensate in totally asymmetric zero range processes. *Communications in Mathematical Physics*, 330(1):1–32, 2012.
1 citation(s) on 1 page(s): 22.

[84] P Chleboun and S Grosskinsky. A dynamical transition and metastability in a size-dependent zero-range process. *Journal of Physics A: Mathematical and Theoretical*, 48(5), 2015.
1 citation(s) on 1 page(s): 22.

[85] H Hinrichsen. Critical phenomena in nonequilibrium systems. *arXiv preprint cond-mat/0001070*, 2000.
1 citation(s) on 1 page(s): 22.

[86] R Holley. A class of interactions in an infinite particle system. *Advances in Mathematics*, 5:291–309 (1970), 1970.
1 citation(s) on 1 page(s): 24.

[87] P Chleboun. *Large Deviations and Metastability in Condensing Stochastic Particle Systems*. PhD thesis, The University of Warwick, The University of Warwick, 2012.
11 citation(s) on 8 page(s): 26, 28, 29, 32, 44, 124, 129, and 131.

[88] S Reuveni, I Eliazar, and U Yechiali. Asymmetric inclusion process as a showcase of complexity. *Physical Review Letters*, 109(2):020603, 2012.
1 citation(s) on 1 page(s): 26.

[89] S Reuveni, O Hirschberg, I Eliazar, and U Yechiali. Occupation probabilities and fluctuations in the asymmetric simple inclusion process. *Physical Review E*, 89(4):042109, 2014.
1 citation(s) on 1 page(s): 26.

[90] K Vafayi and M H Duong. Weakly nonequilibrium properties of a symmetric inclusion process with open boundaries. *Physical Review E*, 90(5), 2014.
1 citation(s) on 1 page(s): 26.

[91] J T Lewis and C E Pfister. Thermodynamic probability theory: some aspects of large deviations. *Russian Mathematical Surveys*, 50(2):279–317, 2007.
1 citation(s) on 1 page(s): 29.

[92] J Beltrán, M Jara, and C Landim. A martingale problem for an absorbed diffusion: the nucleation phase of condensing zero range processes. *arXiv.org*, 2015.
1 citation(s) on 1 page(s): 31.

[93] A Opoku and F Redig. Coupling and hydrodynamic limit for the inclusion process. *Journal of Statistical Physics*, pages 1–16, 2015.
2 citation(s) on 2 page(s): 31 and 104.

[94] G Grimmett. *Probability and Random Processes*. Oxford University Press, USA, 2001.
5 citation(s) on 5 page(s): 37, 110, 124, 126, and 128.

[95] F Family and T Vicsek. *Dynamics of Fractal Surfaces*. World Scientific, 1991.
1 citation(s) on 1 page(s): 49.

[96] K Johansson. Shape fluctuations and random matrices. *Communications in Mathematical Physics*, 209(2):437–476, 2000.
1 citation(s) on 1 page(s): 56.

[97] B Derrida and A Gerschenfeld. Current fluctuations of the one dimensional symmetric simple exclusion process with step initial condition. *Journal of Statistical Physics*, 136(1):1–15, 2009.
1 citation(s) on 1 page(s): 56.

[98] C A Tracy and H Widom. On ASEP with step Bernoulli initial condition. *Journal of Statistical Physics*, 137(5-6):825–838, 2009.
1 citation(s) on 1 page(s): 56.

[99] C A Tracy and H Widom. Total current fluctuations in the asymmetric simple exclusion process. *Journal of Mathematical Physics*, 50(9):095204, 2009.
1 citation(s) on 1 page(s): 56.

[100] C A Tracy and H Widom. Asymptotics in ASEP with step initial condition. *Communications in Mathematical Physics*, 290(1):129–154, 2009.
1 citation(s) on 1 page(s): 56.

[101] L Bertini, C Landim, and M Mourragui. Dynamical large deviations for the boundary driven weakly asymmetric exclusion process. *Annals of Probability*, 37(6):2357–2403, 2009.
2 citation(s) on 2 page(s): 56 and 82.

[102] B Derrida, C Enaud, C Landim, and S Olla. Fluctuations in the weakly asymmetric exclusion process with open boundary conditions. *Journal of Statistical Physics*, 118(5-6):795–811, 2005.
2 citation(s) on 2 page(s): 56 and 82.

[103] A Demasi, E Presutti, and E Scacciatelli. The weakly asymmetric simple exclusion process. *Annales de l'Institut Henri Poincaré, Probabilités et Statistiques*, 25(1):1–38, 1989.
1 citation(s) on 1 page(s): 56.

[104] P Dittrich and J Gartner. A central limit theorem for the weakly asymmetric simple exclusion process. *Mathematische Nachrichten*, 151(1):75–93, 1991.
1 citation(s) on 1 page(s): 56.

[105] P Dittrich. Travelling waves and long-time behaviour of the weakly asymmetric exclusion process. *Probability Theory and Related Fields*, 86(4):443–455, 1990.
2 citation(s) on 2 page(s): 56 and 82.

[106] C Enaud and B Derrida. Large deviation functional of the weakly asymmetric exclusion process. *Journal of Statistical Physics*, 114(3-4):537–562, 2004.
2 citation(s) on 2 page(s): 56 and 82.

[107] D Simon. Bethe ansatz for the weakly asymmetric simple exclusion process and phase transition in the current distribution. *Journal of Statistical Physics*, 142(5):931–951, 2011.
2 citation(s) on 2 page(s): 56 and 82.

[108] L Bertini and G Giacomin. Stochastic burgers and KPZ equations from particle systems. *Communications in Mathematical Physics*, 183(3):571–607, 1997.
1 citation(s) on 1 page(s): 56.

[109] R Juhász, L Santen, and F Iglói. Partially asymmetric zero-range process with quenched disorder. *Physical Review E*, 72(4):046129, 2005.
2 citation(s) on 1 page(s): 56.

[110] R Juhász, L Santen, and F Iglói. Partially asymmetric exclusion models with quenched disorder. *Physical Review Letters*, 94(1):010601, 2005.
1 citation(s) on 1 page(s): 56.

[111] T M Liggett. Exponential L2 convergence of attractive reversible nearest particle systems. *Annals of Probability*, 17:403–432, 1989.

1 citation(s) on 1 page(s): 81.

[112] C Landim, S Sethuraman, and S Varadhan. Spectral gap for zero-range dynamics. *Annals of Probability*, 24(4):1871–1902, 1996.
1 citation(s) on 1 page(s): 81.

[113] Y Nagahata. Spectral gap for zero-range processes with jump rate g(x)=xγ. *Stochastic Processes and their Applications*, 120(6):949–958, 2010.
1 citation(s) on 1 page(s): 81.

[114] B Morris. Spectral gap for the zero range process with constant rate. *Annals of Probability*, 34(5):1645–1664, 2006.
1 citation(s) on 1 page(s): 81.

[115] A Galves and H Guiol. Relaxation time of the one-dimensional symmetric zero range process with constant rate. *Markov Processes and Related Fields*, 3(3):323–332, 1997.
1 citation(s) on 1 page(s): 81.

[116] J de Gier and F H L Essler. Exact spectral gaps of the asymmetric exclusion process with open boundaries. *Journal of Statistical Mechanics: Theory and Experiment*, 2006(12):P12011–P12011, 2006.
1 citation(s) on 1 page(s): 81.

[117] T Sasamoto and H Spohn. The crossover regime for the weakly asymmetric simple exclusion process. *Journal of Statistical Physics*, 140(2):209–231, 2010.
1 citation(s) on 1 page(s): 82.

[118] E Lazar and R Pemantle. Coarsening in one dimension: invariant and asymptotic states. *arXiv.org*, 2015.
1 citation(s) on 1 page(s): 82.

[119] C Landim and H T Yau. Fluctuation-dissipation equation of asymmetric simple exclusion processes. *Probability Theory and Related Fields*, 108(3):321–356, 1997.
1 citation(s) on 1 page(s): 85.

[120] H T Yau. $\log(t)^{2/3}$ Law of the two dimensional asymmetric simple exclusion process. *Annals of Mathematics*, 159(1):377–405, 2004.
1 citation(s) on 1 page(s): 85.

[121] R L Greenblatt and J L Lebowitz. Product measure steady states of generalized zero range processes. *Journal of Physics A: Mathematical and General*, 39(7):1565–1573, 2006.
1 citation(s) on 1 page(s): 85.

[122] C Bernardin. Superdiffusivity of asymmetric energy model in dimensions 1 and 2. *Journal of Mathematical Physics*, 49(10):103301–21, 2008.
1 citation(s) on 1 page(s): 85.

[123] R M Munasinghe, R Rajesh, and O V Zaboronski. Multiscaling of correlation functions in single species reaction-diffusion systems. *Physical Review E*, 73(5):051103–10, 2006.
1 citation(s) on 1 page(s): 95.

[124] R Munasinghe, R Rajesh, R Tribe, and O Zaboronski. Multi-scaling of the n-point density function for coalescing Brownian motions. *Communications in Mathematical Physics*, 268(3):717–725, 2006.
1 citation(s) on 1 page(s): 95.

[125] E W Montroll. Random walks on lattices. III. calculation of first-passage times with application to exciton trapping on photosynthetic units. *Journal of Mathematical Physics*, 10(4):753–14, 1969.
2 citation(s) on 2 page(s): 95 and 101.

[126] M Bramson and D Griffeath. Asymptotics for interacting particle systems on Zd. *Zeitschrift für Wahrscheinlichkeitstheorie und Verwandte Gebiete*, 53(2):183–196, 1980.
2 citation(s) on 2 page(s): 99 and 112.

[127] S Sawyer. A limit theorem for patch sizes in a selectively-neutral migration model. *Journal of Applied Probability*, 16(3):482, 1979.
1 citation(s) on 1 page(s): 99.

[128] F P Kelly. The asymptotic behaviour of an invasion process. *Journal of Applied Probability*, 14(3):584, 1977.
1 citation(s) on 1 page(s): 99.

[129] A Sudbury. The size of the region occupied by one type in an invasion process. *Journal of Applied Probability*, 13(2):355–356, 1976.
1 citation(s) on 1 page(s): 99.

[130] J T Cox. Coalescing random-walks and voter model consensus times on the torus in Zd. *Annals of Probability*, 17(4):1333–1366, 1989.
1 citation(s) on 1 page(s): 99.

[131] J T Cox and D Griffeath. Mean field asymptotics for the planar stepping stone model. *Proceedings of the London Mathematical Society*, 3(1):189–208, 1990.
1 citation(s) on 1 page(s): 99.

[132] P Lévy. Processus stochastiques et mouvement brownien, 1948.
1 citation(s) on 1 page(s): 103.

[133] S Karlin and J McGregor. The classification of birth and death processes. *Transactions of the American Mathematical Society*, pages 366–400, 1957.
1 citation(s) on 1 page(s): 103.

[134] D V Lindley. The theory of queues with a single server. In *Mathematical Proceedings of the Cambridge Philosophical Society*, volume 48(02), pages 277–289. Cambridge University Press, 1952.
1 citation(s) on 1 page(s): 103.

[135] D Siegmund. The equivalence of absorbing and reflecting barrier problems for stochastically monotone Markov processes. *Annals of Probability*, pages 914–924, 1976.
1 citation(s) on 1 page(s): 103.

[136] A Sudbury and P Lloyd. Quantum operators in classical probability theory: II. The concept of duality in interacting particle systems. *Annals of Probability*, pages 1816–1830, 1995.
1 citation(s) on 1 page(s): 103.

[137] W Vervaat. Algebraic duality of Markov processes. *Stochastic Processes and their Applications*, 26:185–186, 1987.
1 citation(s) on 1 page(s): 103.

[138] S N Ethier and T G Kurtz. *Markov Processes.* Characterization and Convergence. John Wiley & Sons, 2009.
2 citation(s) on 1 page(s): 103.

[139] P Clifford and A Sudbury. A sample path proof of the duality for stochastically monotone Markov processes. *Annals of Probability*, pages 558–565, 1985.
1 citation(s) on 1 page(s): 103.

[140] J T Cox and U Rösler. A duality relation for entrance and exit laws for Markov processes. *Stochastic Processes and their Applications*, 16(2):141–156, 1984.
1 citation(s) on 1 page(s): 103.

[141] R Holley and D W Stroock. Dual processes and their application to infinite interacting systems. *Advances in Mathematics*, 32(2):149–174, 1979.
1 citation(s) on 1 page(s): 103.

[142] S Jansen and N Kurt. On the notion (s) of duality for Markov processes. *Probability Surveys*, 11:59–120, 2014.
4 citation(s) on 4 page(s): 103, 104, 105, and 107.

[143] R Getoor. Duality theory for Markov processes: Part 1. *arXiv.org*, 2010.
1 citation(s) on 1 page(s): 103.

[144] K L Chung and J B Walsh. *Markov Processes, Brownian Motion, and Time Symmetry*. Springer Science & Business Media, 2006.
1 citation(s) on 1 page(s): 103.

[145] S Asmussen. *Applied Probability and Queues*, volume 51 of *Applications of Mathematics (New York)*. Springer-Verlag, New York, second edition, 2003.
1 citation(s) on 1 page(s): 103.

[146] A Sudbury. Dual families of interacting particle systems on graphs. *Journal of Theoretical Probability*, 13(3):695–716, 2000.
1 citation(s) on 1 page(s): 103.

[147] M Möhle. The concept of duality and applications to Markov processes arising in neutral population genetics models. *Bernoulli. Official Journal of the Bernoulli Society for Mathematical Statistics and Probability*, 5(5):761–777, 1999.
1 citation(s) on 1 page(s): 103.

[148] P Diaconis and J A Fill. Strong stationary times via a new form of duality. *Annals of Probability*, 18(4):1483–1522, 1990.
1 citation(s) on 1 page(s): 103.

[149] D A Dawson and A Greven. *Spatial Fleming-Viot Models with Selection and Mutation*, volume 2092 of *Lecture Notes in Mathematics*. Springer, Cham, 2014.
1 citation(s) on 1 page(s): 103.

[150] K Kuoch and F Redig. Ergodic theory of the symmetric inclusion process. *arXiv.org*, 2015.
1 citation(s) on 1 page(s): 104.

[151] G Carinci, C Giardinà, F Redig, and T Sasamoto. A generalized Asymmetric Exclusion Process with $U_q(sl_2)$ stochastic duality. *arXiv.org*, 2014.
1 citation(s) on 1 page(s): 104.

[152] G Carinci, C Giardinà, F Redig, and T Sasamoto. Asymmetric stochastic transport models with $\mathcal{U}_q(\mathfrak{su}(1,1))$ symmetry. *arXiv.org*, 2015.
2 citation(s) on 2 page(s): 104 and 115.

[153] B Van Ginkel and F Redig. Duality and stationary distributions of the" Immediate Exchange Model" and its generalizations. *arXiv.org*, 2015.
1 citation(s) on 1 page(s): 104.

[154] G Carinci, C Giardinà, C Giberti, and F Redig. Dualities in population genetics: a fresh look with new dualities. *Stochastic Processes and their Applications*, 125(3):941–969, 2015.
1 citation(s) on 1 page(s): 104.

[155] Y Chau, C Connaughton, and S Grosskinsky. Explosive condensation in symmetric mass transport models. *arXiv.org*, 2015.
1 citation(s) on 1 page(s): 117.

[156] K P N Murthy and K W Kehr. Mean first-passage time of random walks on a random lattice. *Physical Review A*, 40(4):2082–2087, 1989.
1 citation(s) on 1 page(s): 124.

[157] D T Gillespie. A general method for numerically simulating the stochastic time evolution of coupled chemical reactions. *Journal of Computational Physics*, 22(4):403–434, 1976.
1 citation(s) on 1 page(s): 131.

[158] D T Gillespie. Exact stochastic simulation of coupled chemical reactions. *The Journal of Physical Chemistry*, 81(25):2340–2361, 1977.
1 citation(s) on 1 page(s): 131.

[159] A B Bortz, M H Kalos, and J L Lebowitz. A new algorithm for Monte Carlo simulation of Ising spin systems. *Journal of Computational Physics*, 17(1):10–18, 1975.
1 citation(s) on 1 page(s): 131.

[160] M Saito and M Matsumoto. SIMD-oriented fast mersenne twister: a 128-bit pseudorandom number generator. In *Monte Carlo and Quasi-Monte Carlo Methods 2006*, pages 607–622. Springer Berlin Heidelberg, Berlin, Heidelberg, 2008.
1 citation(s) on 1 page(s): 131.

[161] M Matsumoto and T Nishimura. Mersenne twister: a 623-dimensionally equidistributed uniform pseudo-random number generator. *Transactions on Modeling and Computer Simulation*, 8(1):3–30, 1998.
1 citation(s) on 1 page(s): 131.